# Lateglacial and Holocene paleoceanography of the central Nordic Seas

**Dissertation**

in fulfilment of the requirements for the degree „Dr. rer. nat."

of the Faculty of Mathematics and Natural Sciences

at Kiel University

submitted by

**Maciej Mateusz Telesiński**

Kiel, 2014

| | |
|---|---|
| First referee: | Prof. Dr. Martin Frank |
| Second referee: | Prof. Dr. Dirk Nürnberg |
| | |
| Date of the oral examination: | 29. 07. 2014 |
| Approved for publication: | 29. 07. 2014 |

Signed: Prof. Dr. Wolfgang J. Duschl, Dean

## Summary

Five sediment cores of millennial to multicentennial resolution from the Greenland and Lofoten basins, central Nordic Seas, were analyzed for planktic foraminiferal fauna, planktic and benthic stable oxygen and carbon isotopes, and ice-rafted debris. The Nordic Seas are an important region for the global oceanic system because they constitute the main surface and the only deep water connection between the Artic and North Atlantic oceans. They are also a crucial area for deepwater formation. However, due to a lack of high resolution sediment records the paleoceanography of their central part has been poorly investigated in close detail yet.

The results in this report show that on a larger spatial and temporal scale the oceanographic evolution of the Nordic Seas is governed mainly by orbital forcing, but other processes can play an equally important role in shorter-scale, more local changes. The most important of these factors are the intensity of Polar and Atlantic waters inflow, the influence of freshwater discharges, sea-ice processes and deep convection.

The circum-Nordic Seas marine-based ice sheets collapsed 18,000-16,000 years before present, releasing large amounts of icebergs and freshwater, which affected the overturning circulation and contributed to the Heinrich stadial 1. Between 12,800 and 11,700 years before present the central Nordic Seas were affected by the last major freshwater outburst related with the Younger Dryas. Most likely it entered the area through the Fram Strait, suggesting an Arctic origin for the trigger of this cold event.

The Holocene Thermal Maximum in the central Nordic Seas was delayed compared to their eastern part and stretched well into the middle Holocene. The deep convection, developing in the Greenland Basin since the early Holocene, reached its

maximum intensity 7,000-6,000 years before present. Neoglacial cooling increased the stratification of the water column and around 3,000 years before present it led to a drop in the deepwater production rate. Ca. 2,000 years before present the subsurface water layer in the central Nordic Seas was warmed by enhanced Atlantic Water inflow to a level comparable with the Holocene Thermal Maximum.

## Zusammenfassung

An fünf Sedimentkernen aus dem Grönlandbecken und dem Lofotenbecken (zentrales Europäisches Nordmeer) wurden die planktischen Foraminiferen, planktische und benthische stabile Sauerstoff- und Kohlenstoffisotope und eistransportiertes Material mit einer zeitlichen Auflösung von Jahrhunderten bis Jahrtausenden untersucht. Das Europäische Nordmeer ist eine wichtige Region für das globale Ozeanzirkulationssystem, weil es die wichtigste bzw. einzige Verbindung für den Austausch von Oberflächen- und Tiefenwasser zwischen dem Arktischen und dem Atlantischen Ozean darstellt. Es ist auch ein äußerst wichtiges Gebiet für die Tiefwasserbildung im Weltozean. Wegen nur weniger vorhandener zeitlich hochauflösender Sedimentkerne ist der zentrale Teil des Europäischen Nordmeeres bisher aber relativ unvollkommen untersucht.

Die Ergebnisse in dieser Arbeit zeigen, dass die ozeanographische Entwicklung im Arbeitsgebiet großräumlich und auf längeren Zeitskalen vor allem durch orbitale Veränderungen beeinflusst wird. Andere Faktoren können jedoch regional und auf kürzeren Zeitskalen eine ebenso wichtige Rolle spielen. Die wichtigsten dieser Faktoren sind die Intensität der Advektion von polaren und atlantischen Wassermassen, der Einstrom von Süßwasser, sowie Prozesse in Zusammenhang mit der Tiefenwassererneuerung und der Bildung von Meereis.

Die rund um das Europäische Nordmeer existierenden marinen Eisschelfe kollabierten ca. 18,000-16,000 Jahre vor heute (J. v. h.). Sie setzten große Mengen von Eisbergen und Süßwasser frei, die die thermohaline Zirkulation beeinflussten und zur Entstehung des Heinrich-Stadials 1 beigetrugen. Zwischen 12.800 und 11.700 J. v. h. wurde das zentrale Europäische Nordmeer vom letzten großen Süßwasserausstoß betroffen, der mit der Jüngeren Dryas assoziiert war. Wahrscheinlich erreichte das

Süßwasser das Europäische Nordmeer durch die Framstraße, was auf einen arktischen Ursprung für den Auslöser dieser kalten Klimaphase hindeutet.

Das holozäne Temperaturmaximum (HTM) im zentralen Europäischen Nordmeer begann im Vergleich zu seinem östlichen Teil etwas verzögert und zog sich bis ins mittleren Holozän hinein. Die Tiefenwassererneuerung, die sich im Grönlandbecken seit dem frühen Holozän entwickelte, erreichte ihre maximale Intensität ca. 7,000-6,000 J. v. h. Die neoglaziale Kühlung verstärkte die Schichtung der Wassersäule und führte ca. 3.000 J. v. h. zu einer Verringerung in der Tiefwasserproduktionsrate. Ab ca. 2000 J. v. h. zeigen die Daten eine Erwärmung der oberflächennahen Schichten im zentralen Europäischen Nordmeer ähnlich wie im HTM an, was auf einen erneuten verstärkten Atlantikwasserzustrom deutet.

## Streszczenie

Pięć rdzeni osadów morskich o rozdzielczości rzędu stu do tysiąca lat, pochodzących z basenów Grenlandzkiego i Lofockiego (centralna część Mórz Nordyckich) zostało poddanych analizie mikropaleontologicznej (otwornice planktoniczne), izotopowej (stabilne izotopy tlenu i węgla) oraz litologicznej. Morza Nordyckie są regionem istotnym dla globalnego systemu oceanicznego, ponieważ stanowią główne połączenie dla wód powierzchniowych, a jedyne dla wód głębinowych pomiędzy Oceanem Arktycznym i północnym Atlantykiem. Są również kluczowym obszarem formowania się wód głębinowych. Jednakże, z powodu braku zapisów kopalnych o dostatecznej rozdzielczości, historia rozwoju oceanograficznego ich centralnej części była dotychczas słabo poznana.

Przedstawione w tej pracy wyniki pokazują, że rozwój oceanograficzny Mórz Nordyckich w dłuższej skali czasowej, jak i w większej skali geograficznej jest determinowany głównie przez zmiany parametrów orbity ziemskiej. Jednakże w krótszej skali czasowej i na miejszych obszarach inne czynniki mogą odgrywać równie znaczącą rolę. Do najważniejszych z nich należą: intensywność napływu wód polarnych i atlantyckich, wpływ wód o niskim zasoleniu, procesy związane z lodem morskim oraz głęboka konwekcja.

Czoła lądolodów położonych wokół Mórz Nordyckich zaczęły wycofywać się 18-16 tysięcy lat temu, uwalniając duże ilości gór lodowych oraz wody słodkiej, która wpłynęła na cyrkulację termohalinową, przyczyniając się do genezy tzw. Zdarzenia Heinricha 1. Pomiędzy 12,8 i 11,7 tys. lat temu, w czasie Młodszego dryasu, po raz ostatni znaczące ilości wody słodkiej dotarły do centralnej części Mórz Nordyckich.

Najprawdopodobniej woda ta przedostała się w ten rejon od strony cieśniny Fram, co sugeruje że źródła tej zimnej fazy klimatycznej należy szukać w Arktyce.

Optimum klimatyczne holocenu w centralnej części Mórz Nordyckich było opóźnione w porównaniu z ich wschodnią częścią i trwało aż do środkowego holocenu. Głęboka konwekcja, która rozwijała się w Basenie Grenlandzkim od wszesnego holocenu, osiągnęła swoją maksymalną intensywność około 7-6 tys. lat temu. Ochłodzenie neoglacjalne wzmocniło stratyfikację termohalinową wód i około 3 tys. lat temu doprowadziło do spadku tempa produkcji wód głębinowych. Około 2 tys. lat temu temperatura podpowierzchniowych warstw wód w centralnej części Mórz Nordyckich wzrosła do poziomu porównywalnego z optimum klimatycznym holocenu w wyniku zwiększonego napływu wód atlantyckich.

## Acknowledgements

My warm and sincere thanks go to:

- Dr. Robert F. Spielhagen for introducing me to my work and supervising it, for his kindness, support and countless advices,
- Prof. Dr. Martin Frank for entrusting me this work, overseeing and examining it,
- Prof. Dr. Dirk Nürnberg for being the co-referee,
- Dr. Henning A. Bauch for numerous discussions, advices, his interest and criticism,
- Dr. Kirstin Werner for valuable help and support, not only in scientific matters,
- Dr. Christelle Not and Lulzim Haxhiaj for performing the stable isotope measurements,
- my co-authors, reviewers and others who helped me in this work,
- the entire Arctic group at GEOMAR (aka "Kaffeerunde") for discussions on almost every possible subject as well as many moments of laugh and relax,
- all the people involved in the CASE ITN – the PIs, ESRs, and visiting scientists – for the time spent together in different places across the Europe, for the scientific input and personal exchange,
- Dr. Jacques Giraudeau and Isabelle Deme for coordinating the entire CASE project and their kind support,

- my family and friends for their invaluable support, encouragement during my work and for moments of respite, especially to my Grandfather for his concern about my forams,
- my Parents – certainly more difficult than to earn a doctoral degree is to raise the children in such a way that they can achieve it, so they deserve this title more than I do.

This work is a contribution to the CASE Initial Training Network funded by the European Community's 7th Frame- work Programme FP7 2007/2013, Marie-Curie Actions, under Grant Agreement no. 238111.

## Erklärung

Hiermit versichere ich an Eides statt, dass ich diese Dissertation selbständig und nur mit Hilfe der angegebenen Quellen und Hilfsmittel und der Beratung durch meinen Betreuer unter Einhaltung der Regeln guter wissenschaftlicher Praxis der Deutschen Forschungsgemeinschaft angefertigt habe. Ferner versichere ich, dass der Inhalt dieser Arbeit weder in dieser, noch in veränderter Form einer weiteren Prüfungsbehörde vorliegt.

Kiel, den 5. Juni 2014

# Table of contents

1. Introduction 1
   1.1. The Nordic Seas – morphology and geological evolution 1
   1.2. “The heat pump” and “the lungs of the ocean” 4
   1.3. State of the art: the Nordic Seas since the Last Glacial Maximum 5
   1.4. Research questions and outline of the thesis 11
   1.5. Synthesis/major results 14
   References 20
2. Material and methods 29
   2.1. Sediment cores 29
   2.2. Sample preparation 31
   2.3. Chronology 31
   2.4. Planktic foraminifera counts 34
   2.5. Subsurface temperature reconstruction 34
   2.6. Ice-rafted debris and volcanic glass shards 35
   2.7. Stable oxygen and carbon isotopes 36
   References 36
3. A high-resolution Lateglacial and Holocene palaeoceanographic record from the Greenland Sea 39
4. Water mass evolution of the Greenland Sea since late glacial times 53
5. Evolution of the central Nordic Seas over the last 20 thousand years 69
   Abstract 70
   5.1. Introduction 71
   5.2. Study area 73
   5.3. Material and methods 75
   5.4. Chronology 78
   5.5. Results 81
      5.5.1. Planktic foraminifera and reconstructed subsurface temperatures 81
      5.5.2. Stable isotopes 83
      5.5.3. IRD 84
   5.6. Discussion 84
      5.6.1. Deglaciation 84
      5.6.2. Holocene 91
   5.7. Sumary and conclusions 101
   Acknowledgements 103
   References 103

# 1. Introduction

## 1.1. The Nordic Seas – morphology and geological evolution

The Nordic Seas (Fig. 1.1.) is a collective name for the body of water consisting of two deep ocean regions: the Norwegian Sea and the Greenland Sea. They are bordered by Greenland to the west, the Svalbard archipelago to the northeast, the Scandinavian Peninsula to the southeast and Iceland to the southwest. In the north the Nordic Seas have a deep (sill depth ca. 2200 m, Hansen & Østerhus, 2000) connection with the Arctic Ocean through Fram Strait. In the east they neighbor the shallow Barents Sea shelf. In the south, the Greenland-Scotland Ridge forms a continuous barrier divided by Iceland and the Faroe Islands into three gaps – the Denmark Strait, the Iceland-Faroe Ridge and the Faroe-Shetland Channel – that connect the Nordic Seas with the North Atlantic (Hansen and Østerhus, 2000).

The Norwegian Sea is separated from the Greenland Sea by submarine ridges – the Mohns Ridge in the north and the Jan Mayen Ridge (or Microcontinent as it consists of continental crust, cf. Talwani and Eldholm, 1977) in the south. It can be subdivided into the southern Norwegian and northern Lofoten basins. Between them are the northwest-southeast running Jan Mayen fracture zone (JMFZ) and the Vøring Plateau – a marginal plateau of igneous origin (Mjelde et al., 2001). Characteristic features of the eastern margin of the Norwegian Sea are glacigenic sediment fans (e.g., the Bear Island Trough Mouth Fan).

The Greenland Sea is bordered to the west by the broad Greenland continental shelf. Its northern part is divided by the northwest-southeast oriented Greenland fracture zone into the northern Boreas and southern Greenland basins. The southernmost part of

the Greenland Sea, also referred to as the Iceland Sea (Hansen and Østerhus, 2000) is shallower compared to the rest of the Nordic Seas basins. It is cut by the northeast-southwest stretching Kolbeinsey Ridge, an active section of the Mid-Atlantic Ridge, and separated by the JMFZ from the rest of the Greenland Sea.

The early Tertiary lithospheric breakup between Eurasia and Greenland occurred close to the Paleocene/Eocene boundary, ca. 56 milion years ago (Ma). The late syn-rift phase led to extensive uplift and formation of a land area along the subsequent breakup axis (Thiede et al., 1995). The Nordic Seas started to open in the early Eocene (Ypresian, ca. 53 Ma) with a NNW-SSE relative displacement between the Greenland and European plates (Dauteuil and Brun, 1993). The opening occurred along stable continental margins without offsets across minor fracture zones (Olesen et al., 2007). The Mohns ridge formed perpendicular to the spreading direction (Dauteuil and Brun, 1993). The Greenland Sea only came into existence subsequent to about 38 Ma. Prior to this time a land bridge existed between Svalbard and Greenland (Talwani and Eldholm, 1977). During the Oligocene (27 Ma) a major reorganization of North Atlantic plate boundaries occurred when spreading in the Labrador Sea ceased and the Greenland Plate rotated counterclockwise relative to the Eurasian Plate. This kinematic change induced WNW-ESE spreading. In the early Miocene (17.5 Ma) Fram Strait opened wide enough to permit deepwater exchange and to turn the Arctic Ocean from an oxygen-poor ‘lake stage’ to the fully ventilated ‘ocean’ phase (Jakobsson et al., 2007) From 12 to 5 Ma, the spreading rate slowly decreased and then increased to its present value of 1.8 cm $a^{-1}$. In spite of these kinematic changes, the Mohns Ridge retained its old trend and is now oblique to the 110-120° spreading direction (Dauteuil and Brun, 1996, 1993).

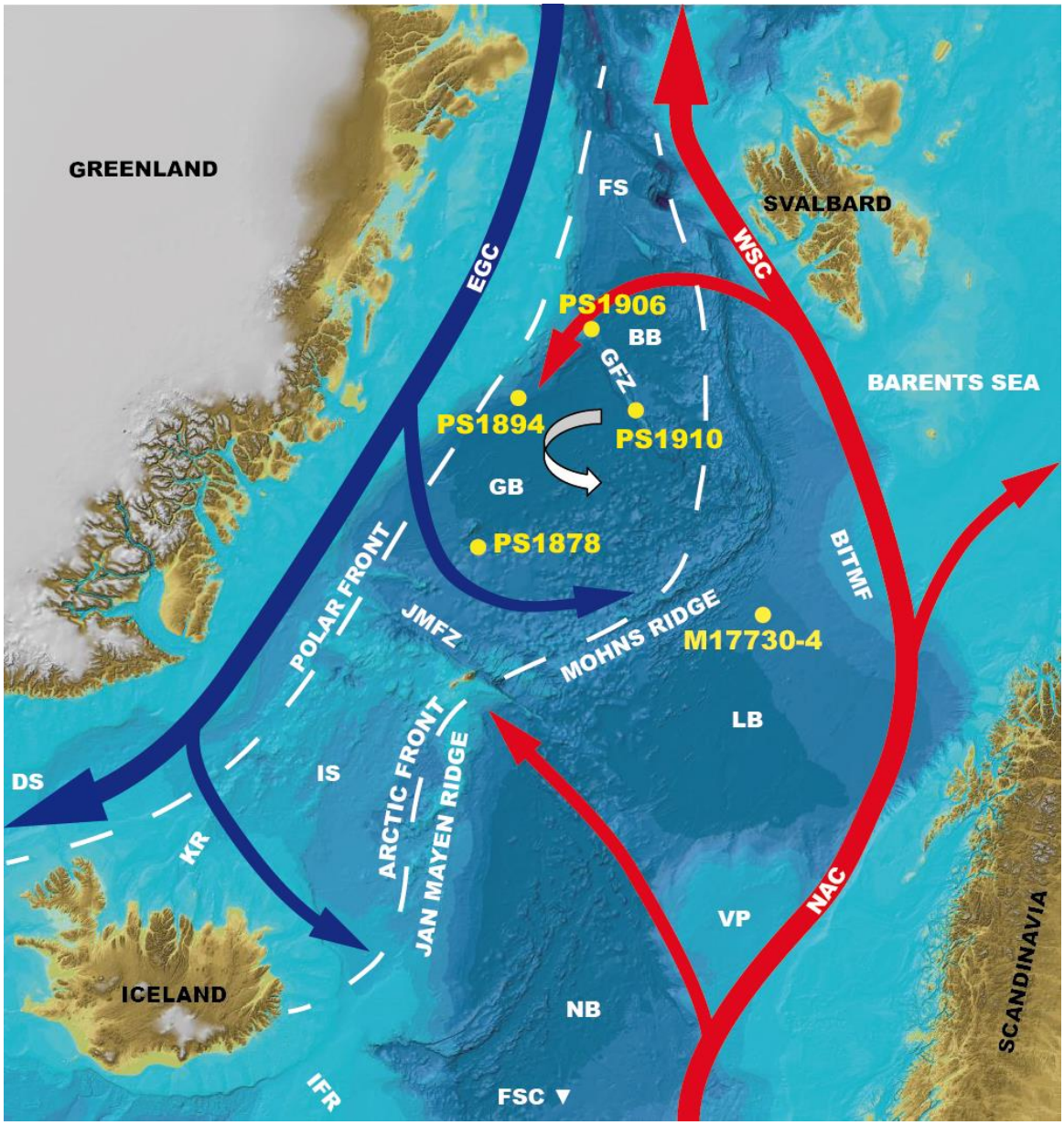


Fig. 1.1. Present day morphology and surface water circulation in the Nordic Seas. Cores used in this study are marked with yellow dots. Red arrows indicate Atlantic Water, blue arrows – Polar Water, white broken lines – oceanographic fronts. White arrow – present-day deep convection (Marshall and Schott, 1999). BB - Boreas Basin, BITMF – Bear Island Trough Mouth Fan, DS – Denmark Strait, EGC – East Greenland Current, FS – Fram Strait, FSC - Faroe-Shetland Channel, GB – Greenland Basin, GFZ – Greenland Fracture Zone, IFR – Iceland-Faroe Ridge, IS – Iceland Sea, JMFZ – Jan Mayen Fracture Zone, KR – Kolbeinsey Ridge, NAC – North Atlantic Current, WSC – West Spitsbergen Current, VP – Vøring Plateau. Bathymetry from The International Bathymetric Chart of the Arctic Ocean (http://www.ibcao.org, 2012).

## 1.2. "The heat pump" and "the lungs of the deep ocean"

The Nordic Seas have been termed "the heat pump" of the oceans (Weinelt, 1993) because they play a key role in the warmth transport from low to high latitudes. They constitute the main surface and the only deep water connection between the Artic and North Atlantic oceans. Relatively warm, saline (T~6–11°C, S>35) Atlantic Water (AW) is advected to the area by the North Atlantic Current (NAC) mainly through the Faroe-Shetland Channel but also over the Iceland-Faroe Ridge and through the Denmark Strait. The AW then flows northward along the Norwegian coast. Part of it enters the Barents Sea while the rest continues northward along the shelf edge to eventually reach the Arctic Ocean through the eastern Fram Strait. Cold, low saline (T<0°C, S<34.4) Polar Water (PW) enters the Nordic Seas through the western Fram Strait and flows southward as the East Greenland Current (EGC) along the Greenland shelf margin to finally leave the basin through the Denmark Strait (Rudels et al., 1999). The EGC sends its branches into the central part of the Nordic Seas (e.g., the Jan Mayen Current) where they meet western branches of the NAC (e.g., the Return Atlantic Current). The distribution of surface water masses in the Nordic Seas results in a threefold division of the basin. The eastern Atlantic domain is separated by the Arctic Front from the central Arctic domain, an area of AW and PW mixing (Swift, 1986). In the west, along the Greenland coast, is the Polar domain, separated by the Polar Front. The AW is partially being subducted below the EGC-derived Arctic Surface Water, supplying the Atlantic Intermediate Water. Below resides the weakly stratified Greenland Sea Deep Water, a product of deep convection (Marshall and Schott, 1999).

The Nordic Seas are also "the lungs of the deep ocean" (Weinelt, 1993) as they are one of the major areas in the world where deep water convection takes place (e.g., Marshall and Schott, 1999; Rudels and Quadfasel, 1991). The western branches of the

NAC and the eastern branches of the EGC create a cyclonic circulation in the Greenland Sea (known as the Greenland Sea gyre) and lead to a doming of the upper water layers. Sea ice plays an important preconditioning role in the Greenland Sea compared to other convection areas. In early winter, the formation of sea ice leads to brine rejection. The surface layer increases its density. The mixed layer under the ice cools to freezing temperature and sinks to about 150 m by mid-January. The sea ice cover forms a wedge (Is Odden) extending far to the northeast. Preconditioning continues later in the winter, with mixed-layer deepening in the ice-free area (Nord Bukta) to 300–400 m, induced by strong winds blown over the ice. Typically in March, near-surface densities are high enough to develop deep convection (down to >2000 m) in the Greenland Sea, if the meteorological conditions are favorable (Marshall and Schott, 1999). Subsequently, the water leaves the Nordic Seas as the Denmark Strait and Iceland-Scotland Overflow Waters (DSOW and ISOW, respectively) together with Arctic Ocean Intermediate and Deep Water entering the Nordic Sea through the deeper parts of the Fram Strait (Hansen and Østerhus, 2000).

## 1.3. State of the art: the Nordic Seas since the Last Glacial Maximum

A huge discrepancy in the state of knowledge exists between the eastern and the central part of the Nordic Seas. While there are a lot of paleoceanographic studies from sites located along the main NAC flow, little is known – despite its importance for the global oceanographic system – about the evolution of the remaining part of the basin even since the Last Glacial Maximum (LGM). One major reason is the difference in the temporal resolution of the available sediment records. While a number of sites with several meters thick marine Holocene sedimentary sequences are known from the eastern

Nordic Seas – even far north, off Svalbard (e.g., Hald et al., 2007; Ślubowska-Woldengen et al., 2007; Werner et al., 2013), there are very few records of submillennial or higher temporal resolution from the central Nordic Seas (e.g., Bauch and Weinelt, 1997; Bauch et al., 2001a; Fronval and Jansen, 1997). The typical sedimentation rates in this deep, cold and often ice-covered area hardly reach 5 cm $kyr^{-1}$ (e.g., Nørgaard-Pedersen et al., 2003). With such low sedimentation rates bioturbational mixing becomes a severe problem, resulting in unusually old surface sediment ages (e.g., Bauch et al., 2001a; Fronval and Jansen, 1997). Another matter is the accessibility of the sites. While the eastern Nordic Seas can be reached relatively easily and in a short time from Scandinavia or Svalbard, coring farther to the west requires long expeditions with ice-strengthened research vessels.

Since the LGM, ca. 18-23 ka (Sarnthein et al., 2003a), the Nordic Seas experienced an evolution from fully glacial climatic and oceanographic conditions to the full interglacial. The LGM was an orbitally driven climax of the Weichselian glaciation. As the sea-level was ca. 120 m lower than at present (Lambeck and Chappell, 2001), the Nordic Seas constituted the only connection between the Arctic and Atlantic oceans. All the land masses surrounding the Nordic Seas, including the Barents Sea shelf, were covered with ice sheets (Funder and Hansen, 1996; Hubbard et al., 2006; Svendsen et al., 2004). Despite such cold conditions, sea ice did not cover the entire basin but was restricted to the northwestern margin of the Nordic Seas during summer and advanced to the south of Iceland and Faroe during winter (Pflaumann et al., 2003). This was due to AW, which continued to enter the Nordic Seas although the inflow was much more unstable than during interstadials (Rasmussen and Thomsen, 2008). The AW subducted under the cold and relatively fresh surface layer and was warming the deepwater masses.

The deep convection and the outflow of deepwater from the Nordic Seas stopped (Rasmussen and Thomsen, 2008, 2004).

Due to the rapidly increasing insolation, the ice sheets surrounding the Nordic Seas started to retreat shortly after the LGM (Lehman et al., 1991). The early (ca. 19 ka) deglaciation of the Fennoscandian Ice Sheet resulted in enhanced freshwater fluxes to the North Atlantic and the Nordic Seas, forcing the ocean into a state with weak Atlantic Meridional Overturning Circulation (AMOC) and NADW formation, similar to a stadial period (Hall et al., 2006). This led to subsurface warming and a subsequent collapse of the ice sheets and iceberg purges, a sequence of events known as Heinrich event 1 (H1) (Álvarez-Solas et al., 2011; Stanford et al., 2011). The released freshwater (Sarnthein et al., 1995) acted as a positive feedback for the entire process which led to the near or complete elimination of the AMOC (Álvarez-Solas et al., 2011; McManus et al., 2004).

At 14.6 ka meltwater pulse 1A (mwp-1A) originating from the Antarctic Ice Sheet raised the sea-level by ca. 20 m and caused a rapid reactivation of the AMOC, thereby warming the North Atlantic region and initiating the Bølling-Allerød (BA) period (McManus et al., 2004; Weaver et al., 2003).

The Younger Dryas (YD), spanning ca. 12.8–11.7 ka (Rasmussen et al., 2006), was the coldest phase within the overall climate warming in the transition from the LGM to the Holocene. This millennial-scale event involved a significant reduction in the AMOC attributed to enhanced meltwater inputs into the North Atlantic (e.g., Broecker et al., 2010; Not and Hillaire-Marcel, 2012). It is still unclear whether the freshwater pulse reached the Nordic Seas as a sediment-loaded plume from the Hudson Strait (Rashid et al., 2011), as a meltwater discharge through the St Lawrence river system and via the Gulf Stream (e.g., Broecker et al., 1989) or through the Mackenzie River basin and via

the Arctic Ocean (e.g., Not and Hillaire-Marcel, 2012; Tarasov and Peltier, 2006). Despite a dispute on terrestrial evidence (Fisher and Lowell, 2012; Murton et al., 2010), the latter concept has gained increasing support recently through modelling results of Condron and Winsor (2012). They showed that only a meltwater discharge from the Arctic, in contrast to the outflow through the St Lawrence Valley, was able to reach the deepwater formation regions of the subpolar North Atlantic and weaken the AMOC significantly.

The Holocene interglacial, which began after the YD (Rasmussen et al., 2006), was climatically a relatively stable interval compared to the last glacial, especially when looking at the ice core records (e.g., Grootes et al., 1993). Other proxy records, however, reveal rapid variations of significant amplitude throughout the Holocene (e.g., Bond et al., 1997; Mayewski et al., 2004). The onset of the Holocene was related to high insolation in the high northern latitudes (Risebrobakken et al., 2011). After the transitional Preboreal period, Northern Hemisphere insolation and AW advection into the Nordic Seas reached their maximum (Risebrobakken et al., 2011). The Holocene Thermal Maximum (HTM), the warmest part of the Holocene related with these maxima, occurred relatively early in the eastern Nordic Seas, along the main NAC flow, and was quite short (11-9 ka, Risebrobakken et al., 2011). In other parts of the Nordic Seas, however, the climatic optimum was reached later and/or lasted much longer (e.g., Andersen et al., 2004b; Bauch et al., 2001b; Sarnthein et al., 2003b; Werner et al., 2013). This delay partly resulted from the influence of the melting Greenland Ice Sheet which acted as a negative feedback to the orbitally forced climatic optimum (Blaschek and Renssen, 2013). On the other hand, it was related to the development of the stable and modern-like oceanic circulation in the Nordic Seas that was reached only ca. 7-8 ka (Bauch et al., 2001a; Hall et al., 2004; Thornalley et al., 2010).

Many studies report a number of relatively short events during the Holocene with surface water cooling (Wanner et al., 2011; Werner et al., 2013), increased ice-rafting (Bond et al., 2001, 1997) or reduced AMOC intensity (Hass, 2002) in the North Atlantic region. Despite numerous attempts (Bond et al., 2001, 1997; Risebrobakken et al., 2003; Sarnthein et al., 2003b) no clear cyclicity has been found and most of these events apparently did not occur simultaneously on a global or even regional scale (Wanner et al., 2011). Only the event at ca. 8.2 ka seems to be recorded worldwide, although the anomalies in many records span 400 to 600 years (Rohling and Pälike, 2005). This so-called '8.2 ka event' is also recorded in Greenland ice cores where it appears as the most prominent abrupt climatic event during the Holocene (Kobashi et al., 2007). This event, characterized by a generally cool, dry and windy climate, is commonly assigned to the final outburst drainage of proglacial lakes Agassiz and Ojibway into the North Atlantic and a slowdown of NADW formation (Barber et al., 1999; Kobashi et al., 2007; Rohling and Pälike, 2005). In the Nordic Seas it was associated with lower sea-surface temperatures (Risebrobakken et al., 2003; Sarnthein et al., 2003b), salinities (Werner et al., 2013), increased sea-ice and iceberg abundance (Bond et al., 1997; Müller et al., 2012) and reduced ISOW flow speed (Hall et al., 2004).

Apparently, the 8.2 ka event interrupted the HTM but did not disturb the long-term climatic and oceanographic evolution of the Holocene. Although in some areas the orbitally induced (Andersen et al., 2004a) Neoglacial cooling started already after 9 ka (Hald et al., 2007; Risebrobakken et al., 2011), in most of the Nordic Seas the climatic optimum ended well after the 8.2 ka perturbation (e.g., Andersen et al., 2004b; Bauch et al., 2001a; Fronval and Jansen, 1997; Sarnthein et al., 2003b). While at some sites the cooling was gradual (e.g., Andersen et al., 2004a; Marchal et al., 2002), in other places it showed a stepwise pattern (e.g., Calvo et al., 2002; Werner et al., 2013). The flooding of

the Arctic shelves at 9-5 ka which increased the sea-ice production (Bauch et al., 2001b) and the roughly contemporary shift of the Transpolar Drift in the Arctic Ocean that increased the southward transport through the Fram Strait (Dyke et al., 1997; Prange and Lohmann, 2003) may have triggered the stepwise cooling episodes (Werner et al., 2013).

At least since the establishment of the stable and modern-like oceanic circulation in the Nordic Seas ca. 7-8 ka (Bauch et al., 2001a; Thornalley et al., 2010) open ocean deep convection has taken place in the Nordic Seas (Marshall and Schott, 1999; Rudels and Quadfasel, 1991). Benthic carbon isotope records (Bauch et al., 2001a; Sarnthein et al., 2003b) indicate that ca. 6 ka it reached its maximum velocity and depth. The development of convective activity was enabled by the activation of the Greenland Sea gyre. The resulting increased inflow of both AW and PW strengthened the heat transport to the eastern Nordic Seas (hence delaying the Neoglacial cooling) as well as enhanced cooling and sea-ice delivery from the Arctic (Giraudeau et al., 2010).

Around 3 ka a strong solar irradiance minimum triggered another significant oceanographic and climatic shift in the Nordic Seas (Renssen et al., 2006). The resulting expansion of drift ice (Bond et al., 2001; Müller et al., 2012) not only changed the surface water structure (stronger halocline) but also caused a perturbation in the AMOC (Hall et al., 2004). This event is a sound stratigraphic time marker (Bauch and Weinelt, 1997) as it is recorded all across the Nordic Seas as a distinct decrease in the planktic carbon isotope ratios (Bauch et al., 2001a; Fronval and Jansen, 1997; Risebrobakken et al., 2011; Sarnthein et al., 2003b; Vogelsang, 1990; Werner et al., 2013).

The late Holocene was a time of low insolation in the high northern latitudes (Wanner et al., 2008). Several climatic and oceanographic fluctuations are known from this time interval in the North Atlantic region. The Roman Warm Period (RWP), peaking

ca. 2 ka, was a period of warm weather over the Northern Hemisphere (Ljungqvist, 2010) as well as faster ISOW flow (Bianchi and McCave, 1999). It coincided with a major change in the North Atlantic Oscillation mode from variable, intermittently negative to generally positive (Olsen et al., 2012). The latter state is characterized by stronger westerlies, which intensify the AW advection into the Nordic Seas. The RWP was followed by the Dark Ages Cold Period and the Medieval Warm Period (or Medieval Climate Anomaly), centered around 1.5 ka and 1 ka, respectively (Crowley and Lowery, 2000; Ljungqvist, 2010). Finally, the Little Ice Age, centered ca. 0.3 ka, was a period of cooling and advances of mountain glaciers in the Northern Hemisphere. It occurred when low summer insolation coincided with solar activity minima and several strong tropical volcanic eruptions (Eddy, 1976; Wanner et al., 2008). Since ca. 0.2 ka the Northern Hemisphere temperatures keep increasing (Kaufman et al., 2009; Moberg et al., 2005).

## 1.4. Research questions and outline of the thesis

The aim of this study was to reconstruct the paleoceanography of the central part of the Nordic Seas with highest possible temporal resolution. For this purpose undisturbed records from sites with sufficient sedimentation rates are needed. Due to the scarcity of such sites, lower resolution records from the research area were also used to obtain a better view of the spatial range of at least part of the observed processes. As the target time interval the period between the LGM and present day was chosen as it encompasses a full transition between glacial and interglacial climatic and oceanographic conditions as well as the evolution of the present interglacial. To obtain a most comprehensive image a set of different proxies was applied. Planktic and benthic stable oxygen and carbon isotopes give hints on water temperature and salinity, ventilation and

structure of the water column. Planktic foraminiferal assemblages allow to reconstruct surface water temperature (also absolute temperatures by means of transfer functions), bioproductivity (and thus, indirectly, ventilation, sea-ice coverage, food availability etc.) and different water masses. Finally, ice rafted debris (IRD) informs on the abundance of drift ice and the identification of its origin allows to reconstruct surface water currents.

The presented thesis addresses the following research questions:

- Is it possible to find sedimentary records of submillennial temporal resolution in the central Nordic Seas? What are the problems with the stratigraphy, dating and correlation of records from this region?
- How severe were the conditions in the central Nordic Seas during the LGM? Was there any ice-free water? Did Atlantic Water (AW) reach the area?
- When did the deglaciation start? Was it synchronous across the area? What were the sources of freshwater outbursts and how did they affect the oceanic circulation?
- How was the Younger Dryas expressed in the area? Are there any indications on the origin of this cold event?
- Was the onset of the early Holocene warming simultaneous across the Nordic Seas? How warm was the Holocene Thermal Maximum and did it affect the entire Nordic Seas at the same time?
- Can any indications of the 8.2 ka event and other brief Holocene cooling events be found in the central Nordic Seas records?
- When did the Neoglacial cooling start? Was it gradual or rapid/stepwise?
- How did the overturning circulation in the area develop throughout the Holocene?

- What were the reasons, character and results of the oceanic circulation changes around and after 3 ka? Were the effects of local or regional scale?

The thesis consists of two introductory sections (1. and 2.) and three sections in the form of manuscripts that have either been published or are prepared for submission (3.-5.). Section 1 describes the general morphological features of the Nordic Seas basin and its geological history (1.1.), the present-day oceanography in the area (1.2.), the current state of knowledge on the Nordic Seas paleoceanography from the LGM until present (1.3.), the main research questions and the outline of the thesis (1.4.) as well as summarizes the main results of our research (1.5.). Section 2 presents the material and methods used in the study.

Section 3 presents a new high-resolution record of the surface water paleoceanography of the central Greenland Sea (published in *Boreas*). My contribution included the sampling of the sedimentary record, the preparation of the samples for AMS $^{14}C$ dating and stable isotope analysis, counting planktic foraminifera and IRD, interpreting the data, preparing the figures and writing the manuscript. Robert F. Spielhagen contributed to the discussion and the improvement of the manuscript. Ewa M. Lind performed the geochemical analysis of the volcanic glass shards, interpreted the result, prepared one figure (Fig. 4) and contributed to the part of the manuscript concerning the tephra layer.

In Section 4 the central Greenland Sea record (Section 3.), supplemented with benthic stable isotope data and subsurface temperature reconstruction, is compared to lower-resolution records from the northern Greenland Sea to gain a more complete spatial image of the paleoceanography in the area, including the deep water environment (published in *Climate of the Past*). I contributed to this section by sampling cores

PS1878 and PS1910-1, preparing the material for AMS $^{14}C$ dating and stable isotope analysis, counting planktic foraminifera and IRD (all cores), performing the transfer function calculations, interpreting the data, preparing the figures and writing the manuscript. Robert F. Spielhagen and Henning A. Bauch provided part of the data from the northern Greenland Sea records (PS1894-7 and PS1906-1) and contributed to the discussion and the improvement of the manuscript.

Section 5 compares two high-resolution records from the central Nordic Seas and attempts to summarize the previous results to gain a paleoceanographic reconstruction of the entire area. My contribution included the sampling of the sedimentary record, the preparation of the samples for AMS $^{14}C$ dating and stable isotope analysis, counting planktic foraminifera and IRD, interpreting the data, preparing the figures and writing the manuscript. Henning A. Bauch and Robert F. Spielhagen contributed to the discussion and the improvement of the manuscript. E. S. Kandiano performed the transfer function calculations.

## 1.5. Synthesis/major results

Two sedimentary records of multicentennial resolution retrieved from the Lofoten Basin, Norwegian Sea, and the central Greenland Sea are presented. As only a few submillennial records are known from this region (Bauch et al., 2001a; Fronval and Jansen, 1997), our results greatly improve the understanding of the paleoceanographic evolution of the Nordic Seas on a higher spatial and temporal level. Due to the importance of this region for the global ocean circulation, they also contribute to our knowledge on the processes governing the global ocean-climate system.

The results show that during the LGM the central Nordic Seas were strongly affected by PW. Due to the perennial sea-ice cover the ocean-atmosphere gas exchange and sunlight penetration were limited, resulting in poor ventilation of the upper water layers and low bioproductivity dominated by polar species. Occasionally during the warmer summer seasons the sea-ice cover diminished somewhat, allowing the foraminiferal fauna to bloom. These open water events also increased the mobility of icebergs and ice-rafted material delivery. It is impossible, however, to determine from the data whether the events were simultaneous across the region.

The deglaciation in the Nordic Seas started already around 19 ka with a small but conspicuous "precursor" freshwater event. It was probably caused by the sea-level rise (Clark et al., 2004) and originated from multiple sources. Between 18 and 16 ka the main deglacial event, associated with Heinrich stadial 1 (HS1), occurred roughly simultaneously across the Nordic Seas. Massive freshwater discharges originated from different circum-Nordic Seas ice sheets (Lekens et al., 2005; Nørgaard-Pedersen et al., 2003; Sarnthein et al., 1995). The eastern Greenland Ice Sheet was a source of a particularly strong outburst as in the central Greenland Sea the planktic $\delta^{18}O$ values during HS1 fell to almost 0‰, a level not observed in any other Nordic Seas or North Atlantic record. Freshwater also affected deep parts of the Nordic Seas, either as supercooled cascades descending down the continental slope (Lofoten Basin) or as fine sediment-loaded hyperpycnal plumes (Greenland Basin), though these two mechanisms do not exclude each other. The freshwater lid on top of the water column led to a collapse of the AMOC during HS1 (Stanford et al., 2011). Our results suggest that the Nordic Seas played a crucial role in this process and that the ice sheets surrounding them were an important source of icebergs and freshwater. This is in contrast to many earlier studies

(e.g., Broecker, 1994; Hemming, 2004) which regarded the Laurentide Ice Sheet and the Labrador Sea as the key regions for the onset of HS1.

The HS1-related freshwater discharges ended ca. 16 ka. The following interval (until ca. 13 ka) was still cold in the Nordic Seas and no indications of the Bølling-Allerød warming can be found except for a slightly increased bioproductivity. On the other hand, the AMOC was reactivated (Stanford et al., 2011) and the circulation system in the area started to develop towards its modern shape. As the Barents Sea Ice Sheet had already collapsed by this time (Bischof, 1994), the Greenland Ice Sheet remained the main source for icebergs and freshwater, still releasing them in minor discharges.

During the YD interval (12.8-11.7 ka) the Nordic Seas were affected by the last major freshwater discharge resulting from the drainage of glacial Lake Agassiz (Murton et al., 2010). The presence of clear freshwater indications in the Greenland and Lofoten basins as well as in the Fram Strait (Fahl and Stein, 2012) together with a lack of such evidence farther to the south (e.g., Risebrobakken et al., 2003) points to the Arctic Ocean as the source area of the freshwater and supports the hypothesis of a drainage through the Mackenzie Valley (Condron and Winsor, 2012; Tarasov and Peltier, 2006) as the most probable mechanism to trigger the YD cold event. Our results extend the range of the YD freshwater plume to the central part of the Nordic Seas. Such a broad extent of the freshwater lid is in agreement with the sharp AMOC decline (McManus et al., 2004) and increased sea-ice abundance in the Nordic Seas (Cabedo-Sanz et al., 2013; Müller et al., 2009) during the early YD.

The onset of the Holocene in the Nordic Seas was associated with a major decrease in ice rafting, diminishing sea-ice cover, enhanced AW inflow and increasing bioproductivity. After a short transitional period, subsurface water temperatures reached

their maximum in the eastern Nordic Seas (Hald et al., 2007; Risebrobakken et al., 2011). Our results, however, show that farther to the west the warming was more gradual and somewhat delayed. This was, on the one hand, caused by the activation and stabilization of the Greenland Sea gyre. On the other hand, the deglacial freshwater from the Greenland Ice Sheet acted as a negative feedback to the warming and AMOC development in the central Nordic Seas (Blaschek and Renssen, 2013). In the Lofoten Basin the maximum Holocene temperatures were reached between 10 and 9 ka, while in the central Greenland Sea only after 8 ka. Also the duration of the thermal maximum in the central Nordic Seas was different than in the east. While along the eastern continental margin the warmest interval was restricted to ca. 2 kyr (Hald et al., 2007; Risebrobakken et al., 2011; Sarnthein et al., 2003b), farther to the west it stretched well into the middle Holocene.

The early-mid Holocene thermal maximum was, however, not a uniform interval. In the entire North Atlantic region it was interrupted by several short-scale cooling events (Wanner et al., 2011; Werner et al., 2013), the most prominent and widespread of which was the 8.2 ka event. In the central Nordic Seas it was reflected by a limited bioproductivity. The cooling of the upper water layers was more pronounced in the Lofoten Basin, probably due to the weakened AW transport (Born and Levermann, 2010), as the temperatures in this area depend more on that factor than in the Greenland Sea. Our data also indicate a modest freshwater influence in the Greenland Basin and suggest a brief AMOC reduction at that time (cf. Hall et al., 2004). Several other events of cooling and reduced bioproductivity can be found in our records but a correlation of them seems difficult.

Our benthic isotope records indicate the development of deep convection in the Greenland Sea at least since the early Holocene. Only after 8-7 ka, when the freshwater

input from the Greenland Ice Sheet ceased (Blaschek and Renssen, 2013; Seidenkrantz et al., 2012), the surface and deepwater circulation reached its modern pattern (Thornalley et al., 2010). Around 7-6 ka the convection rates reached their maximum and remained on this level until ca. 3 ka. The convection center was most probably located close to its present-day location (cf. Marshall and Schott, 1999), migrating slightly together with the sea-ice edge.

The transition between the thermal maximum and the Neoglacial cooling was forced by the decreasing summer insolation in the high northern latitudes (Andersen et al., 2004a). However, its course differed across the Nordic Seas. In the northern Greenland Sea and, e.g., over the Vøring Plateau (Andersen et al., 2004a), surface water cooled down with decreasing insolation. In other areas the cooling had a more stepwise character. These rapid cooling steps were apparently triggered by different local or regional forcings. The early termination of the thermal maximum in the eastern Nordic Seas, for instance, was a result of a decrease in AW advection (Hald et al., 2007; Risebrobakken et al., 2011; Sarnthein et al., 2003b). The rapid cooling in the eastern Fram Strait (Werner et al., 2013) and in the central Greenland Sea coincided with – and was probably a result of – an enhanced sea-ice production and export from the Arctic Ocean caused by the flooding of the Siberian shelves (Bauch et al., 2001b; Werner et al., 2013). In the Lofoten Basin the cooling started only after 4 ka and was likely delayed by an enhanced AW advection into the Greenland Sea gyre related to the high convection pace. The cooling led to the expansion of the sea-ice cover and a thickening of the low-salinity surface layer in the Nordic Seas (Müller et al., 2012; Werner et al., 2013).

The Neoglacial cooling reached its apogee in the central Nordic Seas around 3 ka. It resulted not only from decreasing insolation. Between 2.85 and 2.6 ka the strongest Holocene solar irradiance minimum occurred (Renssen et al., 2006; Vonmoos et al.,

2006). By amplifying the Neoglacial cooling, it caused a significant sea-ice expansion (Müller et al., 2012). Our benthic isotope data suggest that this led to a decrease in the rate and/or depth of convection. The convection center was probably also relocated somewhat southeastwards together with the expanding sea-ice cover (Renssen et al., 2006). The convection slowdown was recorded only at three sites located closest to the convection center where the ventilation of the bottom water was most efficient. At other sites the bottom waters were not as well ventilated before 3 ka and therefore the relative decrease in ventilation was not large enough to be recorded in the sediment archive.

After 3 ka the water column in the Nordic Seas became more stratified and the deep convection rate did not recover. Ca. 2 ka a variability analogous to the modern North Atlantic Oscillation changed its mode from variable, intermittently negative to generally positive, inducing stronger westerlies over the region (Olsen et al., 2012). This enhanced the AW inflow into the Nordic Seas and, despite the ongoing, orbitally forced cooling of the surface waters (e.g., Calvo et al., 2002; Marchal et al., 2002), it led to a subsurface warming. Although the warming can be observed in records from across the entire region (Andersen et al., 2004b; Giraudeau et al., 2010; Hald et al., 2007; Risebrobakken et al., 2011; Werner et al., 2013), apparently most of the advected AW was routed northwestwards towards the central Greenland Sea. As a result, the late Holocene subsurface temperatures in this area were at a level comparable with the early-middle Holocene thermal maximum.

The results show that the paleoceanographical evolution of the Nordic Seas was much more complex than previously thought and that even the highest resolution records from their eastern part are not representative for the entire region. While the insolation was the primary factor controlling the environmental evolution on the supraregional and millennial scale, the more local and shorter-scale variability was mostly controlled by the

routing and intensity of AW inflow into the area. Other factors – such as sea-ice processes, deep convection, freshwater discharges, etc. – also played an important role.

## References

Álvarez-Solas, J., Montoya, M., Ritz, C., Ramstein, G., Charbit, S., Dumas, C., Nisancioglu, K., Dokken, T.M., Ganopolski, A., 2011. Heinrich event 1: an example of dynamical ice-sheet reaction to oceanic changes. Clim. Past 7, 1297–1306.

Andersen, C., Koç, N., Jennings, A.E., Andrews, J.T., 2004a. Nonuniform response of the major surface currents in the Nordic Seas to insolation forcing: Implications for the Holocene climate variability. Paleoceanography 19, PA2003.

Andersen, C., Koç, N., Moros, M., 2004b. A highly unstable Holocene climate in the subpolar North Atlantic : evidence from diatoms. Quat. Sci. Rev. 23, 2155–2166.

Barber, D.C., Dyke, A., Hillaire-Marcel, C., Jennings, A.E., Andrews, J.T., Kerwin, M.W., Bilodeau, G., McNeely, R., Southon, J., Morehead, M.D., Gagnon, J.-M., 1999. Forcing of the cold event of 8,200 years ago by catastrophic drainage of Laurentide lakes. Nature 400, 344–348.

Bauch, H.A., Erlenkeuser, H., Spielhagen, R.F., Struck, U., Matthiessen, J., Thiede, J., Heinemeier, J., 2001a. A multiproxy reconstruction of the evolution of deep and surface waters in the subarctic Nordic seas over the last 30,000 yr. Quat. Sci. Rev. 20, 659–678.

Bauch, H.A., Mueller-Lupp, T., Taldenkova, E., Spielhagen, R.F., Kassens, H., Grootes, P.M., Thiede, J., Heinemeier, J., Petryashov, V. V., 2001b. Chronology of the Holocene transgression at the North Siberian margin. Glob. Planet. Change 31, 125–139.

Bauch, H.A., Weinelt, M.S., 1997. Surface water changes in the Norwegian Sea during last deglacial and Holocene times. Quat. Sci. Rev. 16, 1115–1124.

Bianchi, G.G., McCave, I.N., 1999. Holocene periodicity in North Atlantic climate and deep-ocean flow south of Iceland. Nature 397, 515–517.

Bischof, J.F., 1994. The decay of the Barents ice sheet as documented in nordic seas ice-rafted debris. Mar. Geol. 117, 35–55.

Blaschek, M., Renssen, H., 2013. The Holocene thermal maximum in the Nordic Seas: the impact of Greenland Ice Sheet melt and other forcings in a coupled atmosphere–sea-ice–ocean model. Clim. Past 9, 1629–1643.

Bond, G.C., Kromer, B., Beer, J., Muscheler, R., Evans, M.N., Showers, W., Hoffmann, S., Lotti-Bond, R., Hajdas, I., Bonani, G., 2001. Persistent solar influence on North Atlantic climate during the Holocene. Science 294, 2130–2136.

Bond, G.C., Showers, W., Cheseby, M., Lotti, R., Almasi, P., DeMenocal, P., Priore, P., Cullen, H., Hajdas, I., Bonani, G., 1997. A Pervasive Millennial-Scale Cycle in North Atlantic Holocene and Glacial Climates. Science 278, 1257–1266.

Born, A., Levermann, A., 2010. The 8.2 ka event: Abrupt transition of the subpolar gyre toward a modern North Atlantic circulation. Geochemistry, Geophys. Geosystems 11, Q06011.

Broecker, W.S., 1994. Massive iceberg discharges as triggers for global climate change. Nature 372, 421–424.

Broecker, W.S., Denton, G.H., Edwards, R.L., Cheng, H., Alley, R.B., Putnam, A.E., 2010. Putting the Younger Dryas cold event into context. Quat. Sci. Rev. 29, 1078–1081.

Broecker, W.S., Kennett, J.P., Flower, B.P., Teller, J.T., Trumbore, S., Bonani, G., Wolfli, W., 1989. Routing of meltwater from the Laurentide Ice Sheet during the Younger Dryas cold episode. Nature 341, 318–321.

Cabedo-Sanz, P., Belt, S.T., Knies, J., Husum, K., 2013. Identification of contrasting seasonal sea ice conditions during the Younger Dryas. Quat. Sci. Rev. 79, 74–86.

Calvo, E., Grimalt, J., Jansen, E., 2002. High resolution $U_{37}^{K}$ sea surface temperature reconstruction in the Norwegian Sea during the Holocene 21, 1385–1394.

Clark, P.U., McCabe, A.M., Mix, A.C., Weaver, A.J., 2004. Rapid rise of sea level 19,000 years ago and its global implications. Science 304, 1141–1144.

Condron, A., Winsor, P., 2012. Meltwater routing and the Younger Dryas. Proc. Natl. Acad. Sci. U. S. A. 109, 19928–19933.

Crowley, T.J., Lowery, T.S., 2000. How Warm Was the Medieval Warm Period? AMBIO A J. Hum. Environ. 29, 51–54.

Dauteuil, O., Brun, J.-P., 1993. Oblique rifting in a slow-spreading ridge. Nature 361, 145–148.

Dauteuil, O., Brun, J.-P., 1996. Deformation partitioning in a slow spreading ridge undergoing oblique extension: Mohns Ridge, Norwegian Sea. Tectonics 15, 870–884.

Dyke, A.S., England, J., Reimnitz, E., Jetté, H., 1997. Changes in driftwood delivery to the Canadian Arctic Archipelago: The hypothesis of postglacial oscillations of the Transpolar Drift. Arctic 50, 1–16.

Eddy, J.A., 1976. The Maunder Minimum. Science 192, 1189–1202.

Fahl, K., Stein, R., 2012. Modern seasonal variability and deglacial/Holocene change of central Arctic Ocean sea-ice cover: New insights from biomarker proxy records. Earth Planet. Sci. Lett. 351-352, 123–133.

Fisher, T.G., Lowell, T. V., 2012. Testing northwest drainage from Lake Agassiz using extant ice margin and strandline data. Quat. Int. 260, 106–114.

Fronval, T., Jansen, E., 1997. Eemian and early Weichselian (140-60 ka) paleoceanography and paleoclimate in the Nordic seas with comparisons to Holocene conditions. Paleoceanography 12, 443–462.

Funder, S., Hansen, L., 1996. The Greenland ice sheet - a model for its culmination and decay during and after the last glacial maximum. Bull. Geol. Soc. Denmark 42, 137–152.

Giraudeau, J., Grelaud, M., Solignac, S., Andrews, J.T., Moros, M., Jansen, E., 2010. Millennial-scale variability in Atlantic water advection to the Nordic Seas derived from Holocene coccolith concentration records. Quat. Sci. Rev. 29, 1276–1287.

Grootes, P.M., Stuiver, M., White, J.W.C., Johnsen, S.J., Jouzel, J., 1993. Comparison of oxygen isotope records from the GISP2 and GRIP Greenland ice cores. Nature 366, 552–554.

Hald, M., Andersson, C., Ebbesen, H., Jansen, E., Klitgaard-kristensen, D., Risebrobakken, B., Salomonsen, G.R., Sarnthein, M., Petter, H., Telford, R.J., 2007. Variations in temperature and extent of Atlantic Water in the northern North Atlantic during the Holocene. Quat. Sci. Rev. 26, 3423–3440.

Hall, I.R., Bianchi, G.G., Evans, J.R., 2004. Centennial to millennial scale Holocene climate-deep water linkage in the North Atlantic. Quat. Sci. Rev. 23, 1529–1536.

Hall, I.R., Moran, S.B., Zahn, R., Knutz, P.C., Shen, C.-C., Edwards, R.L., 2006. Accelerated drawdown of meridional overturning in the late-glacial Atlantic triggered by transient pre-H event freshwater perturbation. Geophys. Res. Lett. 33, L16616.

Hansen, B., Østerhus, S., 2000. North Atlantic–Nordic Seas exchanges. Prog. Oceanogr. 45, 109–208.

Hass, H.C., 2002. A method to reduce the influence of ice-rafted debris on a grain size record from northern Fram Strait, Arctic Ocean. Polar Res. 21, 299–306.

Hemming, S.R., 2004. Heinrich events: Massive late Pleistocene detritus layers of the North Atlantic and their global climate imprint. Rev. Geophys. 42, 1–43.

Hubbard, A., Sugden, D., Dugmore, A., Norddahl, H., Pétursson, H.G., 2006. A modelling insight into the Icelandic Last Glacial Maximum ice sheet. Quat. Sci. Rev. 25, 2283–2296.

Jakobsson, M., Backman, J., Rudels, B., Nycander, J., Frank, M., Mayer, L., Jokat, W., Sangiorgi, F., O'Regan, M., Brinkhuis, H., King, J., Moran, K., 2007. The early Miocene onset of a ventilated circulation regime in the Arctic Ocean. Nature 447, 986–990.

Kaufman, D.S., Schneider, D.P., McKay, N.P., Ammann, C.M., Bradley, R.S., Briffa, K.R., Miller, G.H., Otto-Bliesner, B.L., Overpeck, J.T., Vinther, B.M., 2009. Recent warming reverses long-term arctic cooling. Science 325, 1236–9.

Kobashi, T., Severinghaus, J.P., Brook, E.J., Barnola, J.-M., Grachev, A.M., 2007. Precise timing and characterization of abrupt climate change 8200 years ago from air trapped in polar ice. Quat. Sci. Rev. 26, 1212–1222.

Lambeck, K., Chappell, J., 2001. Sea level change through the last glacial cycle. Science 292, 679–686.

Lehman, S.J., Jones, G.A., Keigwin, L.D., Andersen, E.S., Butenko, G., Østmo, S.R., 1991. Initiation of Fennoscandian ice-sheet retreat during the last deglaciation. Nature 349, 513–516.

Lekens, W.A.H., Sejrup, H.P., Haflidason, H., Petersen, G., Hjelstuen, B., Knorr, G., 2005. Laminated sediments preceding Heinrich event 1 in the Northern North Sea and Southern Norwegian Sea: Origin, processes and regional linkage. Mar. Geol. 216, 27–50.

Ljungqvist, F.C., 2010. A New Reconstruction of Temperature Variability in the Extra-Tropical Northern Hemisphere During the Last Two Millennia. Geogr. Ann. Ser. A, Phys. Geogr. 92, 339–351.

Marchal, O., Cacho, I., Stocker, T.F., Grimalt, J.O., Calvo, E., Martrat, B., Shackleton, N., Vautravers, M., Cortijo, E., van Kreveld, S., Andersson, C., Koç, N., Chapman, M.R., Sbaffi, L., Duplessy, J.-C., Sarnthein, M., Turon, J.-L., Duprat, J., Jansen, E., 2002. Apparent long-term cooling of the sea surface in the northeast Atlantic and Mediterranean during the Holocene. Quat. Sci. Rev. 21, 455–483.

Marshall, J., Schott, F., 1999. Open-ocean convection: Observations, theory, and models. Rev. Geophys. 37, 1–64.

Mayewski, P.A., Rohling, E.E., Stager, J.C., Karle, W., Maasch, K.A., Meeker, L.D., Meyerson, E.A., Gasse, F., van Kreveld, S., Holmgren, K., Lee-thorp, J., Rosqvist, G., Rack, F., Staubwasser, M., Schneider, R.R., Steig, E.J., 2004. Holocene climate variability. Quat. Res. 62, 243–255.

McManus, J.F., Francois, R., Gherardi, J.-M., Keigwin, L.D., Brown-Leger, S., 2004. Collapse and rapid resumption of Atlantic meridional circulation linked to deglacial climate changes. Nature 428, 834–837.

Mjelde, R., Digranes, P., Schaack, M. Van, Shimamura, H., Shiobara, H., Kodaira, S., Naess, O., Sørenes, N., Vågnes, E., 2001. Crustal structure of the outer Vøring

Plateau, offshore Norway, from ocean bottom seismic and gravity data. J. Geophys. Res. 106, 6769–6791.

Moberg, A., Sonechkin, D.M., Holmgren, K., Datsenko, N.M., Karlén, W., 2005. Highly variable Northern Hemisphere temperatures reconstructed from low- and high-resolution proxy data. Nature 433, 613–617.

Müller, J., Massé, G., Stein, R., Belt, S.T., 2009. Variability of sea-ice conditions in the Fram Strait over the past 30,000 years. Nat. Geosci. 2, 772–776.

Müller, J., Werner, K., Stein, R., Fahl, K., Moros, M., Jansen, E., 2012. Holocene cooling culminates in sea ice oscillations in Fram Strait. Quat. Sci. Rev. 47, 1–14.

Murton, J.B., Bateman, M.D., Dallimore, S.R., Teller, J.T., Yang, Z., 2010. Identification of Younger Dryas outburst flood path from Lake Agassiz to the Arctic Ocean. Nature 464, 740–743.

Nørgaard-Pedersen, N., Spielhagen, R.F., Erlenkeuser, H., Grootes, P.M., Heinemeier, J., Knies, J., 2003. Arctic Ocean during the Last Glacial Maximum: Atlantic and polar domains of surface water mass distribution and ice cover. Paleoceanography 18, 1–19.

Not, C., Hillaire-Marcel, C., 2012. Enhanced sea-ice export from the Arctic during the Younger Dryas. Nat. Commun. 3.

Olesen, O., Ebbing, J., Lundin, E., Mauring, E., Skilbrei, J.R., Torsvik, T.H., Hansen, E.K., Henningsen, T., Midbøe, P., Sand, M., 2007. An improved tectonic model for the Eocene opening of the Norwegian–Greenland Sea: Use of modern magnetic data. Mar. Pet. Geol. 24, 53–66.

Olsen, J., Anderson, N.J., Knudsen, M.F., 2012. Variability of the North Atlantic Oscillation over the past 5,200 years. Nat. Geosci. 5, 808–812.

Pflaumann, U., Sarnthein, M., Chapman, M.R., D'Abreu, L., Funnel, B., Huels, M., Kiefer, T., Maslin, M.A., Schulz, H., Swallow, J., van Kreveld, S., Vautravers, M., Vogelsang, E., Weinelt, M.S., 2003. Glacial North Atlantic: Sea-surface conditions reconstructed by GLAMAP 2000. Paleoceanography 18, 1065.

Prange, M., Lohmann, G., 2003. Effects of mid-Holocene river runoff on the Arctic ocean/sea-ice system: a numerical model study. The Holocene 13, 335–342.

Rashid, H., Piper, D.J.W., Flower, B.P., 2011. The role of Hudson Strait outlet in Younger Dryas sedimentation in the Labrador Sea. Abrupt Clim. Chang. Patterns, Impacts. Geophys. Monogr. Ser. 193, 93–110.

Rasmussen, S.O., Andersen, K.K., Svensson, A.M., Steffensen, J.P., Vinther, B.M., Clausen, H.B., Siggaard-Andersen, M.-L., Johnsen, S.J., Larsen, L.B., Dahl-Jensen, D., Bigler, M., Röthlisberger, R., Fischer, H., Goto-Azuma, K., Hansson, M.E., Ruth, U., 2006. A new Greenland ice core chronology for the last glacial termination. J. Geophys. Res. 111, D06102.

Rasmussen, T.L., Thomsen, E., 2004. The role of the North Atlantic Drift in the millennial timescale glacial climate fluctuations. Palaeogeogr. Palaeoclimatol. Palaeoecol. 210, 101–116.

Rasmussen, T.L., Thomsen, E., 2008. Warm Atlantic surface water inflow to the Nordic seas 34-10 calibrated ka B.P. Paleoceanography 23, PA1201.

Renssen, H., Goosse, H., Muscheler, R., 2006. Coupled climate model simulation of Holocene cooling events: oceanic feedback amplifies solar forcing. Clim. Past 2, 79–90.

Risebrobakken, B., Dokken, T.M., Smedsrud, L.H., Andersson, C., Jansen, E., Moros, M., Ivanova, E. V., 2011. Early Holocene temperature variability in the Nordic Seas: The role of oceanic heat advection versus changes in orbital forcing. Paleoceanography 26, PA4206.

Risebrobakken, B., Jansen, E., Andersson, C., Mjelde, E., Hevrøy, K., 2003. A high-resolution study of Holocene paleoclimatic and paleoceanographic changes in the Nordic Seas. Paleoceanography 18, 1017.

Rohling, E.J., Pälike, H., 2005. Centennial-scale climate cooling with a sudden cold event around 8,200 years ago. Nature 434, 975–979.

Rudels, B., Friedrich, H.J., Quadfasel, D., 1999. The Arctic Circumpolar Boundary Current. Deep Sea Res. Part II Top. Stud. Oceanogr. 46, 1023–1062.

Rudels, B., Quadfasel, D., 1991. Convection and deep water formation in the Arctic Ocean-Greenland Sea System. J. Mar. Syst. 2, 435–450.

Sarnthein, M., Gersonde, R., Niebler, S., Pflaumann, U., Spielhagen, R.F., Thiede, J., Wefer, G., Weinelt, M.S., 2003a. Overview of Glacial Atlantic Ocean Mapping (GLAMAP 2000). Paleoceanography 18, 1030.

Sarnthein, M., Jansen, E., Weinelt, M.S., Arnold, M., Duplessy, J.C., Erlenkeuser, H., Flatøy, A., Johannessen, G., Johannessen, T., Jung, S.J.A., Koç, N., Labeyrie, L.D., Maslin, M., Pflaumann, U., Schulz, H., 1995. Variations in Atlantic surface ocean paleoceanography, 50°-80°N: A time-slice record of the last 30,000 years. Paleoceanography 10, 1063–1094.

Sarnthein, M., van Kreveld, S., Erlenkeuser, H., Grootes, P.M., Kucera, M., Pflaumann, U., Schulz, M., 2003b. Centennial-to-millennial-scale periodicities of Holocene climate and sediment injections off the western Barents shelf, 75°N. Boreas 32, 447–461.

Seidenkrantz, M.-S., Ebbesen, H., Aagaard-Sørensen, S., Moros, M., Lloyd, J.M., Olsen, J., Knudsen, M.F., Kuijpers, A., 2012. Early Holocene large-scale meltwater discharge from Greenland documented by foraminifera and sediment parameters. Palaeogeogr. Palaeoclimatol. Palaeoecol. 391, 71–81.

Ślubowska-Woldengen, M., Rasmussen, T.L., Koç, N., Klitgaard-Kristensen, D., Nilsen, F., Solheim, A., 2007. Advection of Atlantic Water to the western and northern Svalbard shelf since 17,500 cal yr BP. Quat. Sci. Rev. 26, 463–478.

Stanford, J.D., Rohling, E.J., Bacon, S., Roberts, A.P., Grousset, F.E., Bolshaw, M., 2011. A new concept for the paleoceanographic evolution of Heinrich event 1 in the North Atlantic. Quat. Sci. Rev. 30, 1047–1066.

Svendsen, J.I., Alexanderson, H., Astakhov, V.I., Demidov, I., Dowdeswell, J.A., Funder, S., Gataullin, V., Henriksen, M., Hjort, C., Houmark-Nielsen, M., Hubberten, H.W., Ingólfsson, Ó., Jakobsson, M., Kjær, K.H., Larsen, E., Lokrantz, H., Lunkka, J.P., Lysså, A., Mangerud, J., Matiouchkov, A., Murray, A., Möller, P., Niessen, F., Nikolskaya, O., Polyak, L., Saarnisto, M., Siegert, C., Siegert, M.J., Spielhagen, R.F., Stein, R., 2004. Late Quaternary ice sheet history of northern Eurasia. Quat. Sci. Rev. 23, 1229–1271.

Swift, J., 1986. The Arctic waters, in: Hurdle, B. (Ed.), The Nordic Seas. New York, pp. 129–151.

Talwani, M., Eldholm, O., 1977. Evolution of the Norwegian-Greenland sea. Geol. Soc. Am. Bull. 88, 969–999.

Tarasov, L., Peltier, W.R., 2006. A calibrated deglacial drainage chronology for the North American continent: evidence of an Arctic trigger for the Younger Dryas. Quat. Sci. Rev. 25, 659–688.

Thiede, J., Myhre, A.M., Firth, J.V. and the S.S.P., 1995. Cenozoic northern hemisphere polar and subpolar ocean paleoenvironments (summary of ODP Leg 151 drilling results), in: Thiede, J., Myhre, A.M., Firth, J. V. (Eds.), Proceedings of the Ocean Drilling Program, Initial Reports. Ocean Drilling Program, College Station, Texas, pp. 397–420.

Thornalley, D.J.R., Elderfield, H., McCave, I.N., 2010. Intermediate and deep water paleoceanography of the northern North Atlantic over the past 21,000 years. Paleoceanography 25, 1–17.

Vogelsang, E., 1990. Paläo-Ozeanographie des Europäischen Nordmeeres an Hand stabiler Kohlenstoff- und Sauerstoffisotope – Paleo- ceanography of the Nordic seas on the basis of stable carbon and oxygen isotopes. Berichte aus dem Sonderforschungsbereich 313 23, 136.

Vonmoos, M., Beer, J., Muscheler, R., 2006. Large variations in Holocene solar activity: Constraints from 10 Be in the Greenland Ice Core Project ice core. J. Geophys. Res. 111, A10105.

Wanner, H., Beer, J., Bütikofer, J., Crowley, T.J., Cubasch, U., Flückiger, J., Goosse, H., Grosjean, M., Joos, F., Kaplan, J.O., Küttel, M., Müller, S.A., Prentice, I.C., Solomina, O., Stocker, T.F., Tarasov, P., Wagner, M., Widmann, M., 2008. Mid- to Late Holocene climate change: an overview. Quat. Sci. Rev. 27, 1791–1828.

Wanner, H., Solomina, O., Grosjean, M., Ritz, S.P., Jetel, M., 2011. Structure and origin of Holocene cold events. Quat. Sci. Rev. 30, 3109–3123.

Weaver, A.J., Saenko, O.A., Clark, P.U., Mitrovica, J.X., 2003. Meltwater pulse 1A from Antarctica as a trigger of the Bølling-Allerød warm interval. Science 299, 1709–1713.

Weinelt, M.S., 1993. Veränderungen der Oberflächenzirkulation im Europäischen Nordmeer während der letzten 60.000 Jahre. Berichte aus dem Sonderforschungsbereich 313 41, 105.

Werner, K., Spielhagen, R.F., Bauch, D., Hass, H.C., Kandiano, E.S., 2013. Atlantic Water advection versus sea-ice advances in the eastern Fram Strait during the last 9 ka: Multiproxy evidence for a two-phase Holocene. Paleoceanography 28, 283–295.

# 2. Material and methods

## 2.1. Sediment cores

For the study presented here four giant box cores and two kasten cores taken at five different sites (Table 2.1.) were used. All cores consisted of brown to olive grey deep-sea sediments (clay to silty sand).

Table 2.1. Cores used in the study.

| Core | Latitude | Longitude | Water depth (m) | Core type | Analyzed core length (cm) |
|---|---|---|---|---|---|
| PS1878-2 | 73°15.1 N | 9°00.9 W | 3038 | BC | 27 |
| PS1878-3 | 73°15.3 N | 9°00.7 W | 3048 | KC | 108 |
| PS1894-7 | 75°48.8 N | 8°15.5 W | 1992 | BC | 42 |
| PS1906-1 | 76°50.5 N | 2°09.0 W | 2990 | BC | 33 |
| PS1910-1 | 75°37.0 N | 1°19.0 E | 2448 | BC | 33 |
| M17730-4 | 72°06.7'N | 7°23.3'E | 2749 | KC | 118 |

BC – giant box core, KC – kasten core

The Greenland Sea cores (PS1878-2, PS1878-3, PS1894-7, PS1906-1 and PS1910-1) were retrieved during the ARK-VII/1 expedition of RV *Polarstern* to the Greenland Sea in 1990 (Thiede and Hempel, 1991). Cores PS1878-2 and -3 were taken at the southern, lower foot of Vesterisbanken seamount in the central Greenland Sea. The location on the lee side (relative to ocean currents) of this volcano, which rises from the abyssal plain to a water depth of only 133 m (Nowaczyk and Antonow, 1997), provided relatively high sedimentation rates, possibly because velocities of southward-directed ocean currents decrease behind the obstacle, allowing the settling of fine-grained material. The site is, however, apparently located far enough from the steep seamount slope to be protected from downslope mass flows. The cores were spliced to one composite record (PS1878) using AMS $^{14}$C dating and other proxies. The tie point was

located at 12.5 cm depth in core PS1878-2 and 11.5 cm in core PS1878-3. Thus the depth scale of core PS1878-3 had to be shifted by 1 cm. All the depths referring to the compiled record PS1878 are given on the composite depth scale. An 11-cm-thick dark tephra layer was found at 47–58 cm core depth. Cores PS1894-7, PS1906-1 and PS1910-1 come from the northern Greenland Sea and were retrieved on the Greenland continental slope, on the northern and on the southern part of the Greenland Fracture Zone crest, respectively.

Core M17730-4 was taken during the M13/2 expedition of RV *Meteor* in 1990. It was retrieved from the northern part of the Lofoten Basin, west of the Bear Island Trough Mouth Fan and southeast of the Mohns Ridge. It has previously been studied by Weinelt (1993) and Bauch and Weinelt (1997) but with a lower temporal resolution. As the original depth scale of the core (Weinelt, 1993) did not fit with our measurements (likely due to some drying up and some shrinking of the material during storage) we had to correlate the two depth scales using characteristic lithological horizons in the actual core material and in the original core photographs to be able to apply the $^{14}C$ dates of Weinelt (1993) to our record. Thus, a new depth scaling was established (Table 2.2.) and all the depths given here refer to it unless otherwise indicated.

Table 2.2. Tie points between the original depth scale of core M17730-4 (Weinelt, 1993) and the depth scale used in this study.

| Depth (Weinelt, 1993) (cm) | Depth (this study) (cm) |
|---:|---:|
| 21,0 | 21,5 |
| 32,0 | 32,5 |
| 64,6 | 63,5 |
| 88,5 | 85,5 |
| 110,0 | 104,5 |
| 131,0 | 123,5 |

## 2.2. Sample preparation

The cores were sampled continuously every 1 cm. Additionally, surface sediments of cores PS1894, PS1906 and PS1910 were analyzed. Further preparation included freeze-drying, wet-sieving with deionized water through a 63µm mesh, and dry-sieving into size fractions using 100, 125, 250, 500 and 1000 µm sieves. Each size fraction was weighed.

## 2.3. Chronology

Age control of the records is based on AMS $^{14}C$ dates performed on monospecific samples of *Neogloboquadrina pachyderma* (sin.) (Table 2.3.). All radiocarbon ages were corrected for a reservoir age of 400 years, calibrated using Calib Rev 6.1.0 software (Stuiver and Reimer, 1993) and the Marine09 calibration curve (Reimer et al., 2009), and are given in thousand calendar years before AD 1950 (ka).

Assuming that the tephra layer found at 47–58 cm in core PS1878 (volcanic glass shards making up >75% of a sample) reflects a short-term volcanic event (duration less than ca. 5 yr), we set its sedimentation time to zero. Linear interpolation assigned the tephra layer an age of 11.9 ka. The interval between 73.5 and 96.5 cm shows a sedimentation rate that is anomalously high for this record (see Chapters 3-5). To estimate the age of the lowermost section of the core by extrapolation we used the same sedimentation rate as for the 59.5 to 73.5 cm interval. This gave an age of 24.4 ka for the end of the analyzed interval and an average sedimentation rate of ca. 4.7 cm $kyr^{-1}$ (including the tephra layer) or ca. 4.2 cm $kyr^{-1}$ (without the tephra).

Table 2.3. AMS $^{14}C$ measurements and their calibrated ages for the cores used in the study.

| Lab. no. | Depth, cm | $^{14}C$ Age ± Standard deviation | Calibrated Age BP |
|---|---|---|---|
| | | Core PS1878-2 | |
| Poz-45376 | 0.5 | 775 ± 35 | 426 |
| Poz-45377 | 12.5 | 3300 ± 40 | 3143 |
| | | Core PS1878-3 | |
| Poz-45378 | 11.5 | 3295 ± 35 | 3139 |
| Poz-45380 | 19.5 | 4525 ± 35 | 4746 |
| Poz-54381 | 25.5 | 5580 ± 50 | 5961 |
| Poz-54382 | 30.5 | 6760 ± 50 | 7295 |
| Poz-45384 | 39.5 | 8410 ± 60 | 9028 |
| Poz-45385 | 58.5 | 11100 ± 60 | 12613 |
| Beta-367894 | 72.5 | 14050 ± 60 | 16800 |
| KIA 47284 | 95.5 | 16620 ± 110 | 19266 |
| | | Core PS1894-7 | |
| KIA 7088 | 0.5 | 3845 ± 40 | 3794 |
| KIA 47258 | 5.5 | 5390 ± 35 | 5773 |
| KIA 7089 | 9.5 | 5745 ± 40 | 6174 |
| KIA 47259 | 16.5 | 8075 ± 45 | 8528 |
| KIA 7090 | 21.5 | 8910 ± 55 | 9564 |
| KIA 7091 | 35.5 | 14430 ± 70 | 17051 |
| | | Core PS1906-1 | |
| KIA 7084 | 4.5 | 4360 ± 30 | 4482 |
| KIA 7083 | 11.5 | 7965 ± 40 | 8420 |
| KIA 7082 | 22.5 | 17040 ± 80 | 19731 |
| KIA 7081 | 32.5 | 19130 ± 90 | 22334 |
| | | Core PS1910-1 | |
| KIA 44390 | 0.5 | 2655 ± 30 | 2336 |
| Poz-45386 | 4.5 | 4820 ± 35 | 5122 |
| Poz-45387 | 11.5 | 6950 ± 50 | 7457 |
| KIA 44393 | 17.5 | 11340 ± 50 | 12794 |
| Poz-45388 | 30.5 | 16880 ± 100 | 19625 |
| | | Core M17730-4 | |
| Beta-367895 | 12.5 | 2240 ± 30 | 1850 |
| (Weinelt, 1993) | 20.5 | 3330 ± 100 | 3200 |
| (Weinelt, 1993) | 40.1 | 5610 ± 70 | 5990 |
| (Weinelt, 1993) | 49.7 | 6800 ± 110 | 7320 |
| (Weinelt, 1993) | 68.5 | 8470 ± 90 | 9080 |
| Beta-367896 | 78.5 | 8980 ± 40 | 9620 |
| (Weinelt, 1993) | 95.6 | 9520 ± 590 | 10400 |
| Beta-367897 | 101.5 | 10490 ± 50 | 11690 |
| (Weinelt, 1993) | 106.3 | 11590 ± 100 | 13110 |
| (Weinelt, 1993) | 116.3 | 13030 ± 120 | 15000 |
| Beta-367898 | 125.5 | 15590 ± 60 | 18540 |

The three box cores from the northern Greenland Sea (PS1894-7, PS1906-1 and PS1910-1) have average sedimentation rates of 1.5–2.0 cm $kyr^{-1}$. These low rates, together with bioturbation and uncertain reservoir ages, make age models for these records unreliable if based only on $^{14}C$ datings. This is best illustrated by relatively old ages yielded from the surface samples of these cores (2.3–3.8 ka). However, as the surface sample of core PS1878 yielded a younger age (0.426 ka) and contained living (rose bengal stained) benthic foraminifera, we assume that sedimentation in the entire study area did not terminate in the late Holocene. To account for the apparent inaccuracy of the $^{14}C$-based age models we attempted to improve them by correlating the stable isotope data (and, in a few cases, also other proxies) and using linear interpolation between correlated points and reliable $^{14}C$-dated samples. In addition to our own data, we also used three nearby records of comparable sedimentation rates, time range and water depths. These include cores PS2887 (Nørgaard-Pedersen et al., 2003) as well as PS1230 from the western Fram Strait and PS1243 from the SW Norwegian Sea (Bauch et al., 2001). As the base for the correlation we used core PS1878, which has a relatively high temporal resolution and a reliable chronological framework based on $^{14}C$ datings in the younger part of the record. Due to poorer $^{14}C$ age control and more speculative reservoir ages in the older part of the records, the improved age models for the northern Greenland Sea records are restricted to the last 15 kyr.

The average sedimentation rate of core M17730-4 amounts to ca. 6.6 cm $kyr^{-1}$ and the record represents the time period between 19.6 and 1.9 ka. The dating at 95.6 cm (Weinelt, 1993; original depth 100 cm) gave an anomalously large error (±590 $^{14}C$ years BP). The obtained calibrated age (10.4 ka) fits relatively well into our age model and thus we did not leave out this dating. However, it should be kept in mind that the possible age at this level varies from 9.6 to 11.1 ka (1σ range).

## 2.4. Planktic foraminifera counts

Counts of planktic foraminiferal assemblages were conducted on representative splits (>300 specimens). In the Arctic environment subpolar foraminiferal species (e.g., *Turborotalita quinqueloba*) reach smaller test sizes compared to warmer conditions (Bauch, 1994; Kandiano and Bauch, 2002). To obtain representative results, in records from the Arctic domain (all cores from the Greenland Sea) we used the 100–250 μm size fraction, while in core M17730-4, located in the Atlantic domain, the >150 μm size fraction was analyzed. Individual species were identified and counted. Samples containing less than 100 specimens were excluded from the statistical analysis. The number of planktic foraminifera per 1 g dry sediment was calculated to serve as a semiquantitative proxy for bioproductivity.

## 2.5. Subsurface temperature reconstruction

Absolute summer subsurface temperatures (SSTs) at 100 m water depth were calculated at site PS1878 between 15 and 0 ka using transfer functions based on a modern training set from the Arctic (Husum and Hald, 2012) and the C2 software, version 1.7.2 (Juggins, 2011). A weighted average partial least-squares statistical model with three components (WA-PLS C3) and leave-one-out ("jack knifing") cross validation was used. The root mean-squared error of prediction is 0.52°C. Unlike Husum and Hald (2012), who used the >100μm size fraction, we ran the transfer function using the 100–250 μm size fraction. Although the coarser sediments contained relatively few foraminifera, we acknowledge that this might have slightly biased the results. Further, reconstructed SSTs below 2°C are considered to be uncertain as the modern training set contains very few data points below 2°C (Husum and Hald, 2012).

To retrieve SSTs from foraminiferal census data in core M17730-4 the SIMMAX technique, a variation of the modern analogue technique (MAT) approach, was applied. The relation between foraminiferal diversities and SSTs was established by using the North Atlantic part of the surface sediment samples foraminiferal database (Pflaumann et al., 2003) linked to oceanographic atlas SST data of 100 m water depth layer (Levitus and Boyer, 1994). The used winter and summer temperatures represent average values for February to April and August to October, respectively.

## 2.6. Ice-rafted debris and volcanic glass shards

Mineral grains >250 μm (in Greenland Sea cores) or >150 μm (M17730-4) were identified and counted to provide information on ice-rafting and tephra layers. As ice-rafted debris (IRD) we interpret all lithic grains >250/150 μm, except for unweathered volcanic glass. Such coarse particles are transported into an ice-covered deep ocean basin preferentially by icebergs while sea ice mainly transports finer material (Nürnberg et al., 1994). To provide clues on the origin of IRD, in cores PS1878 and M17730-4 several types were identified, the most common of them being crystalline and clastic rock fragments. Organic-rich clastic IRD grains are common in glacial sediments from the eastern Nordic Seas (e.g., Bischof, 1994; Bischof et al., 1997) and are interpreted as originating from the wide and shallow western Eurasian shelves (Wagner and Henrich, 1994). The unweathered volcanic glass shards were used to identify tephra layers. The geochemistry of the tephra layer found in core PS1878 was analyzed by Ewa M. Lind (University of Stockholm).

## 2.7. Stable oxygen and carbon isotopes

For the analysis of stable oxygen and carbon isotopes, specimens of the planktic foraminiferal species *N. pachyderma* (sin.) (all cores) and two benthic species – the epibenthic *Cibicidoides wuellerstorfi* and the shallow infaunal *Oridorsalis umbonatus* (cores PS1878, PS1894, PS1910 and M17730-4) – were used. Because of departures from isotopic calcite equilibrium, the measured $\delta^{18}O$ values of the two latter species were corrected by +0.64 and +0.36‰, respectively (cf. Duplessy et al., 1988). Approximately twenty-five specimens were picked from the 125–250µm (*N. pachyderma* (sin.) and *O. umbonatus*) and 250–500µm (*C. wuellerstorfi*) size fractions. All stable isotope analyses were carried out in the isotope laboratories of the GEOMAR Helmholtz Centre for Ocean Research Kiel and the Leibniz Laboratory, University of Kiel, on Finnigan MAT 251 and Thermo MAT 253 mass spectrometer systems and a Kiel IV Carbonate Preparation Device. Results are expressed in the δ notation referring to the PDB (Pee Dee Belemnite) standard and are given as $\delta^{18}O$ and $\delta^{13}C$ with an analytical accuracy of <0.06 and <0.03‰, respectively.

## References

Bauch, H.A., 1994. Significance of variability in *Turborotalita quinqueloba* (Natland) test size and abundance for paleoceanographic interpretations in the Norwegian-Greenland Sea. Mar. Geol. 121, 129–141.

Bauch, H.A., Erlenkeuser, H., Spielhagen, R.F., Struck, U., Matthiessen, J., Thiede, J., Heinemeier, J., 2001. A multiproxy reconstruction of the evolution of deep and surface waters in the subarctic Nordic seas over the last 30,000 yr. Quat. Sci. Rev. 20, 659–678.

Bauch, H.A., Weinelt, M.S., 1997. Surface water changes in the Norwegian Sea during last deglacial and Holocene times. Quat. Sci. Rev. 16, 1115–1124.

Bischof, J.F., 1994. The decay of the Barents ice sheet as documented in nordic seas ice-rafted debris. Mar. Geol. 117, 35–55.

Bischof, J.F., Lund, J.J., Ecke, H.-H., 1997. Palynomorphs of ice rafted clastic sedimentary rocks in Late Quaternary glacial marine sediments of the Norwegian Sea as provenance indicators. Palaeogeogr. Palaeoclimatol. Palaeoecol. 129, 329–360.

Duplessy, J.C., Labeyrie, L.D., Blanc, P.L., 1988. Norwegian Sea Deep Water Variations over the Last Climatic Cycle: Paleo-Oceanographical Implications, in: Wanner, H., Siegenthaler, U. (Eds.), Long and Short Term Variability of Climate. Springer, New York, pp. 83–116.

Husum, K., Hald, M., 2012. Arctic planktic foraminiferal assemblages: Implications for subsurface temperature reconstructions. Mar. Micropaleontol. 96-97, 38–47.

Juggins, S., 2011. C2, Software for Ecological and Palaeoecological Data Analysis and Visualization.

Kandiano, E.S., Bauch, H.A., 2002. Implications of planktic foraminiferal size fractions for the glacial-interglacial paleoceanography of the polar North Atlantic. J. Foraminifer. Res. 32, 245–251.

Levitus, S., Boyer, T.P., 1994. World Ocean Atlas 1994, vol. 4, Temperature, NOAA Atlas, U.S. Department of Commerce, Washington, D.C.

Nørgaard-Pedersen, N., Spielhagen, R.F., Erlenkeuser, H., Grootes, P.M., Heinemeier, J., Knies, J., 2003. Arctic Ocean during the Last Glacial Maximum: Atlantic and polar domains of surface water mass distribution and ice cover. Paleoceanography 18, 1–19.

Nowaczyk, N.R., Antonow, M., 1997. High-resolution magnetostratigraphy of four sediment cores from the Greenland Sea-I. Identification of the Mono Lake excursion, Laschamp and Biwa I/Jamaica geomagnetic polarity events. Geophys. J. Int. 131, 310–324.

Nürnberg, D., Wollenburg, I., Dethleff, D., Eicken, H., Kassens, H., Letzig, T., Reimnitz, E., Thiede, J., 1994. Sediments in Arctic sea ice: Implications for entrainment, transport and release. Mar. Geol. 119, 185–214.

Pflaumann, U., Sarnthein, M., Chapman, M.R., D'Abreu, L., Funnel, B., Huels, M., Kiefer, T., Maslin, M.A., Schulz, H., Swallow, J., van Kreveld, S., Vautravers, M., Vogelsang, E., Weinelt, M.S., 2003. Glacial North Atlantic: Sea-surface conditions reconstructed by GLAMAP 2000. Paleoceanography 18, 1065.

Reimer, P.J., Baillie, M.G.L., Bard, E., Bayliss, A., 2009. IntCal09 and Marine09 radiocarbon age calibration curves, 0–50,000 years cal BP. Radiocarbon 51, 1111–1150.

Stuiver, M., Reimer, P.J., 1993. Radiocarbon calibration program. Radiocarbon 35, 215–230.

Thiede, J., Hempel, G., 1991. Die Expedition ARKTIS-VII/1 mit FS “Polarstern” 1990. Berichte zur Polarforsch. 80, 137pp.

Wagner, T., Henrich, R., 1994. Organo-and lithofacies of glacial-interglacial deposits in the Norwegian-Greenland Sea: Responses to paleoceanographic and paleoclimatic changes. Mar. Geol. 120, 335–364.

Weinelt, M.S., 1993. Veränderungen der Oberflächenzirkulation im Europäischen Nordmeer während der letzten 60.000 Jahre. Berichte aus dem Sonderforschungsbereich 313 41, 105.

# 3. A high-resolution Lateglacial and Holocene palaeoceanographic record from the Greenland Sea

From [Telesiński, M.M., Spielhagen, R.F., Lind, E.M., 2014. A high-resolution Lateglacial and Holocene palaeoceanographic record from the Greenland Sea. Boreas 43, 273–285.]. Reprinted with permission from John Wiley & Sons, Inc.

Data available online at http://doi.pangaea.de/10.1594/PANGAEA.832384

BOREAS An international journal of Quaternary research

# A high-resolution Lateglacial and Holocene palaeoceanographic record from the Greenland Sea

MACIEJ M. TELESIŃSKI, ROBERT F. SPIELHAGEN AND EWA M. LIND

BOREAS

Telesiński, M. M., Spielhagen, R. F. & Lind, E. M. 2014 (April): A high-resolution Lateglacial and Holocene palaeoceanographic record from the Greenland Sea. *Boreas*, Vol. 43, pp. 273–285. 10.1111/bor.12045. ISSN 0300-9483.

We present an unprecedented multicentennial sediment record from the foot of Vesterisbanken Seamount, central Greenland Sea, covering the past 22.3 thousand years (ka). Based on planktic foraminiferal total abundances, species assemblages, and stable oxygen and carbon isotopes, the palaeoenvironments in this region of modern deepwater renewal were reconstructed. Results show that during the Last Glacial Maximum the area was affected by harsh polar conditions with only episodic improvements during warm summer seasons. Since 18 ka extreme freshwater discharges from nearby sources occurred, influencing the surface water environment. The last major freshwater event took place during the Younger Dryas. The onset of the Holocene was characterized by an improvement of environmental conditions suggesting warming and increasing ventilation of the upper water layers. The early Holocene saw a stronger Atlantic waters advection to the area, which began around 10.5 and ended quite rapidly at 5.5 ka, followed by the onset of Neoglacial cooling. Surface water ventilation reached a maximum in the middle Holocene. Around 3 ka the surface water stratification increased leading to subsequent amplification of the warming induced the North Atlantic Oscillation at 2 ka.

*Maciej M. Telesiński (mtelesinski@geomar.de), GEOMAR Helmholtz Centre for Ocean Research Kiel, Wischhofstrasse 1-3, 24148 Kiel, Germany; Robert F. Spielhagen, GEOMAR Helmholtz Centre for Ocean Research Kiel, Wischhofstrasse 1-3, 24148 Kiel, Germany and Academy of Sciences, Humanities, and Literature, 53151 Mainz, Germany; Ewa M. Lind, Department of Physical Geography and Quaternary Geology, Stockholm University, SE 106 91 Stockholm, Sweden;* *received 27th May 2013, accepted 1st September 2013.*

The Greenland Sea is an important region for the Atlantic Meridional Overturning Circulation (AMOC), and thus the global ocean circulation, as deep water convection takes place here (e.g. Marshall & Schott 1999), leading to the formation of North Atlantic Deep Water (NADW). It also plays an important role as the main gateway for the surface- and deep-water exchange between the Arctic and North Atlantic oceans (e.g. Hansen & Østerhus 2000). Despite its importance, little is known so far about the palaeoceanographic evolution in this area since the Last Glacial Maximum (LGM). In deep, cold, often ice-covered environments sedimentation rates are generally low (e.g. Nørgaard-Pedersen *et al.* 2003). Therefore high-resolution, undisturbed sediment records from the Greenland Sea are lacking, in contrast to the eastern Nordic Seas (e.g. Sarnthein *et al.* 2003; Hald *et al.* 2007; Risebrobakken *et al.* 2011; Werner *et al.* 2013). The only published record of submillennial-scale resolution from the central, deep Greenland Sea stems from core HM94-34 (Fronval & Jansen 1997; Fig. 1), which holds ~40 cm of Holocene sediments. However, the surface sample from this site was dated to ~3000 $^{14}$C years before present, which indicates strong sediment mixing by bioturbation.

Here we present a palaeoceanographic record of unprecedented high resolution from the southern foot of Vesterisbanken seamount in the central Greenland Sea, covering the past 22 300 years (22.3 ka). Records of planktic foraminifer associations and stable isotopes allow reconstruction of the Lateglacial and Holocene palaeoceanography of the central Greenland Sea on a multicentennial time scale.

## Study area

The oceanographic regime of the Nordic Seas is governed by two major surface-water masses (Fig. 1). Relatively warm, saline ($T$~6–11°C, $S$>35 psu) Atlantic Water (AW) is advected to the area by the North Atlantic Current (NAC) and eventually reaches the Arctic Ocean through the eastern Fram Strait and across the Barents Sea. Cold, low saline ($T$<0°C, $S$<34.4 psu) Polar Water (PW) flows southward as the East Greenland Current (EGC) along the Greenland shelf margin. Both NAC and EGC show a relatively small seasonal variability (Foldvik *et al.* 1988; Hansen & Østerhus 2000; Sutherland & Pickart 2008) but significant decadal variations (Hansen & Østerhus 2000; Eldevik *et al.* 2009). The central part of the Nordic Seas is the domain of Arctic Water, a result of PW and AW mixing (Swift 1986). It is an area of deep-water formation, as AW cools down when it mixes with PW and subsequently sinks to the bottom (Hansen & Østerhus 2000). Arctic Water is separated from PW by the Polar Front and from AW by the Arctic Front.

Today, the site PS1878 investigated in this study is located within the Arctic Water domain, which is most sensitive to changes in the relative influence of PW and AW. The temperature and salinity of the surface water

DOI 10.1111/bor.12045 

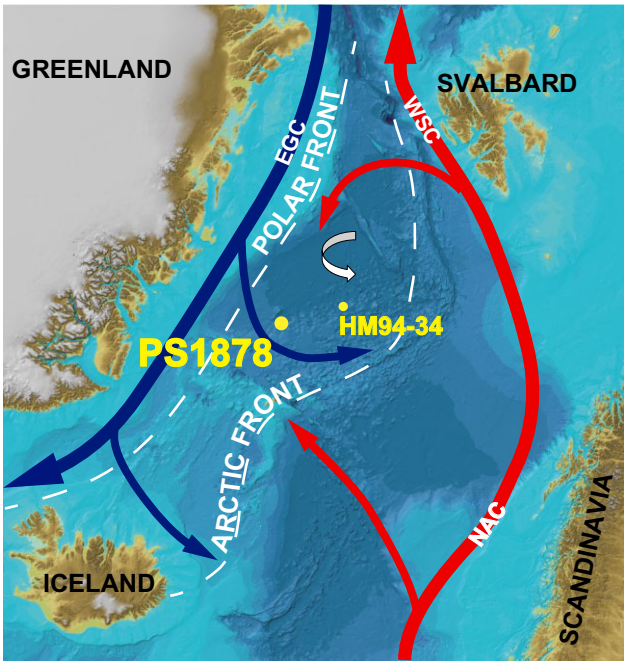


*Fig. 1.* Present day surface water circulation in the Nordic Seas. Cores PS1878 (this study) and HM94-34 (Fronval & Jansen 1997) are marked with yellow dots. Red arrows indicate Atlantic Water (AW), blue arrows – Polar Water (PW), white broken lines – oceanographic fronts. White arrow – present-day deep convection (Marshall & Schott 1999). EGC = East Greenland Current; NAC = North Atlantic Current; WSC = West Spitsbergen Current. Bathymetry from The International Bathymetric Chart of the Arctic Ocean (http://www.ibcao.org, 2012).

can change significantly within a short distance and is closely related to the lack or presence of sea ice. In the ice-covered areas the temperature amounts to ~0°C at the surface, increases to ~2°C at 50–100 m water depth and decreases to −1–0°C in the deeper parts. The salinity increases with depth from 32–34 at the surface to ~35 psu below 50–100 m. Further to the east, in the ice free areas, the temperature reaches 2–3°C and decreases to ~−1°C below 50 m, while the salinity increases from ~34 psu at the surface to ~35 psu below 50 m (Thiede & Hempel 1991).

The core was retrieved from the southern, lower foot of Vesterisbanken seamount in the central Greenland Sea. The location on the lee side of this volcano, which rises from the abyssal plain to a water depth of only 133 m (Nowaczyk & Antonow 1997), may provide relatively high sedimentation rates, possibly because velocities of southward-directed ocean current decrease behind the obstacle, allowing the settling of fine-grained material. The site is, however, apparently located far enough from the steep seamount slope to be protected from downslope mass flows.

## Material and methods

Sediment core PS1878 (73°15′N, 9°01′W, water depth 3048 m) was retrieved during the ARK-VII/1 expedition of *RV Polarstern* in 1990. It is compiled from giant box core PS1878-2 and a kasten core PS1878-3. The material consisted of brown to olive grey sediments of silty clay to silty sand. A 11-cm-thick dark tephra layer was found at 47–58 cm core depth. Sediment samples were taken continuously as 1-cm-thick slabs from the uppermost 114 cm of PS1878. Samples were freeze-dried, weighed, wet-sieved with deionized water through a 63 μm mesh, and subsequently split into size fractions using 100, 125, 250, 500 and 1000 μm sieves.

Counts of planktic foraminiferal assemblages were conducted on representative splits (>300 specimens) of the 100–250 μm size fraction. Samples containing less than 100 specimens were excluded from the statistical analysis. Individual species were identified and counted. The number of planktic foraminifera per 1 g dry sediment was calculated.

Unweathered volcanic glass and other rock fragments >250 μm were distinguished and counted, providing information on the intensity of ice-rafting and allowing the identification of the tephra layer. As IRD we interpret all lithic grains >250 μm (except for unweathered volcanic glass). Such coarse particles will be transported into a deep ocean basin preferentially by icebergs while sea ice mainly transports finer material (Nürnberg *et al.* 1994).

Stable oxygen and carbon isotope analyses were conducted on planktic species *Neogloboquadrina pachyderma* (sin.). Twenty-five specimens were picked from the 125–250 μm size fraction. All stable isotope analyses were carried out in the stable isotope laboratory of GEOMAR. Results are expressed in the δ notation referring to the PDB standard and are given as $\delta^{18}O$ and $\delta^{13}C$. Analysis for tephra geochemistry was performed on the 100–250 μm size fraction at 49–50 cm core depth. Fresh-looking shards were mounted in epoxy and the preparation of slides for microprobe analysis followed Dugmore *et al.* (1995). Dataset outliers with abnormal geochemical composition that could reflect microlites or impurities in the glass were removed and totals below 95% were omitted. Analysed tephra was compared with published tephra horizons from Iceland and Jan Mayen on the basis of a TAS plot (total alkali vs. silica), $K_2O$, CaO, MgO and $SiO_2$. All plots of geochemical data were normalized to 100%.

## Chronology

Age control of PS1878 is based on nine AMS $^{14}C$ dates measured on *N. pachyderma* (sin.) (Table 1). All radiocarbon ages were corrected for a reservoir age of 400 years, calibrated using Calib Rev 6.1.0 software (Stuiver & Reimer 1993) and the Marine09 calibration curve (Reimer *et al.* 2009), and are given in thousand calendar years before AD 1950 (ka).

*Table 1.* AMS $^{14}$C measurements and calibrated ages of core PS1878.

| Laboratory number | Depth (cm) | Species dated | $^{14}$C age±error | Calibrated age (ka) |
|---|---|---|---|---|
| Core PS1878-2 | | | | |
| Poz-45376 | 0.5 | *N. pachyderma* (sin.) | 775±35 | 426 |
| Poz-45377 | 12.5 | *N. pachyderma* (sin.) | 3300±40 | 3143 |
| Core PS1878-3 | | | | |
| Poz-45378 | 11.5 | *N. pachyderma* (sin.) | 3295±35 | 3139 |
| Poz-45380 | 19.5 | *N. pachyderma* (sin.) | 4525±35 | 4746 |
| Poz-54381 | 25.5 | *N. pachyderma* (sin.) | 5580±50 | 5961 |
| Poz-54382 | 30.5 | *N. pachyderma* (sin.) | 6760±50 | 7295 |
| Poz-45384 | 39.5 | *N. pachyderma* (sin.) | 8410±60 | 9028 |
| Poz-45385 | 58.5 | *N. pachyderma* (sin.) | 11 100±60 | 12 613 |
| KIA 47284 | 95.5 | *N. pachyderma* (sin.) | 16 620±110 | 19 266 |

The age–depth relation of PS1878 is shown in Fig. 2. The average sedimentation rate amounts to ~5.1 cm ka$^{-1}$. Assuming that the tephra layer found at 47–58 cm in the core (volcanic glass shards making up >75% of a sample) reflects a short-term event, we set its sedimentation time to zero. Linear interpolation assigned the tephra layer an age of 11.9 ka. The obtained calibrated AMS $^{14}$C dates, together with the proxy records, were used to compile a composite record (PS1878) from the giant box core and the kasten core at the depth of 12.5 cm below the sea floor. As the calculated sedimentation rate was relatively stable throughout the record (except for the tephra interval) we extrapolated the age beyond the oldest dated sample (19.3 ka at 96.5 cm) using the sedimentation rate of the above interval (59.5–96.5 cm; ~5.6 cm ka$^{-1}$) and extended the age model back to 22.3 ka at 113.5 cm. However, as discussed below, it is possible that there was a short interval of increased sedimentation rate in the deglacial part of our record (~18 ka). If this was indeed the case, then the 'normal' sedimentation rate in the remaining part of the >12.6 ka interval would have been lower and the extrapolation would give an older age of the bottom of the record. Due to these uncertainties we consider the older part of the age model (>12.6 ka) as uncertain and interpret it with caution. Nevertheless, the bottom of the record is certainly older than 19.3 ka.

The surface sample yielded a comparatively young age (0.426 ka) and contained living (rose bengal stained) benthic foraminifera. Therefore we assume that the record represents the time period between 22.3 ka and the retrieval year AD 1990.

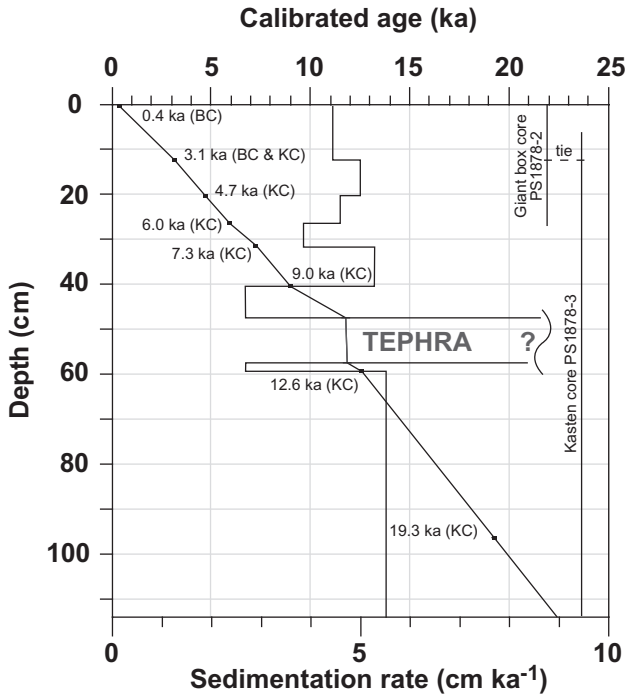


*Fig. 2.* PS1878 age–depth plot.

## Results

### *Planktic foraminifera and ice-rafted debris*

The record starts in the Last Glacial Maximum (LGM) with low foraminiferal abundances. The fauna is strongly dominated by *N. pachyderma* (sin.) (Fig. 3), a polar species dwelling at water depths of ~50–200 m (Carstens *et al.* 1997). However, there are a number of prominent, short-lived peaks of relatively high foraminiferal abundance. The IRD content is relatively high and seems to be positively correlated with the foraminiferal abundance. The peaks in both proxies coincide clearly (59.5, 73.5, 89.5, 96.5, 99.5, 105.5 and 111.5 cm below the sea floor).

The Holocene part of the record (after 12 ka) contains generally little IRD. The foraminiferal abundance is significantly higher than in the earlier part. It reaches a maximum around 9 ka and remains high until 5.5 ka. Subsequently it decreases quite rapidly, but remains higher than in the pre-Holocene part of the record. Finally, the abundance increases again after 2 ka. Superimposed on these longer-term changes, a quasi-millennial scale variability of a comparable magnitude is observed.

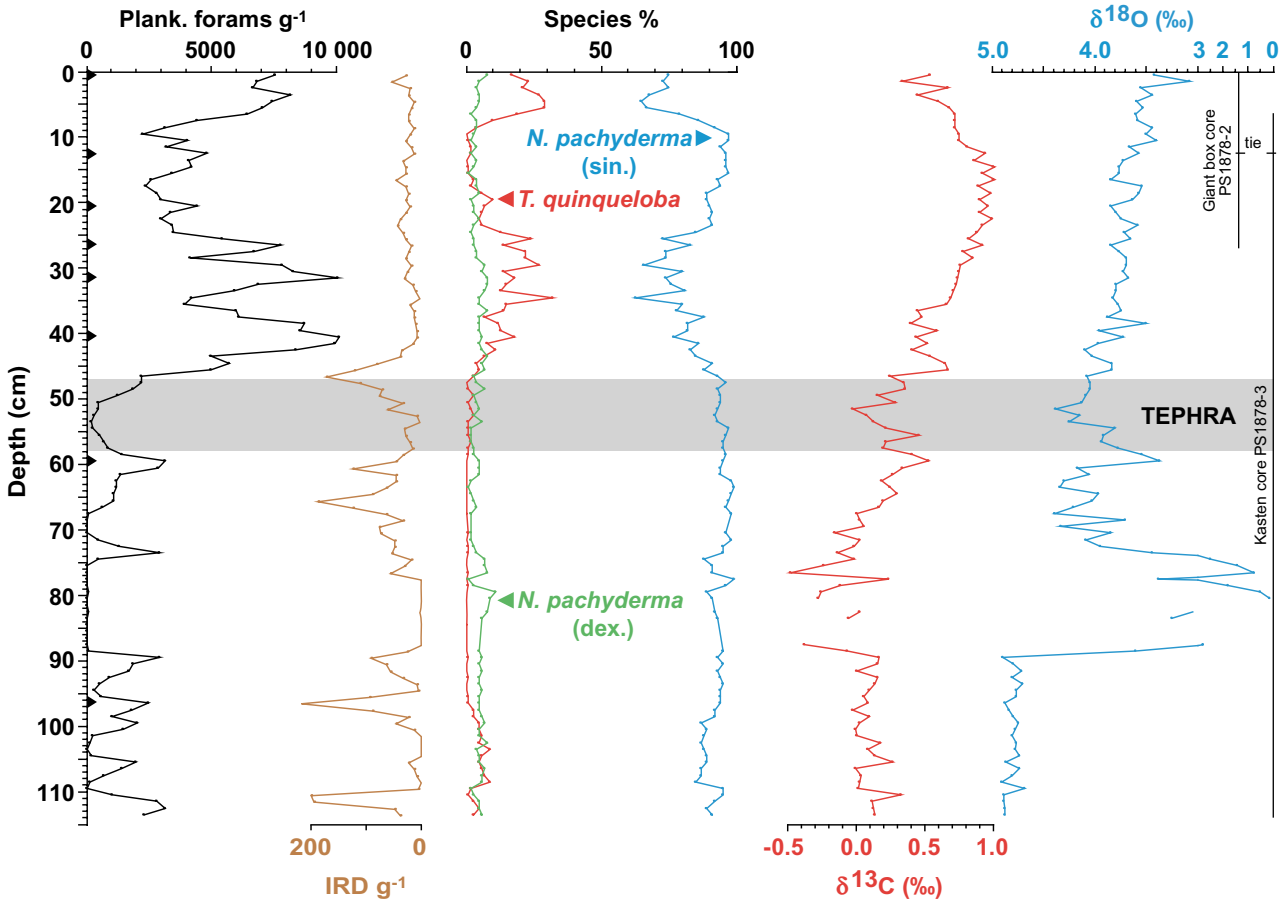


*Fig. 3.* PS1878 proxy records versus depth: total abundance of planktic foraminifera, total abundance of IRD, relative abundance of three dominant planktic foraminiferal species, stable carbon and oxygen isotope ratios of planktic foraminifer *N. pachyderma* (sin). Black triangles mark the AMS $^{14}$C dates. Grey bar indicates the tephra layer. This figure is available in colour at http://www.boreas.dk.

The changes in species composition show similarities to the abundance record. The percentage of subpolar species (mainly *N. pachyderma* (dex) and *Turborotalita quinqueloba*) increases gradually to reach its maximum (30–40%) between 10.5 and 5.5 ka. Afterwards, the percentage of *N. pachyderma* (sin.) increases again and returns to the pre-Holocene values of >80–90%. Another significant and relatively rapid increase in subpolar fauna occurs after 2.5 ka (up to >30%).

We did not find any significant signs of dissolution in the studied foraminifera. Both tests of robust *N. pachyderma* and more fragile subpolar species are well preserved throughout the cores.

### *Stable isotopes*

The planktic oxygen isotope record reveals relatively heavy and stable values of 4.3–4.9‰ in its older part (Fig. 3). After ~18 ka sharp peaks of very light values (minimum 0.15‰) occur and a trend towards lower $\delta^{18}$O values commences that lasts until the end of the record. A distinct, though irregular, variability within the trend can be observed. The most prominent light isotope excursion within this trend occurs at 12.8–11.9 ka and reaches 3.4‰.

The glacial part of the planktic carbon isotope record (>18 ka) exhibits low and stable values around 0.0–0.3‰ (Fig. 3). Simultaneous with the light $\delta^{18}$O peaks the $\delta^{13}$C values decrease slightly and a trend of increasing values commences thereafter. Around 7 ka the $\delta^{13}$C values reach a high plateau of 0.8–1.0‰, which lasts until 3 ka and ends with a relatively sudden drop. After 1.5 ka the values decrease again and become more variable.

### *Geochemical analysis of the tephra*

Analysed shards have a basanitic to tephritic composition according to the TAS plot (Le Bas *et al.* 1986; Fig. 4A). The analysed tephra can be distinguished from both the Icelandic tephras and the Jan Mayen tephra on the basis of its higher $K_2O$ (1–6 wt%) and decreasing trend of MgO (7–2 wt%) (Fig. 4B, C).

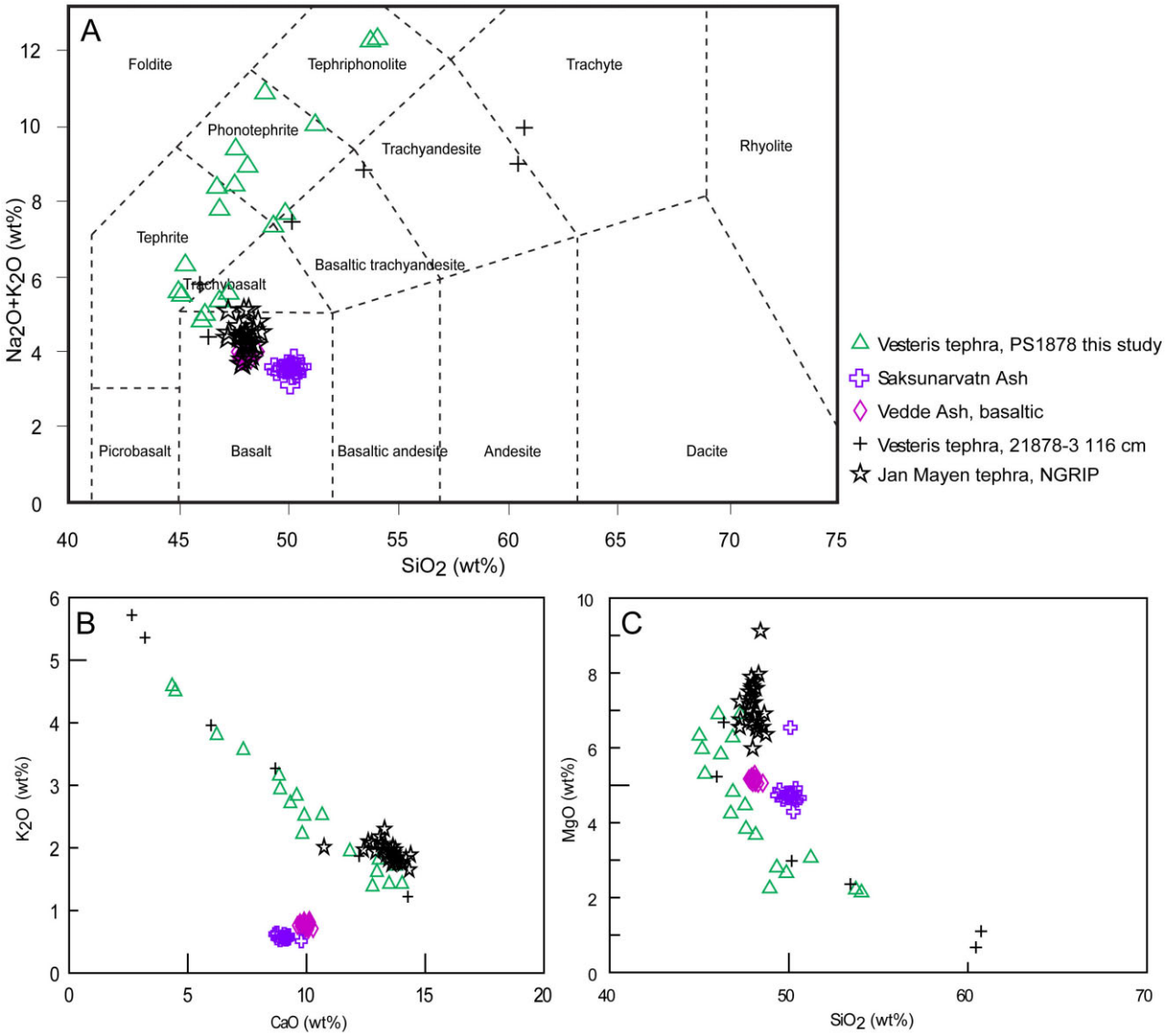


*Fig. 4.* Major element plots of different Nordic Seas tephras: Vesterisbanken tephra from PS1878 at 49–50 cm (this study), Vesterisbanken tephra from PS1878-3 at 116 cm (Haase *et al.* 1996), Saksunarvatn Ash (Davies *et al.* 2012), the basaltic component of the Vedde Ash (Davies *et al.* 2001) and Jan Mayen tephra (Abbott *et al.* 2012). All major data are plotted as normalized values. A. Total alkali–silica plot (after Le Bas *et al.* 1986). B and C. Selected bi-plots. This figure is available in colour at http://www.boreas.dk.

## Discussion

### *Last Glacial Maximum*

Our central Greenland Sea planktic $\delta^{18}O$ record shows LGM values (Fig. 5) that are typical for this interval in the Nordic Seas. They indicate the presence of relatively high-salinity waters and can be interpreted as AW advected to the north (Sarnthein *et al.* 1995; Nørgaard-Pedersen *et al.* 2003). The low foraminiferal abundance and species diversity indicates a low biological productivity in the LGM. Following Duplessy *et al.* (1988) we interpret the low planktic $\delta^{13}C$ values as suggesting a poorly ventilated water mass as the habitat for the foraminifers. From these lines of evidence we propose that the study area was largely covered with sea ice, which strongly inhibited the penetration of sunlight, reduced the productivity of phytoplankton that the foraminifera feed on, and limited the air–sea gas exchange. As even today the sea ice edge is located close to site PS1878, we consider it unlikely that conditions were significantly more favourable in the LGM.

The amount of coarse ice-rafted debris in sediments from the LGM is relatively high (Fig. 5), suggesting the presence of numerous icebergs originating from the circum-Arctic ice sheets. However, the record is highly variable suggesting repeated occurrences of

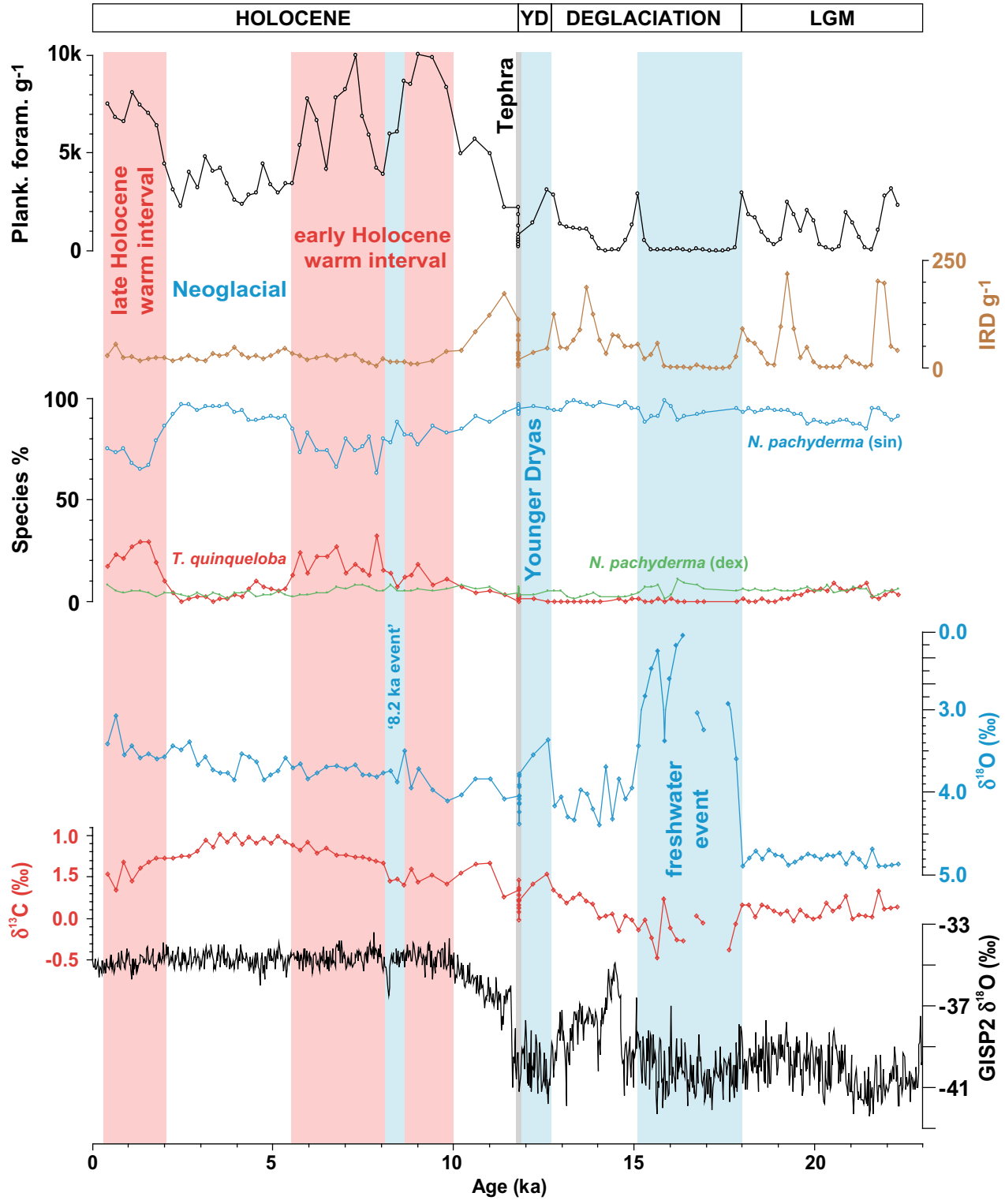


*Fig. 5.* PS1878 palaeoceanographic record: total abundance of planktic foraminifera, total abundance of IRD, relative abundance of three dominant planktic foraminiferal species, stable oxygen and carbon isotope ratios of planktic foraminifer *N. pachyderma* (sin). Also plotted is the oxygen isotope record from the GISP2 ice-core (Grootes *et al.* 1993).

numerous icebergs rather than their constant presence. The IRD peaks coincide with foraminiferal abundance peaks. The clear correlation of these two proxies suggests that the water remained somewhat open, at least during the warmer summer seasons. Any decrease in sea ice cover could have improved the living conditions, leading to a significant increase in planktic productivity. Such open water conditions and possibly even slightly warmer surface waters may have enhanced mobility and melting of icebergs and IRD deposition. These intervals with higher productivity and IRD delivery may have been rather rare in the Greenland Sea during the LGM, but they are distinctly recorded in the sediment, although timewise disproportionately overrepresented due to temporarily higher sedimentation rates. It is not clear, however, why no clear $\delta^{13}C$ response corresponding to open water intervals can be observed.

### *Deglaciation*

The PS1878 deglacial record starts with a massive low $\delta^{18}O$ peak (Fig. 5). Similar but less prominent features can be found in cores PS1230 (Bauch *et al.* 2001) and PS2887 (Nørgaard-Pedersen *et al.* 2003) from the western Fram Strait as well as in the eastern Nordic Seas (e.g. Dokken & Jansen 1999). We interpret them as a result of the discharge of isotopically light meltwater that lowered the regional surface water salinity (Sarnthein *et al.* 1995). This conclusion is supported by the simultaneous decrease of planktic $\delta^{13}C$ values, which are indicative of weakly ventilated subsurface waters. A low-density freshwater-rich surface layer increases the stratification of the upper water layers, thereby decreasing the gas exchange between subsurface waters and the atmosphere (Duplessy *et al.* 1988; Stein *et al.* 1994a, b; Spielhagen *et al.* 2004). Together with the low isotope values, a decrease in the IRD content is observed, pointing at a reduction in the sediment delivery by icebergs. This may suggest that the meltwater originated from terrestrial sources (melting ice sheets or possible outbursts from ice-dammed lakes in glaciated areas around the Arctic Ocean) rather than from locally melting icebergs.

Although the AMS $^{14}C$ dates suggest a different timing (between 20 and 18 ka) for the freshwater outbursts in the western Fram Strait and in the Greenland Sea we argue that the apparent difference may be a result of variable, unknown reservoir ages (possibly up to 2000 years, cf. Waelbroeck *et al.* 2001), as well as low sedimentation rates in some of the cores. We suggest that the first significant freshwater outbursts in the Nordic Seas took place roughly simultaneously around 18 ka. The trigger mechanism remains elusive but may be related to an early sea-level rise (Clark & Mix 2002) and possibly a collapse of marine-based ice sheets (Álvarez-Solas *et al.* 2011).

Sarnthein *et al.* (1995) presented a compilation of $\delta^{18}O$ values from sediment records from the North Atlantic and the Nordic Sea. The deglacial time-slice (14.2–13.2 $^{14}C$ ka) shows two meltwater tongues with $\delta^{18}O$ values <3‰ – one stretching from the Danish Strait towards Jan Mayen and the other from the Barents Sea margin towards the central Norwegian Sea. Sarnthein *et al.* (1995) did not present any datapoints from the Greenland Sea, around site PS1878. Nevertheless, it is clear that in any other record the $\delta^{18}O$ values were as low as in PS1878. This indicates that the meltwater outburst probably originated in the proximity of this site and most likely came from the Greenland Ice Sheet. However, the Fram Strait, also poorly represented in the compilation of Sarnthein *et al.* (1995), was also strongly affected by fresh water (Bauch *et al.* 2001; Nørgaard-Pedersen *et al.* 2003) and it seems unlikely that it propagated northward (i.e. upstream the EGC), from site PS1878 towards sites PS2887 and PS1230. Therefore at least one more outburst that reached the Fram Strait must have occurred in the circum-Arctic region. Nevertheless, they both could have a common trigger mechanism.

The age of the freshwater event in PS1878 (18–15 ka) fits well with Heinrich stadial 1 (HS1). Our planktic carbon isotope record shows extremely low values during this interval (Fig. 5), indicating a ventilation of the (sub)surface water even weaker than during the LGM (cf. Sarnthein *et al.* 1995; Spielhagen *et al.* 2004). Considering the role of the Greenland Sea in modern deepwater renewal, this might support the suggestions of Stanford *et al.* (2011) that the AMOC gradually decreased and virtually collapsed during HS1.

The lack of IRD and the extremely low foraminiferal concentrations (Fig. 5) in sediments deposited during the freshwater outburst might suggest that it was a relatively short event, however, it is represented by sediments of significant thickness (>15 cm, Fig. 3). We speculate that their deposition could have resulted from a sediment plume (Lekens *et al.* 2005) and reflects only a relatively short period of high sedimentation rates, overrepresented in our age model. Biological productivity might have been further reduced by surface-water salinity below the level tolerated by planktic foraminifera and an extensive sea ice cover, which may have resulted from the low surficial salinity and could have further limited sunlight penetration and gas exchange. Such an interpretation would imply that the sedimentation rate before 12.6 ka (except for the sediment plume interval) was in fact lower than that yielded from the linear interpolation between 12.6 and 19.3 ka. Álvarez-Solas *et al.* (2011) suggest that it was the melting of the Fennoscandian ice sheet that triggered HS1 by weakning the deep convection and causing the collapse of the Laurentide ice sheet. Taking into account the relatively early age of our meltwater event (18 ka) and the lack of IRD we argue that if the inter-

pretation of the sediment plume in PS1878 is correct, then the Greenland ice sheet might have also played an initiating role in weakening of the deep convection (as the freshwater outburst occurred close to the Greenland Sea convection centre) and could have contributed to the onset of HS1.

Following the freshwater events, planktic $\delta^{18}O$ returned to values around 4‰ (Fig. 5), indicating that the freshwater influence had decreased by this time. Also the increasing $\delta^{13}C$ values suggest that the ventilation of (subsurface) water was reactivated. Although some minor negative excursions in the planktic $\delta^{18}O$ record after the main freshwater event suggest that meltwater discharges still occurred in the central Greenland Sea, their amplitude decreases, indicating that the development of a more stable oceanographic system commenced. We associate this interval with the Bølling–Allerød (B/A) period. At its onset, the fresh water was purged out of the Nordic Seas and the AMOC was rapidly re-established (McManus *et al.* 2004; Stanford *et al.* 2011). In our record, the HS1–B/A transition seems to be relatively gradual. This might be the result of the stronger EGC influence on site PS1878 compared with the areas further to the south.

### *Younger Dryas*

The Younger Dryas (YD), spanning ~12.8–11.7 ka (Rasmussen *et al.* 2006), was a cold period within the overall climate warming in the transition from the LGM to the Holocene. This millennial-scale event involved a significant reduction in the AMOC attributed to enhanced meltwater inputs into the North Atlantic (e.g. Broecker *et al.* 2010; Not & Hillaire-Marcel 2012). It is still unclear whether the freshwater impulse reached the Nordic Seas as a sediment-loaded plume from the Hudson Strait (Rashid *et al.* 2011), as a meltwater discharge through the St Lawrence river system and via the Gulf Stream (e.g. Broecker *et al.* 1989) or through the Mackenzie River basin and via the Arctic Ocean (e.g. Tarasov & Peltier 2006; Not & Hillaire-Marcel 2012). Despite lacking terrestrial evidence (Fisher & Lowell 2012), the latter concept has gained increasing support recently through modelling results of Condron & Winsor (2012). They showed that only a meltwater discharge from the Arctic, in contrast to the outflow through the St Lawrence Valley, was able to reach the deep-water-formation regions of the subpolar North Atlantic and weaken the AMOC significantly.

In our planktic oxygen isotope record we observe a strong negative excursion at 12.8–11.9 ka that we associate with the YD (Fig. 5). This age fits well with the timing of this cold event in Greenland ice cores (Rasmussen *et al.* 2006) as well as in high-resolution terrestrial and marine records (e.g. Bakke *et al.* 2009; Cabedo-Sanz *et al.* 2012) and may suggest that the reservoir age (400 years) applied for dating of PS1878 is largely correct for this time interval. This value, suggested also for the central Nordic Seas (Bauch *et al.* 2001), is significantly lower than the estimates of 1000 years for the Norwegian Sea (Björck *et al.* 2003) and 700–800 (Bard *et al.* 1994) or ~1000–1500 years (Waelbroeck *et al.* 2001) for the North Atlantic. The proposed low reservoir age, together with rather high planktic $\delta^{13}C$, indicates relatively strong subsurface water ventilation. The explanation could be a thicker but weaker halocline. The strong halocline in the modern Arctic Ocean is maintained by a large contribution of fresh river water (Prange & Gerdes 1999). During cold periods such as the YD, however, this source was significantly limited (Rasmussen & Thomsen 2004) and fresh water originated only from more local and episodic sources (e.g. freshwater outbursts). Because of the weaker halocline the stratification was probably considerably weaker than at present. This could have increased the subsurface water ventilation and resulted in higher planktic $\delta^{13}C$ values. The strong negative planktic $\delta^{18}O$ excursion in PS1878 during the YD together with a similar decrease in the western Fram Strait (Bauch *et al.* 2001) suggests an Arctic source of the freshwater discharge that could be considered as a trigger for the YD (an 'Arctic' trigger in the sense of Condron & Winsor 2012).

### *Holocene*

The onset of the Holocene is marked in our record by a thick (11 cm), dark tephra layer (Figs 2, 3). The interpolated age of the layer (11.9 ka) is close to the age of the Vedde Ash (12 171±114 GICC05 a b2k in the NGRIP ice core; Rasmussen *et al.* 2006), one of the most widely spread Icelandic isochrones for the Lateglacial–early Holocene in the North Atlantic region (Mortensen *et al.* 2005; Lane *et al.* 2012). It is also close in time to the Saksunarvatn Ash in the NGRIP ice core (10 347± 89 GICC05 a b2k; Rasmussen *et al.* 2006), another widespread Icelandic tephra (Lind & Wastegård 2011; Davies *et al.* 2012). However, the concentrations of the fresh-looking volcanic shards with sharp edges in PS1878 (up to 99% of non-biogenic grains >250 μm) and the thickness of the layer suggest a nearby and primary source. The geochemical analysis of the tephra confirms this presumption (Fig. 4). The higher $K_2O$ and lower CaO concentrations of the PS1878 tephra distinguish it from the tephra originating from Jan Mayen (Hunt 2004; Abbott *et al.* 2012). The Icelandic tephras, including Vedde Ash and Saksunarvatn Ash (Mangerud *et al.* 1984, 1986; Davies *et al.* 2001), can be clearly distinguished from the PS1878 tephra based on the TAS-plot but also by the lower CaO concentrations. On the other hand, our tephra shows a strong correlation to an older Vesterisbanken tephra found in core PS1878-3 at 116 cm (Haase *et al.* 1996). Therefore we suggest that

the PS1878 tephra is a local tephra originating from the Vesterisbanken volcano whose eruptions were frequent during the past 60 ka (Haase *et al*. 1996).

In general, the Holocene part of our record is characterized by higher abundances of planktic foraminifera and higher percentages of the subpolar fauna (Fig. 5). These proxies indicate higher bioproductivity and higher water temperatures. Together with the low IRD content, they also suggest limited ice-rafting and sea ice cover. Our carbon isotope record shows rising values until *c*. 5 ka, which accords with a trend commonly observed in the Nordic Seas (e.g. Vogelsang 1990; Fronval & Jansen 1997; Bauch *et al*. 2001; Sarnthein *et al*. 2003) indicating increasing ventilation of subsurface waters (Lubinski *et al*. 2001). However, the changes are not linear and a significant internal variability in the different proxy records can be observed.

From the planktic faunal distribution record a threefold division of the Holocene can be applied (Fig. 5). A period characterized by high percentages of subpolar species and high foraminiferal abundances (~11–5.5 ka) is followed by a transition to a fauna similar to that of the Lateglacial (5.5–2 ka). Finally, around 2 ka, a return of subpolar species and an abundance increase is found.

The PS1878 faunal record shows a strongly different image of the Holocene palaeoenvironmental evolution compared with the ice-core records, for example, GISP2 (Grootes *et al*. 1993). The GISP2 $\delta^{18}O$ record (Fig. 5), which generally reflects the temperature of ice formation (Johnsen *et al*. 1992), shows very little variability during the Holocene, with only a slight trend towards more negative values (i.e. cooling) in the younger part. Even though the more recent reconstruction of the Greenland Holocene temperature (Vinther *et al*. 2009) reveals a more pronounced Holocene climatic optimum, it still shows very little shorter-scale variability. In contrast, the faunal PS1878 record indicates that the intra-Holocene long-term variability as well as millennial-scale changes had a magnitude only slightly lower than the glacial–interglacial transition. This comparison shows that the open-ocean environment was much more susceptible to changes (resulting both from external forcing and internal oscillation) than the climate on top of a large ice-sheet.

We associate the period of highest subpolar fauna percentages (10–5.5 ka) with the Holocene Thermal Maximum (HTM) and the relatively warm interval thereafter (e.g. Werner *et al*. 2013), which we collectively term the early Holocene warm interval (EHWI). Its onset (Fig. 5) accords with that of HTM in many other records from the Nordic Seas (e.g. Bauch *et al*. 2001; Sarnthein *et al*. 2003; Giraudeau *et al*. 2010; Risebrobakken *et al*. 2011; Husum & Hald 2012). While the onset of the HTM is roughly simultaneous in the northern Nordic Seas and occurred shortly after the insolation peak at high northern latitudes (Laskar *et al*. 2004), the subsequent cooling is more gradual and differs among the individual study sites. These regional differences are the expression of the general Holocene evolution of water masses and associated frontal systems combined with local and regional feedback mechanisms (Bauch *et al*. 2001; Risebrobakken *et al*. 2011; Werner *et al*. 2013). However, in our record the EHWI termination was relatively abrupt and took place around 5.5 ka.

The presence of the subpolar species *T. quinqueloba*, which reaches up to 30% of the planktic fauna during the EHWI (Fig. 5), indicates an increased influence of Atlantic waters. In comparison to the Lateglacial the Holocene IRD record shows a significant decrease. Probably only few icebergs penetrated into the central Greenland Sea during the EHWI. The westward shift of the Greenland Sea gyre due to the Atlantic waters advection could have additionally prevented icebergs from reaching the central Greenland Sea (Sarnthein *et al*. 1995).

According to our record, conditions in the central Greenland Sea were variable during the EHWI. The most prominent changes can be observed between ~8.6 and 8.2 ka (Fig. 5). The percentage of polar species increases, reaching highest values of the HTM and indicating a cooling of the (sub)surface water. The faunal composition changes coincide with an interval of decreasing foraminiferal abundance, suggesting decreasing productivity, and are preceded by a light $\delta^{18}O$ peak (indicating freshwater influence) accompanied by a decrease in $\delta^{13}C$ values (pointing to a weaker subsurface water ventilation). Although this must be regarded as relatively obscure evidence for a freshwater-related cooling event, the findings are generally consistent with those from other palaeoclimatic and palaeoceanographic archives recording the cool '8.2 ka event', which was caused by the drainage of Lake Agassiz into the Labrador Sea and further into the North Atlantic, with a subsequent AMOC collapse (Rohling & Pälike 2005; Risebrobakken *et al*. 2003 and references therein; Hillaire-Marcel *et al*. 2007).

No clear evidence of the 8.2 ka event was found in other central and western Nordic Seas records (e.g. Fronval & Jansen 1997; Bauch *et al*. 2001), possibly attributed to the low temporal resolution of these records in the Holocene and the use of the >150 μm fraction for planktic foraminiferal counts of core HM94-34 (Fronval & Jansen 1997). This size fraction misses a significant part of the subpolar specimens because the subpolar species (e.g. *T. quinqueloba*) often do not reach such large test sizes in the Arctic environment (Bauch 1994; Kandiano & Bauch 2002). Therefore the record of Fronval & Jansen (1997) might underestimate indications of the Holocene temperature and water mass variations in the Holocene Greenland Sea. However, our finding that the 8.2 ka event is only weakly expressed in the central Greenland Sea might

indicate that the event did not affect the western Nordic Seas significantly, in contrast to the eastern Nordic Seas where it is clearly recorded (Hald *et al.* 2007; Risebrobakken *et al.* 2003; Werner *et al.* 2013). The middle Holocene (between ~5.5 and 3 ka) was characterized by the return of a more polar planktic fauna strongly dominated by *N. pachyderma* (sin) (Fig. 5). Also the foraminiferal abundance decreased significantly but remained higher than in the Lateglacial sediments. These changes may indicate the onset of the Neoglacial cooling induced by decreasing insolation (e.g. Andersen *et al.* 2004a). The generally stable oxygen isotope ratios (8–3 ka) can be interpreted as opposing effects of cooling and freshening of the (sub-)surface water, though significant short-term variability occurs in this interval as well. The observed changes are similar to those in other records (e.g. Jennings *et al.* 2002; Werner *et al.* 2013) but the increase in the IRD deposition in our record is not as prominent as on the East Greenland shelf (Jennings *et al.* 2002). This is probably due to the larger distance from the iceberg sources.

The $\delta^{13}C$ values reach their maximum between 7 and 3 ka (Fig. 5) indicating intensive water mass ventilation. High $\delta^{13}C$ values are common in the Nordic Seas during this interval (Vogelsang 1990; Fronval & Jansen 1997; Bauch *et al.* 2001; Sarnthein *et al.* 2003) and might indicate maximum ventilation of the subsurface waters and/or reflect relatively stable and modern-like environmental conditions in terms of the oceanic circulation (Bauch *et al.* 2001; Sarnthein *et al.* 2003), as well as weak surface-water stratification (Bauch & Weinelt 1997). Hall *et al.* (2004) report an interval of relatively fast Iceland–Scotland Overflow Water (ISOW) flow between 7 and 4 ka, indicating AMOC strengthening. At first sight this may appear inconsistent with a middle Holocene cooling in the Greenland Sea at ~5.5 ka because an intensified AMOC may require an increased AW inflow. However, as noticed by Giraudeau *et al.* (2010), AW inflow to the Norwegian Sea is on the suborbital scale positively correlated to the PW outflow from the Arctic Ocean to the Greenland Sea. Thus, AMOC intensification might have brought cooler surface waters to the Greenland Sea, intensifying the activity of the gyre system.

Around 3 ka planktic carbon isotopes show a significant decrease (Fig. 5). This change to lower $\delta^{13}C$ values has been noted before (Bauch & Weinelt 1997) and can be recognized as a basinwide stratigraphic feature among many isotope records from the Nordic Seas (e.g. Vogelsang 1990; Bauch *et al.* 2001; Sarnthein *et al.* 2003; Risebrobakken *et al.* 2011). It is not visible in the record from core HM94-34 from the Greenland Sea (Fronval & Jansen 1997), most probably due to the low sedimentation rates and mixing of the uppermost sediment layers by bioturbation. Sarnthein *et al.* (1995, 2003) interpret the $\delta^{13}C$ drop as the result of an increase in AW advection. However, Hall *et al.* (2004) report that the ISOW flow started to decrease around 4 ka (indicating AMOC slow down) and reached a minimum at 2.7 ka. This precludes an intensification of AW inflow and suggests a decrease in water mass ventilation and strengthening of the surface-water stratification as the reasons for the $\delta^{13}C$ drop. The onset of the orbitally forced Neoglacial after ~5.5 ka caused a general cooling in the high northern latitudes and increasing sea ice occurrence (Müller *et al.* 2012). The sea ice and the cold, low salinity (and thus low density) surface layer associated with it may have acted as a lid on top of the water column and limited its vertical mixing. In the Greenland Sea this development was amplified by the more intensive PW inflow (percentages of polar species *N. pachyderma* (sin.) reach the pre-Holocene values), which probably led to even stronger surface water stratification. Possibly around 3 ka the abundance of sea ice and the thickness of the freshwater lid reached a threshold and led to a stepwise AMOC slow down.

In PS1878 we observe distinct changes in almost all available proxies for the past 2–3 ka (Fig. 5). The percentage of subpolar foraminifera increases steadily between 2.5 and 1.5 ka, reaching values similar to those of the HTM (>30%). Parallel to the subpolar fauna reappearance, an increase in the total abundance of the foraminiferal fauna occurs. Significant changes are also found in the stable isotope records. After a relatively short stable interval (2.5–1.5 ka) the carbon isotope ratio decreases and becomes more variable. This might suggest an increase in water-column stratification and a decreasing ventilation of the subsurface water. The oxygen isotope values begin to decrease after the stable interval of the middle Holocene, which might suggest warming of the subsurface water.

Our data fit well in the broader image of the late Holocene in the circum-Nordic Seas region. Various ice-core (e.g. Johnsen *et al.* 2001), terrestrial (e.g. McDermott *et al.* 2001) and marine records (e.g. Sarnthein *et al.* 2003; Andersen *et al.* 2004a, b; Giraudeau *et al.* 2010; Spielhagen *et al.* 2011; Werner *et al.* 2013) indicate warming and/or an increase in AW inflow into the Nordic Seas starting 3–2 ka and peaking 1.5–1.0 ka.

Our data (Fig. 5) suggest two possible mechanisms explaining the observed late Holocene changes – a warming of more stratified water masses and/or an increase in lateral warm Atlantic waters advection. A stronger stratification could be the result of the dense sea-ice cover and the low salinity surface layer, as already discussed for the 3 ka $\delta^{13}C$ drop. Stronger stratification of the upper water column would certainly ease the warming of the subsurface water. However, due to the albedo being increased by the sea ice cover and the low insolation during the late Holocene (Laskar *et al.* 2004), solar radiation must be excluded as a possible heat source. A possible solution

is a stronger inflow of relatively warm Atlantic waters. This mechanism does not exclude a stronger stratification of the water column (Andersen *et al*. 2004a), as the warm and saline AW is stable between the low salinity surface layer and cold and saline deep waters and most of it does not participate in deepwater formation, but becomes part of outflowing water masses at shallow and intermediate depths (Mauritzen 1996). The Atlantic waters also could be responsible for the further decrease of planktic $\delta^{13}C$ after 2 ka as AW is generally poorly ventilated (Sarnthein *et al*. 2003). However, the mechanisms behind the basinwide drop in planktic $\delta^{13}C$ around 3 ka seem not fully understood yet and need further investigations.

The fact that similar late Holocene changes described above are observed in many records from the Nordic Seas suggests that they were a regional phenomenon of AW inflow intensification, rather than just a change in relative strength of individual NAC branches (although the Atlantic waters did not necessarily reach the entire basin at the sea surface). A reconstruction of the North Atlantic Oscillation (NAO) over the past 5.2 ka (Olsen *et al*. 2012) shows that around 2 ka the NAO changed from variable, intermittently negative to generally positive conditions. The positive NAO situation is characterized by stronger westerlies, which can explain the intensification of the AW inflow into the Nordic Seas.

Our central Greenland Sea record is unusual compared with other circum-Nordic Seas records because the faunal data suggest a late Holocene (after 2 ka) onset of HTM-comparable conditions in the upper water layers. We suppose that the stronger surface water stratification after 3 ka amplified the effect of the enhanced Atlantic waters inflow into the area at 2 ka. PS1878 is the first multicentennial record from the deep, central part of the Nordic Sea that documents a late Holocene warming in this area. The unusual character of the observed changes, together with the relatively high temporal resolution, makes it an interesting site for further studies.

## Conclusions

Our record from the deep central Greenland Sea allows us to reconstruct the palaeoceanographic evolution of the area since the Last Glacial Maximum on an unprecedented multicentennial scale.

- In the LGM, the Greenland Sea was strongly influenced by Polar Water. The basin was predominantly ice-covered and intensive ice-rafting took place. The ice lid together with a cold, low-salinity surface layer limited subsurface water ventilation. These conditions resulted in a low biological productivity reflected by a poor planktic fauna dominated by the polar species. Occasionally during the warmer summer seasons the sea ice cover diminished somewhat, significantly improving planktic living conditions.
- Deglaciation started around 18 ka with a freshwater discharge directly from the Greenland Ice Sheet. It lowered the surface salinity and decreased the surface water ventilation leading to a further impoverishment of the planktic fauna.
- The last major freshwater event is recorded in the central Greenland Sea during the Younger Dryas (12.8–11.9 ka) and supports the hypothesis of an 'Arctic' trigger for this cool event.
- The earliest Holocene (11.9–7 ka) was an interval of surface-water warming, increasing productivity and improving surface water ventilation.
- The early Holocene warm interval (~10–5.5 ka) was characterized by high biologic productivity and abundant subpolar foraminiferal species. The interval was interrupted by short-term events, for example, the cool 8.2 ka event.
- Due to the decreasing insolation, the middle Holocene (7–3 ka) was a time of the Neoglacial cooling, amplified by Polar Water inflow. The record indicates that the ventilation of the upper water layers was more intense than at present.
- Thickening of the cold, low salinity surface layer as a result of Neoglacial cooling led to a relatively rapid decrease of the ventilation and a stronger stratification of the upper water layer at 3 ka. This amplified the subsequent late Holocene warming caused by the NAO-induced strengthening of the Atlantic Water inflow into the Nordic Seas at ~2 ka.

*Acknowledgements.* – This work is a contribution to the CASE Initial Training Network funded by the European Community's 7th Framework Programme FP7 2007/2013, Marie-Curie Actions, under Grant Agreement no. 238111. We thank Henning Bauch and Leonid Polyak for valuable discussions and suggestions and two anonymous reviewers for their constructive criticism, which improved the manuscript. We are grateful to Lulzim Haxhiaj for performing the stable isotope measurements and to the Leibniz Laboratory, Kiel University, and the Poznan Radiocarbon Laboratory for the AMS $^{14}C$ dating.

## References

Abbott, P. M., Davies, S. M., Steffensen, J. P., Pearce, N. J. G., Bigler, M., Johnsen, S. J., Seierstad, I. K., Svensson, A. & Wastegård, S. 2012: A detailed framework of Marine Isotope Stages 4 and 5 volcanic events recorded in two Greenland ice-cores. *Quaternary Science Review 36*, 59–77.

Álvarez-Solas, J., Montoya, M., Ritz, C., Ramstein, G., Charbit, S., Dumas, C., Nisancioglu, K., Dokken, T. M. & Ganopolski, A. 2011: Heinrich event 1: an example of dynamical ice-sheet reaction to oceanic changes. *Climate of the Past 7*, 1297–1306.

Andersen, C., Koç, N., Jennings, A. E. & Andrews, J. T. 2004a: Nonuniform response of the major surface currents in the Nordic Seas to insolation forcing: implications for the Holocene climate variability. *Paleoceanography 19*, PA2003, doi: 10.1029/2002PA000873.

Andersen, C., Koç, N. & Moros, M. 2004b: A highly unstable Holocene climate in the subpolar North Atlantic: evidence from diatoms. *Quaternary Science Reviews 23*, 2155–2166.

Bakke, J., Lie, Ø., Heegaard, E., Dokken, T., Haug, G. H., Birks, H. H., Dulski, P. & Nilsen, T. 2009: Rapid oceanic and atmospheric changes during the Younger Dryas cold period. *Nature Geoscience 2*, 202–205.

Bard, E., Arnold, M., Mangerud, J., Paterne, M., Labeyrie, L., Duprat, J., Mélières, M.-A., Sønstegaard, E. & Duplessy, J. 1994: The North Atlantic atmosphere–sea surface $^{14}C$ gradient during the Younger Dryas climatic event. *Earth and Planetary Science Letters 126*, 275–287.

Bauch, H. A. 1994: Significance of variability in *Turborotalita quinqueloba* (Natland) test size and abundance for paleoceanographic interpretations in the Norwegian–Greenland Sea. *Marine Geology 121*, 129–141.

Bauch, H. A. & Weinelt, M. S. 1997: Surface water changes in the Norwegian Sea during last deglacial and Holocene times. *Quaternary Science Reviews 16*, 1115–1124.

Bauch, H. A., Erlenkeuser, H., Spielhagen, R. F., Struck, U., Matthiessen, J., Thiede, J. & Heinemeier, J. 2001: A multiproxy reconstruction of the evolution of deep and surface waters in the subarctic Nordic seas over the last 30,000 yr. *Quaternary Science Reviews 20*, 659–678.

Björck, S., Koç, N. & Skog, G. 2003: Consistently large marine reservoir ages in the Norwegian Sea during the Last Deglaciation. *Quaternary Science Reviews 22*, 429–435.

Broecker, W. S., Denton, G. H., Edwards, R. L., Cheng, H., Alley, R. B. & Putnam, A. E. 2010: Putting the Younger Dryas cold event into context. *Quaternary Science Reviews 29*, 1078–1081.

Broecker, W. S., Kennett, J. P., Flower, B. P., Teller, J. T., Trumbore, S., Bonani, G. & Wolfli, W. 1989: Routing of meltwater from the Laurentide Ice Sheet during the Younger Dryas cold episode. *Nature 341*, 318–321.

Cabedo-Sanz, P., Belt, S. T., Knies, J. & Husum, K. 2012: Identification of contrasting seasonal sea ice conditions during the Younger Dryas. *Quaternary Science Reviews*. Doi: 10.1016/j.quascirev.2012.10.028. In press.

Carstens, J., Hebbeln, D. & Wefer, G. 1997: Distribution of planktic foraminifera at the ice margin in the Arctic (Fram Strait). *Marine Micropaleontology 29*, 257–269.

Clark, P. U. & Mix, A. C. 2002: Ice sheets and sea level of the Last Glacial Maximum. *Quaternary Science Reviews 21*, 1–7.

Condron, A. & Winsor, P. 2012: Meltwater routing and the Younger Dryas. *Proceedings of the National Academy of Sciences 6*, 1–6.

Davies, S. M., Abbott, P. M., Pearce, N. J. G., Wastegård, S. & Blockley, S. P. E. 2012: Integrating the INTIMATE records using tephrochronology: rising to the challenge. *Quaternary Science Review 36*, 11–27.

Davies, S. M., Turney, C. S. M. & Lowe, J. J. 2001: Identification and significance of a visible, basalt-rich Vedde Ash layer in a Late-glacial sequence on the Isle of Skye, Inner Hebrides, Scotland. *Journal of Quaternary Science 16*, 99–104.

Dokken, T. M. & Jansen, E. 1999: Rapid changes in the mechanism of ocean convection during the last glacial period. *Nature 401*, 458–461.

Dugmore, A. J., Larsen, G. & Newton, A. J. 1995: Seven Tephra Isochrones in Scotland. *The Holocene 5*, 257–266.

Duplessy, J.-C., Shackleton, N. J., Fairbanks, R. G., Labeyrie, L. D., Oppo, D. & Kallel, N. 1988: Deepwater source variations during the last climatic cycle and their impact on the global deepwater circulation. *Paleoceanography 3*, 343–360.

Eldevik, T., Nilsen, J. E. Ø., Iovino, D., Anders Olsson, K., Sandø, A. B. & Drange, H. 2009: Observed sources and variability of Nordic seas overflow. *Nature Geoscience 2*, 406–410.

Fisher, T. G. & Lowell, T. V. 2012: Testing northwest drainage from Lake Agassiz using extant ice margin and strandline data. *Quaternary International 260*, 106–114.

Foldvik, A., Aagaard, K. & Tørresen, T. 1988: On the velocity field of the East Greenland Current. *Deep Sea Research 35*, 1335–1354.

Fronval, T. & Jansen, E. 1997: Eemian and early Weichselian (140–60 ka) paleoceanography and paleoclimate in the Nordic seas with comparisons to Holocene conditions. *Paleoceanography 12*, 443–462.

Giraudeau, J., Grelaud, M., Solignac, S., Andrews, J. T., Moros, M. & Jansen, E. 2010: Millennial-scale variability in Atlantic water advection to the Nordic Seas derived from Holocene coccolith concentration records. *Quaternary Science Reviews 29*, 1276–1287.

Grootes, P. M., Stuiver, M., White, J. W. C., Johnsen, S. J. & Jouzel, J. 1993: Comparison of oxygen isotope records from the GISP2 and GRIP Greenland ice cores. *Nature 366*, 552–554.

Haase, K. M., Hartmann, M. & Wallrabe-Adams, H.-J. 1996: The geochemistry of ashes from Vesterisbanken Seamount, Greenland Basin: implications for the evolution of an alkaline volcano. *Journal of Volcanology and Geothermal Research 70*, 1–19.

Hald, M., Andersson, C., Ebbesen, H., Jansen, E., Klitgaard-kristensen, D., Risebrobakken, B., Salomonsen, G. R., Sarnthein, M., Sejrup, H. P. & Telford, R. J. 2007: Variations in temperature and extent of Atlantic Water in the northern North Atlantic during the Holocene. *Quaternary Science Reviews 26*, 3423–3440.

Hall, I. R., Bianchi, G. G. & Evans, J. R. 2004: Centennial to millennial scale Holocene climate–deep water linkage in the North Atlantic. *Quaternary Science Reviews 23*, 1529–1536.

Hansen, B. & Østerhus, S. 2000: North Atlantic–Nordic Seas exchanges. *Progress in Oceanography 45*, 109–208.

Hillaire-Marcel, C., de Vernal, A. & Piper, D. J. W. 2007: Lake Agassiz Final drainage event in the northwest North Atlantic. *Geophysical Research Letters 34*, L15601.

Hunt, J. B. 2004: Tephrostratigraphical evidence for the timing of Pleistocene explosive volcanism at Jan Mayen. *Journal of Quaternary Science 19*, 121–136.

Husum, K. & Hald, M. 2012: Marine Mmicropaleontology Arctic planktic foraminiferal assemblages: implications for subsurface temperature reconstructions. *Marine Micropaleontology 96–97*, 38–47.

Jennings, A. E., Knudsen, K. L., Hald, M., Hansen, C. V. & Andrews, J. T. 2002: A mid-Holocene shift in Arctic sea-ice variability on the East Greenland Shelf. *The Holocene 12*, 49–58.

Johnsen, S. J., Clausen, H. B., Dansgaard, W., Fuhrer, K., Gundestrup, N., Hammer, C. U., Iversen, P., Jouzel, J., Stauffer, B. & Steffensen, J. 1992: Irregular glacial interstadials recorded in a new Greenland ice core. *Nature 359*, 311–313.

Johnsen, S. J., Dahl-Jensen, D., Gundestrup, N., Steffensen, J. P., Henrik, B., Miller, H., Masson-Delmotte, V., Sveinbjörnsdottir, A. E. & White, J. 2001: Oxygen isotope and palaeotemperature records from six Greenland ice-core stations: camp century, Dye-3, GRIP, GISP2, Renland and NorthGRIP. *Journal of Quaternary Science 16*, 299–307.

Kandiano, E. S. & Bauch, H. A. 2002: Implications of planktic foraminiferal size fractions for the glacial-interglacial paleoceanography of the polar North Atlantic. *The Journal of Foraminiferal Research 32*, 245–251.

Lane, C. S., Blockley, S. P. E., Mangerud, J., Smith, V. C., Lohne, O. S., Tomlinson, E. L., Matthews, I. P. & Lotter, A. F. 2012: Was the 12.1 ka Icelandic Vedde Ash one of a kind? *Quaternary Science Review 33*, 87–99.

Laskar, J., Robutel, P., Joutel, F., Gastineau, M., Correia, A. C. M. & Levrard, B. 2004: A long term numerical solution for the insolation quantities of the Earth. *Astronomy & Astrophysics 428*, 261–285.

Le Bas, M. J., Le Maitre, R. W. & Streckeisen, A. 1986: A chemical classification of volcanic rocks based on the total alkali-silica diagram. *Journal of Petrology 27*, 745–750.

Lekens, W. A. H., Sejrup, H. P., Haflidason, H., Petersen, G., Hjelstuen, B. & Knorr, G. 2005: Laminated sediments preceding Heinrich event 1 in the Northern North Sea and Southern Norwegian Sea: origin, processes and regional linkage. *Marine Geology 216*, 27–50.

Lind, E. M. & Wastegård, S. 2011: Tephra horizons contemporary with short early Holocene climate fluctuations: new results from the Faroe Islands. *Quaternary International 246*, 157–167.

Lubinski, D. J., Polyak, L. & Forman, S. L. 2001: Freshwater and Atlantic water inflows to the deep northern Barents and Kara seas since ca 13 $^{14}C$ ka: foraminifera and stable isotopes. *Quaternary Science Reviews 20*, 1851–1879.

Mangerud, J., Furnes, H. & Johansen, J. 1986: A 9000-year-old ash bed on the Faroe Islands. *Quaternary Research 26*, 262–265.

Mangerud, J., Lie, S. E., Furnes, H., Krisiansen, I. L. & Lomo, L. 1984: A Younger Dryas ash bed in Western Norway, and its possible correlations with tephra in cores from the Norwegian Sea and the North-Atlantic. *Quaternary Research 21*, 85–104.

Marshall, J. & Schott, F. 1999: Open-ocean convection: observations, theory, and models. *Reviews of Geophysics 37*, 1–64.

Mauritzen, C. 1996: Production of dense overflow waters feeding the North Atlantic across the Greenland–Scotland Ridge. Part 1: evidence for a revised circulation scheme. *Deep Sea Research 43*, 769–806.

McDermott, F., Mattey, D. P. & Hawkesworth, C. 2001: Centennial-scale Holocene climate variability revealed by a high-resolution speleothem $\delta^{18}O$ record from SW Ireland. *Science 294*, 1328–1331.

McManus, J. F., Francois, R., Gherardi, J.-M., Keigwin, L. D. & Brown-Leger, S. 2004: Collapse and rapid resumption of Atlantic meridional circulation linked to deglacial climate changes. *Nature 428*, 834–837.

Mortensen, A. K., Bigler, M., Grönvold, K., Steffensen, J. P. & Johnsen, S. J. 2005: Volcanic ash layers from the Last Glacial Termination in the NGRIP ice core. *Journal of Quaternary Science 20*, 209–219.

Müller, J., Werner, K., Stein, R., Fahl, K., Moros, M. & Jansen, E. 2012: Holocene cooling culminates in sea ice oscillations in Fram Strait. *Quaternary Science Reviews 47*, 1–14.

Nørgaard-Pedersen, N., Spielhagen, R. F., Erlenkeuser, H., Grootes, P. M., Heinemeier, J. & Knies, J. 2003: Arctic Ocean during the Last Glacial Maximum: Atlantic and polar domains of surface water mass distribution and ice cover. *Paleoceanography 18*, 1–19.

Not, C. & Hillaire-Marcel, C. 2012: Enhanced sea-ice export from the Arctic during the Younger Dryas. *Nature Communications 3*, 647, doi: 10.1038/ncomms1658.

Nowaczyk, N. R. & Antonow, M. 1997: High-resolution magnetostratigraphy of four sediment cores from the Greenland Sea-I. Identification of the Mono Lake excursion, Laschamp and Biwa I/Jamaica geomagnetic polarity events. *Geophysical Journal International 131*, 310–324.

Nürnberg, D., Wollenburg, I., Dethleff, D., Eicken, H., Kassens, H., Letzig, T., Reimnitz, E. & Thiede, J. 1994: Sediments in Arctic sea ice: implications for entrainment, transport and release. *Marine Geology 104*, 185–214.

Olsen, J., Anderson, N. J. & Knudsen, M. F. 2012: Variability of the North Atlantic Oscillation over the past 5,200 years. *Nature Geoscience 5*, 808–812.

Prange, M. & Gerdes, R. 1999: Influence of Arctic river runoff on the circulation in the Arctic Ocean, the Nordic Seas and the North Atlantic. *ICES ASC 1999 – CM 1999/L:11 (Nordic Seas Exchanges)*, 1–5.

Rashid, H., Piper, D. & Flower, B. 2011: The role of Hudson Strait outlet in Younger Dryas sedimentation in the Labrador Sea. *Abrupt Climate Change: Mechanisms, Patterns, and Impacts. Geophysical Monograph Series 193*, 93–110.

Rasmussen, S. O., Andersen, K. K., Svensson, A. M., Steffensen, J. P., Vinther, B. M., Clausen, H. B., Siggaard-Andersen, M.-L., Johnsen, S. J., Larsen, L. B., Dahl-Jensen, D., Bigler, M., Röthlisberger, R., Fischer, H., Goto-Azuma, K., Hansson, M. E. & Ruth, U. 2006: A new Greenland ice core chronology for the last glacial termination. *Journal of Geophysical Research 111*, D06102.

Rasmussen, T. L. & Thomsen, E. 2004: The role of the North Atlantic Drift in the millennial timescale glacial climate fluctuations. *Palaeogeography, Palaeoclimatology, Palaeoecology 210*, 101–116.

Reimer, P., Baillie, M., Bard, E., Bayliss, A., Beck, J. W., Blackwell, P. G., Bronk Ramsey, C., Buck, C. E., Burr, G. S., Edwards, R. L., Friedrich, M., Grootes, P. M., Guilderson, T. P., Hajdas, I., Heaton, T. J., Hogg, A. G., Hughen, K. A., Kaiser, K. F., Kromer, B., McCormac, F. G., Manning, S. W., Reimer, R. W., Richards, D. A., Southon, J. R., Talamo, S., Turney, C. S. M., van der Plicht, J. & Weyhenmeyer, C. E. 2009: IntCal09 and Marine09 radiocarbon age calibration curves, 0–50,000 years cal BP. *Radiocarbon 51*, 1111–1150.

Risebrobakken, B., Jansen, E., Andersson, C., Mjelde, E., & Hevrøy, K. 2003: A high-resolution study of Holocene paleoclimatic and paleoceanographic changes in the Nordic Seas. *Paleoceanography 18*, 1017.

Risebrobakken, B., Dokken, T., Smedsrud, L. H., Andersson, C., Jansen, E., Moros, M. & Ivanova, E. V. 2011: Early Holocene temperature variability in the Nordic Seas: the role of oceanic heat advection versus changes in orbital forcing. *Paleoceanography 26*, PA4206, Doi: 10.1029/2011PA002117.

Rohling, E. J. & Pälike, H. 2005: Centennial-scale climate cooling with a sudden cold event around 8,200 years ago. *Nature 434*, 975–979.

Sarnthein, M., Jansen, E., Weinelt, M., Arnold, M., Duplessy, J. C., Erlenkeuser, H., Flatøy, A., Johannessen, G., Johannessen, T., Jung, S., Koc, N., Labeyrie, L., Maslin, M., Pflaumann, U. & Schulz, H. 1995: Variations in Atlantic surface ocean paleoceanography, 50°–80°N: a time-slice record of the last 30,000 years. *Paleoceanography 10*, 1063–1094.

Sarnthein, M., van Kreveld, S., Erlenkeuser, H., Grootes, P. M., Kucera, M., Pflaumann, U. & Schulz, M. 2003: Centennial-to-millennial-scale periodicities of Holocene climate and sediment injections off the western Barents shelf, 75°N. *Boreas 32*, 447–461.

Spielhagen, R. F., Baumann, K.-H., Erlenkeuser, H., Nowaczyk, N. R., Nørgaard-Pedersen, N., Vogt, C. & Weiel, D. 2004: Arctic Ocean deep-sea record of northern Eurasian ice sheet history. *Quaternary Science Reviews 23*, 1455–1483.

Spielhagen, R. F., Werner, K., Aagaard-Sørensen, S., Zamelczyk, K., Kandiano, E., Budeus, G., Husum, K., Marchitto, T. M. & Hald, M. 2011: Enhanced modern heat transfer to the Arctic by warm Atlantic water. *Science 331*, 450–453.

Stanford, J. D., Rohling, E. J., Bacon, S., Roberts, A. P., Grousset, F. E. & Bolshaw, M. 2011: A new concept for the paleoceanographic evolution of Heinrich event 1 in the North Atlantic. *Quaternary Science Reviews 30*, 1047–1066.

Stein, R., Nam, S. I., Schubert, C., Vogt, C., Ftitterer, D. & Heinemeier, J. 1994a: The last deglaciation event in the eastern central Arctic Ocean. *Science 264*, 692–696.

Stein, R., Schubert, C., Vogt, C. & Ftitterer, D. 1994b: Stable isotope stratigraphy, sedimentation rates and paleosalinity in the latest Pleistocene to Holocene central Arctic Ocean. *Marine Geology 119*, 333–355.

Stuiver, M. & Reimer, P. J. 1993: Radiocarbon calibration program. *Radiocarbon 35*, 215–230.

Sutherland, D. A. & Pickart, R. S. 2008: The East Greenland Coastal Current: structure, variability, and forcing. *Progress in Oceanography 78*, 58–77.

Swift, J. 1986: The Arctic waters. *In* Hurdle, B. (ed.): *The Nordic Seas*, 129–151. Springer, New York.

Tarasov, L. & Peltier, W. R. 2006: A calibrated deglacial drainage chronology for the North American continent: evidence of an Arctic trigger for the Younger Dryas. *Quaternary Science Reviews 25*, 659–688.

Thiede, J. & Hempel, G. 1991: The expedition ARKTIS-VII/1 of RV 'POLARSTERN' in 1990. *Berichte zur Polarforschung 80*, 1–137.

Vinther, B. M., Buchardt, S. L., Clausen, H. B., Dahl-Jensen, D., Johnsen, S. J., Fisher, D. A., Koerner, R. M., Raynaud, D., Lipenkov, V., Andersen, K. K., Blunier, T., Rasmussen, S. O., Steffensen, J. P. & Svensson, A. M. 2009: Holocene thinning of the Greenland ice sheet. *Nature 461*, 385–388.

Vogelsang, E. 1990: Paläo-Ozeanographie des Europäischen Nordmeeres anhand stabiler Kohlenstoff- und Sauerstoffisotope. *Berichte aus dem Sonderforschungsbereich 313*, 1–136. University of Kiel, Kiel.

Waelbroeck, C., Duplessy, J. C., Michel, E., Labeyrie, L., Paillard, D. & Duprat, J. 2001: The timing of the last deglaciation in North Atlantic climate records. *Nature 412*, 724–727.

Werner, K., Spielhagen, R. F., Bauch, D., Hass, H. C. & Kandiano, E. 2013: Atlantic Water advection versus sea-ice advances in the eastern Fram Strait during the last 9 ka – multiproxy evidence for a two-phase Holocene. *Paleoceanography 28*, 283–295.

# 4. Water mass evolution of the Greenland Sea since late glacial times

From [Telesiński, M.M., Spielhagen, R.F., Bauch, H.A., 2014. Water mass evolution of the Greenland Sea since late glacial times. Clim. Past 10, 123–136.]. Reprinted under Creative Commons license.

Data available online at http://doi.pangaea.de/10.1594/PANGAEA.832368

Clim. Past, 10, 123–136, 2014
www.clim-past.net/10/123/2014/
doi:10.5194/cp-10-123-2014


Climate of the Past
Open Access

# Water mass evolution of the Greenland Sea since late glacial times

**M. M. Telesiński**[1], **R. F. Spielhagen**[1,2], **and H. A. Bauch**[1,2]

[1]GEOMAR Helmholtz Centre for Ocean Research Kiel, Wischhofstrasse 1–3, 24148 Kiel, Germany
[2]Academy of Sciences, Humanities, and Literature, 53151 Mainz, Germany

*Correspondence to:* M. M. Telesiński (mtelesinski@geomar.de)

Received: 15 August 2013 – Published in Clim. Past Discuss.: 30 August 2013
Revised: 21 November 2013 – Accepted: 6 December 2013 – Published: 16 January 2014

**Abstract.** Four sediment cores from the central and northern Greenland Sea basin, a crucial area for the renewal of North Atlantic deep water, were analyzed for planktic foraminiferal fauna, planktic and benthic stable oxygen and carbon isotopes as well as ice-rafted debris to reconstruct the environmental variability in the last 23 kyr. During the Last Glacial Maximum, the Greenland Sea was dominated by cold and sea-ice bearing surface water masses. Meltwater discharges from the surrounding ice sheets affected the area during the deglaciation, influencing the water mass circulation. During the Younger Dryas interval the last major freshwater event occurred in the region. The onset of the Holocene interglacial was marked by an increase in the advection of Atlantic Water and a rise in sea surface temperatures (SST). Although the thermal maximum was not reached simultaneously across the basin, benthic isotope data indicate that the rate of overturning circulation reached a maximum in the central Greenland Sea around 7 ka. After 6–5 ka a SST cooling and increasing sea-ice cover is noted. Conditions during this so-called "Neoglacial" cooling, however, changed after 3 ka, probably due to enhanced sea-ice expansion, which limited the deep convection. As a result, a well stratified upper water column amplified the warming of the subsurface waters in the central Greenland Sea, which were fed by increased inflow of Atlantic Water from the eastern Nordic Seas. Our data reveal that the Holocene oceanographic conditions in the Greenland Sea did not develop uniformly. These variations were a response to a complex interplay between the Atlantic and Polar water masses, the rate of sea-ice formation and melting and its effect on vertical convection intensity during times of Northern Hemisphere insolation changes.

## 1 Introduction

The Nordic Seas are an important region for the global oceanic system. First of all, they are the main gateway between the Arctic and North Atlantic oceans (Hansen and Østerhus, 2000). They also play a fundamental role in the overturning circulation being one of the deep water formation regions (Marshall and Schott, 1999). Paleoceanographic studies in this area are crucial to improve our understanding of the pace and amplitude of natural variability during the last glacial–interglacial transition and within the Holocene. While a significant number of detailed studies focuses on the eastern part of the region, along the North Atlantic Current (NAC) flow (e.g., Hald et al., 2007; Risebrobakken et al., 2011), less effort has been devoted to its central and western parts (e.g., Fronval and Janssen, 1997; Bauch et al., 2001). Problems with the accessibility due to the ice cover and low sedimentation rates (Nørgaard-Pedersen et al., 2003; Telesiński et al., 2013), which do not allow high resolution studies, are among the main reasons here.

Recently, Telesiński et al. (2013) presented a new record from the central Greenland Sea that allowed studying the oceanographic changes since the late glacial (22.3 ka) in a relatively high temporal resolution. That study revealed significant variability of the oceanic environment on multicentennial to multimillennial timescales. Although the record was generally in agreement with earlier studies, it also revealed some unusual features such as, e.g., an extreme freshwater-related planktic low-$\delta^{18}$O spike during the deglaciation and microfossil evidence for a late Holocene warming. Here we now correlate and compare that record with three other sediment cores from the northern Greenland Sea and with other paleoceanographic archives from the Nordic Seas to reconstruct the paleoceanography on a larger

regional scale. Furthermore, subsurface temperature reconstructions and a first high-resolution benthic stable isotope record from the Greenland Sea are presented and allow assessing the spatial range of variability found in the central Greenland Sea and the history of the overturning circulation in the area.

## 2 Study area

The Nordic Seas constitute the only deep-water connection between the North Atlantic and the Arctic oceans (Fig. 1). Relatively warm and saline ($T \sim 6$–$11\,^{\circ}C$, $S > 35$) Atlantic Water (AW) flows north along the Norwegian, Barents Sea and Svalbard continental margins and enters the Arctic through the Fram Strait and Barents Sea. In the west, cold, low-saline ($< 0\,^{\circ}C$, $< 34.4$) Polar Water (PW) flows south through the Fram Strait and along the Greenland continental margin to enter the North Atlantic through the Denmark Strait (Rudels et al., 1999). The strong gradient between these two main surface water masses makes the Nordic Seas sensitive to climatic changes. The central part of the Nordic Seas is the domain of Arctic Water (ArW), a result of PW and AW mixing. ArW is separated from PW by the Polar Front and from AW by the Arctic Front (Swift, 1986).

The vertical structure of the water column in the central Greenland Sea consists of three layers. At the surface, there is a thin layer of Arctic Surface Water originating from the East Greenland Current (EGC). Underneath, a layer of Atlantic Intermediate Water exists, which is supplied from the NAC. The weakly stratified Greenland Sea Deep Water, a product of deep convection, is found below (Marshall and Schott, 1999).

The Nordic Seas are one of the areas where deep water convection and the formation of North Atlantic Deep Water (NADW) take place today (e.g., Rudels and Quadfasel, 1991; Marshall and Schott, 1999). The western branches of the NAC and the eastern branches of the EGC create a cyclonic circulation in the Greenland Sea and lead to doming of the upper water layers. As the two water masses mix, they increase their density and sink to the bottom (Hansen and Østerhus, 2000). Subsequently, the water leaves the Nordic Seas as the Denmark Strait and Iceland-Scotland Overflow Waters.

Sea ice plays an important preconditioning role in the Greenland Sea compared to other convectional areas. In early winter, the formation of sea ice leads to brine rejection. The surface layer increases its density and sinks to about 150 m by mid-January. The sea-ice cover forms a wedge (Is Odden) extending far to the northeast, also over the Vesterisbanken area. Preconditioning continues later in the winter, with mixed-layer deepening in the ice-free area (Nord Bukta) to 300–400 m, induced by strong winds blown over the ice. Typically in March, near-surface densities are high enough to develop deep convection (down to $> 2000$ m) in the Greenland Sea, if the meteorological conditions are favorable (Marshall and Schott, 1999).

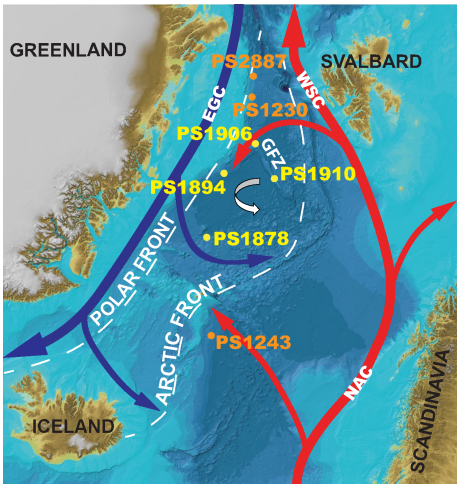


**Fig. 1.** Present day surface water circulation in the Nordic Seas. Cores used in this study are marked by yellow dots; other cores mentioned in text are marked by orange dots. Red arrows indicate Atlantic Water, blue arrows – Polar Water, white broken lines – oceanographic fronts. White arrow – present-day deep convection (Marshall and Schott, 1999). EGC – East Greenland Current, NAC – North Atlantic Current, WSC – West Spitsbergen Current, GFZ – Greenland Fracture Zone. Bathymetry from The International Bathymetric Chart of the Arctic Ocean (http://www.ibcao.org, 2012).

At present, the sites investigated in this study are all located within the ArW domain. A detailed description of site PS1878 was given by Telesiński et al. (2013). The three sites from the northern Greenland Sea, PS1894, PS1906 and PS1910, are located on the Greenland continental slope, on the northern and on the southern part of the Greenland Fracture Zone crest, respectively.

## 3 Material and methods

The sediment cores used in this study were retrieved during the ARK-VII/1 expedition of RV *Polarstern* in 1990 (Fig. 1). Core PS1878 is compiled from a giant box core PS1878-2 and a kasten core PS1878-3 (Telesiński et al., 2013), whereas the three others are giant box cores (Table 1). All cores consisted of brown to olive grey sediments of clay to silty sand. They were sampled continuously every 1 cm. Additionally, surface sediments of cores PS1894, PS1906 and PS1910 were collected. Further preparation included freeze-drying, wet-sieving with deionized water through a 63 µm mesh, and dry-sieving into size fractions using 100, 125, 250, 500 and 1000 µm sieves. Each size fraction was weighed.

In representative splits ($> 300$ specimens) of the 100–250 µm size fraction planktic foraminifera were counted. Samples containing less than 100 specimens were not used

**Table 1.** Cores used in the study.

| Core | Latitude | Longitude | Water depth (m) | Core type | Core length (cm) |
|---|---|---|---|---|---|
| PS1878-2 | 73°15.1′ N | 9°00.9′ W | 3038 | BC[a] | 27 |
| PS1878-3 | 73°15.3′ N | 9°00.7′ W | 3048 | KC[b] | 113 |
| PS1894-7 | 75°48.8′ N | 8°15.5′ W | 1992 | BC[a] | 42 |
| PS1906-1 | 76°50.5′ N | 2°09.0′ W | 2990 | BC[a] | 33 |
| PS1910-1 | 75°37.0′ N | 1°19.0′ E | 2448 | BC[a] | 33 |

[a] BC – giant box core, [b] KC – kasten core.

for the relative species abundance analysis. The number of planktic foraminifera per 1 g dry sediment was calculated to serve as a semiquantitative proxy for bioproductivity.

Identification and counting of several mineral grain types $> 250$ µm was used as a proxy for the intensity of ice-rafting and the identification of tephra layers. As ice-rafted debris (IRD) we interpret all lithic grains $> 250$ µm, except for unweathered volcanic glass. In the high latitudes, such coarse particles can be transported into a deep ocean basin preferentially by icebergs while sea ice mainly transports finer material (Clark and Hanson, 1983; Nürnberg et al., 1994).

For the analysis of stable oxygen and carbon isotopes, specimens of the planktic foraminiferal species *Neogloboquadrina pachyderma* (sin.) (all cores) and two benthic species – the epibenthic *Cibicidoides wuellerstorfi* and the shallow infaunal *Oridorsalis umbonatus* (cores PS1894, PS1910 and PS1878) – were used. Because of departures from isotopic calcite equilibrium, the measured $\delta^{18}$O values of these two species were corrected by $+0.64$ and $+0.36$ ‰, respectively (cf. Duplessy et al., 1988). Twenty-five specimens were picked from the 125–250 µm (*N. pachyderma* (sin.) and *O. umbonatus*) and 250–500 µm (*C. wuellerstorfi*) size fractions. All stable isotope analyses were carried out in the isotope laboratories of GEOMAR Helmholtz Centre for Ocean Research Kiel and the University of Kiel on Finnigan MAT 251 and Thermo MAT 253 mass spectrometers. Results are expressed in the $\delta$ notation referring to the PDB (Pee Dee Belemnite) standard and are given as $\delta^{18}$O and $\delta^{13}$C with an analytical accuracy of $< 0.06$ and $< 0.03$ ‰, respectively.

Absolute summer subsurface temperatures (100 m water depth) were calculated at site PS1878 between 15 and 0 ka using transfer functions based on a modern training set from the Arctic (Husum and Hald, 2012) and the C2 software, version 1.7.2 (Juggins, 2011). A weighted average partial least-squares statistical model with three components (WA-PLS C3) and leave-one-out ("jack knifing") cross validation was used. The root mean-squared error of prediction is 0.52 °C. Unlike Husum and Hald (2012), who used the $> 100$ µm size fraction, we ran the transfer function using the 100–250 µm size fraction. Although the coarser sediments contained relatively few foraminifera, we acknowledge that this might have slightly biased the results. Further, reconstructed temperatures below 2 °C are considered to be uncertain as the modern training set does contain very few data points below 2 °C (Husum and Hald, 2012).

**Table 2.** AMS $^{14}$C measurements and their calibrated ages for the cores used in the study (BP – before present).

| Lab. no. | Depth (cm) | $^{14}$C age ± standard deviation | Calibrated age (yr BP) |
|---|---|---|---|
| Core PS1878-2 | | | |
| Poz-45376 | 0.5 | 775 ± 35 | 426 |
| Poz-45377 | 12.5 | 3300 ± 40 | 3143 |
| Core PS1878-3 | | | |
| Poz-45378 | 11.5 | 3295 ± 35 | 3139 |
| Poz-45380 | 19.5 | 4525 ± 35 | 4746 |
| Poz-54381 | 25.5 | 5580 ± 50 | 5961 |
| Poz-54382 | 30.5 | 6760 ± 50 | 7295 |
| Poz-45384 | 39.5 | 8410 ± 60 | 9028 |
| Poz-45385 | 58.5 | 11 100 ± 60 | 12 613 |
| KIA 47284 | 95.5 | 16 620 ± 110 | 19 266 |
| Core PS1894-7 | | | |
| KIA 7088 | 0.5 | 3845 ± 40 | 3794 |
| KIA 47258 | 5.5 | 5390 ± 35 | 5773 |
| KIA 7089 | 9.5 | 5745 ± 40 | 6174 |
| KIA 47259 | 16.5 | 8075 ± 45 | 8528 |
| KIA 7090 | 21.5 | 8910 ± 55 | 9564 |
| KIA 7091 | 35.5 | 14 430 ± 70 | 17 051 |
| Core PS1906-1 | | | |
| KIA 7084 | 4.5 | 4360 ± 30 | 4482 |
| KIA 7083 | 11.5 | 7965 ± 40 | 8420 |
| KIA 7082 | 22.5 | 17 040 ± 80 | 19 731 |
| KIA 7081 | 32.5 | 19 130 ± 90 | 22 334 |
| Core PS1910-1 | | | |
| KIA 44390 | 0.5 | 2655 ± 30 | 2336 |
| Poz-45386 | 4.5 | 4820 ± 35 | 5122 |
| Poz-45387 | 11.5 | 6950 ± 50 | 7457 |
| KIA 44393 | 17.5 | 11 340 ± 50 | 12 794 |
| Poz-45388 | 30.5 | 16 80 ± 100 | 19 625 |

## 4 Chronology

AMS $^{14}$C datings were performed on monospecific samples of *N. pachyderma* (sin.) (Table 2). All radiocarbon ages were corrected for a reservoir age of 400 yr, calibrated using Calib Rev 6.1.0 software (Stuiver and Reimer, 1993) and the Marine09 calibration curve (Reimer et al., 2009) and are given in thousand calendar years before 1950 AD (ka).

The records cover the last ca. 20–23 kyr. The three box cores from the northern Greenland Sea have average

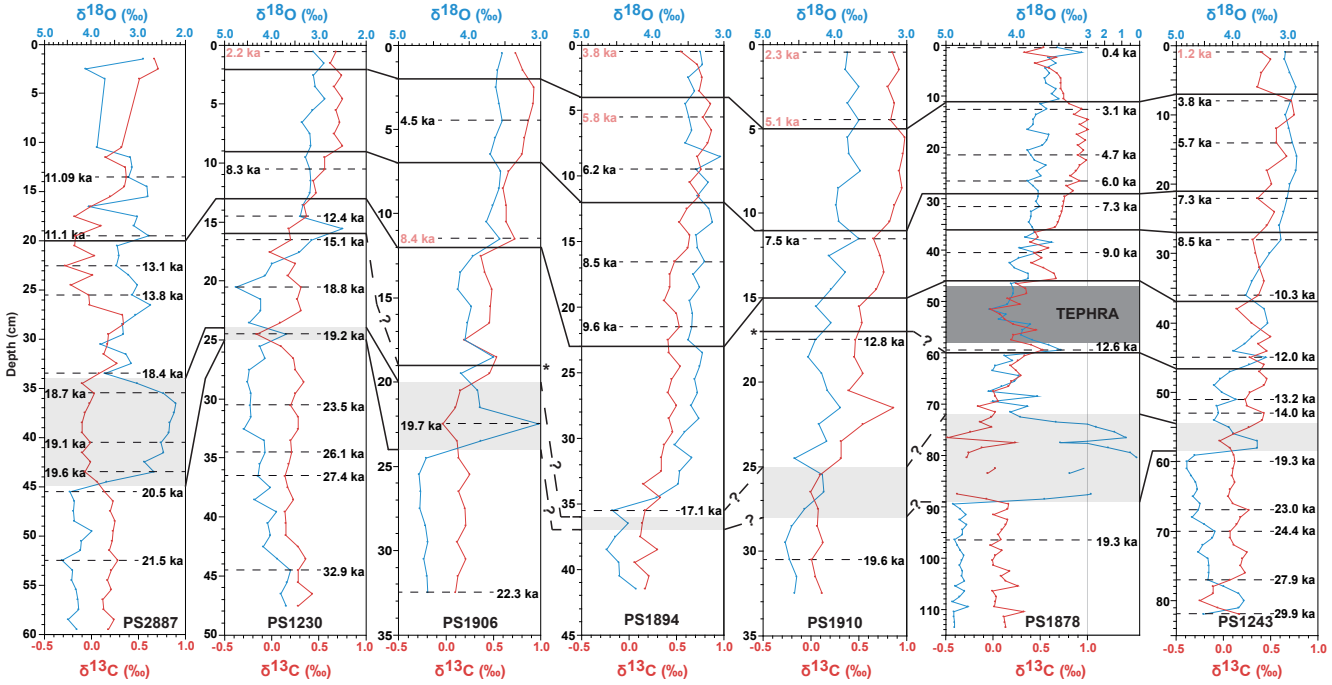


**Fig. 2.** Planktic oxygen and carbon stable isotope records of cores from the Nordic Seas and suggested correlation. Calibrated AMS $^{14}$C dates are shown. Dates excluded from the correlation are marked in pale red. Light grey shadings indicate the light carbon and oxygen isotope excursions interpreted as freshwater discharges, marking the onset of the deglaciation.

sedimentation rates of 1.5–2.0 cm kyr$^{-1}$. These low rates, together with bioturbation and uncertain reservoir ages, make age models of these records unreliable if based only on $^{14}$C datings. This is best illustrated by relatively old ages yielded from the surface samples of these cores (2.3–3.8 ka). However, the surface sample of core PS1878 yielded a younger age (0.426 ka) and contained recent sediments (Telesiński et al., 2013). Therefore we assume that sedimentation in the entire study area did not terminate in the late Holocene. To account for the apparent inaccuracy of part of the AMS $^{14}$C dates we attempted to improve the consistency of the age models of these cores by correlating the stable isotope data (and, in a few cases, also other proxies) and using linear interpolation between correlated points and reliable $^{14}$C-dated samples. In addition to our own data, we also used three nearby records of comparable sedimentation rates, time range and water depths. These include cores PS2887 (Nørgaard-Pedersen et al., 2003) as well as PS1230 from the western Fram Strait and PS1243 from the SW Norwegian Sea (Bauch et al., 2001). As the base for the correlation we used core PS1878, which has the highest temporal resolution and a reliable chronological framework based on $^{14}$C datings in the younger part of the record (Fig. 2). Due to poorer $^{14}$C age control and more speculative reservoir ages in the older part of the records, our improved age model is restricted to the last 15 kyr.

## 5 Results

### 5.1 Planktic foraminifera, ice-rafted detritus (IRD) and reconstructed subsurface temperatures

Four of our faunal records from the Greenland Sea show significantly different planktic foraminiferal abundances (Fig. 3), most likely due to different sedimentation rates. Therefore, absolute numbers of foraminiferal specimens in individual samples are not a meaningful proxy when cores are compared with one another. The records begin with relatively low abundances of the foraminiferal fauna strongly dominated by *N. pachyderma* (sin.) (Fig. 4, between ca. 23 and 12 ka), a polar species dwelling at water depths of ca. 50–200 m (Carstens et al., 1997). There are, however, a number of prominent, short-lived peaks of high foraminiferal abundance. They are most common and most prominent in core PS1878, supposedly due to its highest time resolution, but they are also noticeable in cores PS1906 and PS1894.

A significant early change among the faunal data is observed in core PS1894. Here, an increase to 20–30 % is found for the subpolar species *N. pachyderma* (dex.) and *Turborotalita quinqueloba* already around 17 ka. In the other cores a similar change is not noted until ca. 12 ka when both the percentages of subpolar species and the total abundance increase. Throughout the remaining part of the records the abundance stays high although significant variability can be observed. The portions of subpolar species remain high for

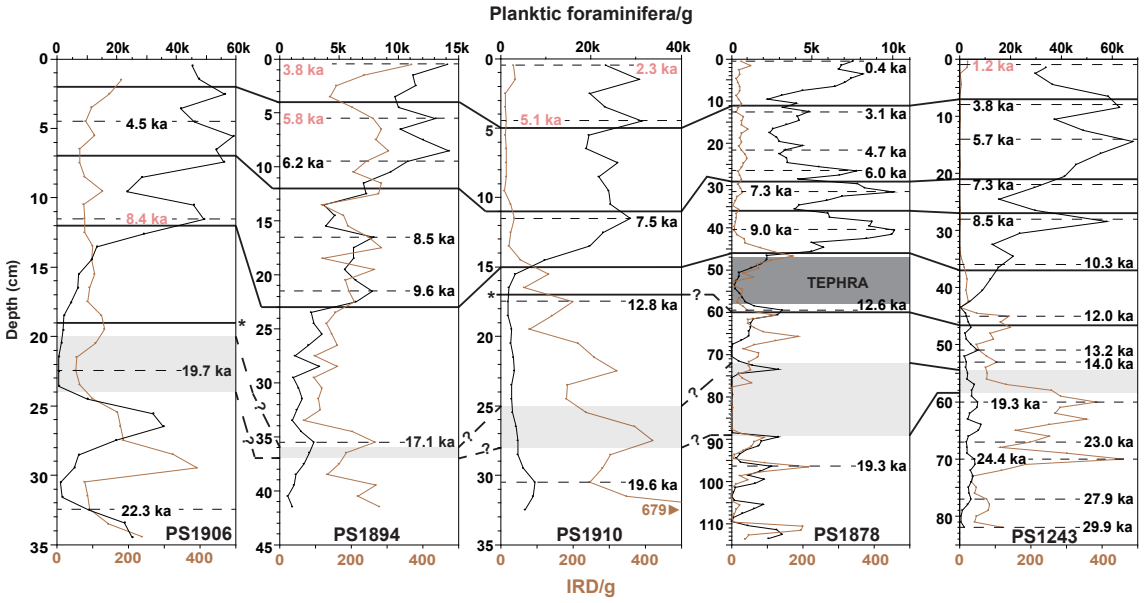


**Fig. 3.** Planktic foraminifera and IRD abundance (per 1 g dry sediment) of cores used in this study and core PS1243. Correlation and ages as in Fig. 2.

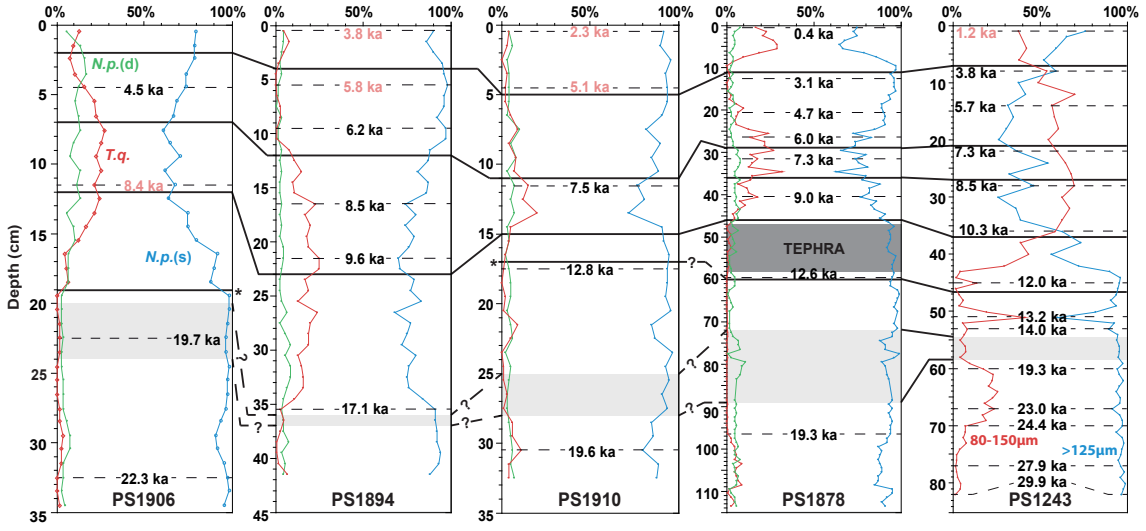


**Fig. 4.** Relative abundances of the three most common planktic foraminifera species in cores used in this study and core PS1243. *N.p.* (s) – *N. pachyderma* (sin.), *N.p.* (d) – *N. pachyderma* (dex.), *T.q.* – *T. quinqueloba*. Correlation and ages as in Fig. 2. Note the different size fractions used in core PS1243.

a few thousand years and then decrease gradually and unsimultaneously to reach pre-Holocene values (< 10–20 %) again after ca. 5 ka. A second, major increase can be observed after 3 ka in core PS1878 and, less clearly, PS1894. We did not find any significant signs of dissolution in the studied foraminifera. Both tests of robust *N. pachyderma* and more fragile subpolar species are generally well preserved throughout the cores.

As expected, the IRD records show high amounts of coarse lithogenic grains in the glacial part and low numbers during the Holocene (Fig. 3). Only the IRD content of core PS1894 remains relatively high throughout the entire record with slightly lower values between ca. 17 and 10 ka. In core PS1894, as well as in the lower part of cores PS1906 and PS1878, the IRD content seems to be positively correlated with the foraminiferal abundance, while in core PS1910 and in the upper part of PS1906 and PS1878 these two proxies appear inversely correlated.

The subsurface temperature record of core PS1878 shows values steadily increasing from around 2 °C around 15 ka

to a maximum of 3–3.5 °C between 8 and 5.7 ka (Fig. 7). Thereafter it decreases stepwise to values around 2 °C between 3.8 and 2.3 ka. Subsequently the record shows rapidly increasing temperatures with a peak value of ca. 3.5 °C at 1.3 ka and a decrease to ca. 3 °C until today.

### 5.2 Stable isotopes

The planktic oxygen isotope records start with relatively heavy and stable values of 4.3–4.9 ‰ (Fig. 2). After ca. 18 ka, sharp peaks of very light values (min. 0.15 ‰) occur (most pronounced in cores PS1906 and PS1878). Similar peaks are also found in cores PS1230, PS1243 (Bauch et al., 2001) and PS2887 (Nørgaard-Pedersen et al., 2003) that we used for the correlation. A trend towards lower $\delta^{18}$O values commences thereafter and lasts until the end of the record. A distinct, though irregular, variability can be observed within the trend (Figs. 2, 5).

The oldest part of all planktic carbon isotope records (> 18 ka) exhibits low and stable values around 0.0–0.3 ‰. Simultaneous with the light $\delta^{18}$O peaks, the $\delta^{13}$C values decrease slightly and a trend of increasing values commences thereafter. Around 7 ka the $\delta^{13}$C values reach a high plateau of 0.7–1.0 ‰, which lasts until 3 ka and ends with a relatively sudden drop.

Because *O. umbonatus* and *C. wuellerstorfi* were partly absent in the lowermost parts of our cores, the benthic stable isotope records cover only the last 16 kyr (Fig. 6). The oxygen isotope ratios of both benthic species generally show a decreasing trend parallel to the planktic record with values ca. 0.7–1.0 ‰ heavier than those of *N. pachyderma* (sin.). The epibenthic (*C. wuellerstorfi*) $\delta^{13}$C data follows the planktic $\delta^{13}$C records in terms of the main trends, but values are 0.2–1.0 ‰ higher and changes are of lower amplitude. The only major exception is the youngest (< 3 ka) part of record PS1894 in which benthic $\delta^{13}$C values continue to rise slightly while the planktic record decreases. All data sets are available from http://www.pangaea.de.

## 6 Discussion

### 6.1 Last Glacial Maximum (LGM)

The heavy $\delta^{18}$O values of > 4.5 ‰ in the Greenland Sea planktic records (Fig. 2) are typical for the late LGM waters in the Nordic Seas and Fram Strait (e.g., Sarnthein et al., 1995; Nørgaard-Pedersen et al., 2003). The low foraminiferal abundance and species diversity (Figs. 3, 4) are evidence of a low biological productivity in the Greenland Sea during the LGM. The latter might be a result of a perennial sea-ice cover that would strongly limit the penetration of sunlight and reduce the growth of phytoplankton that the foraminifera feed on.

Low $\delta^{13}$C values might suggest that the foraminifera lived in poorly ventilated water (cf. Duplessy et al., 1988), which

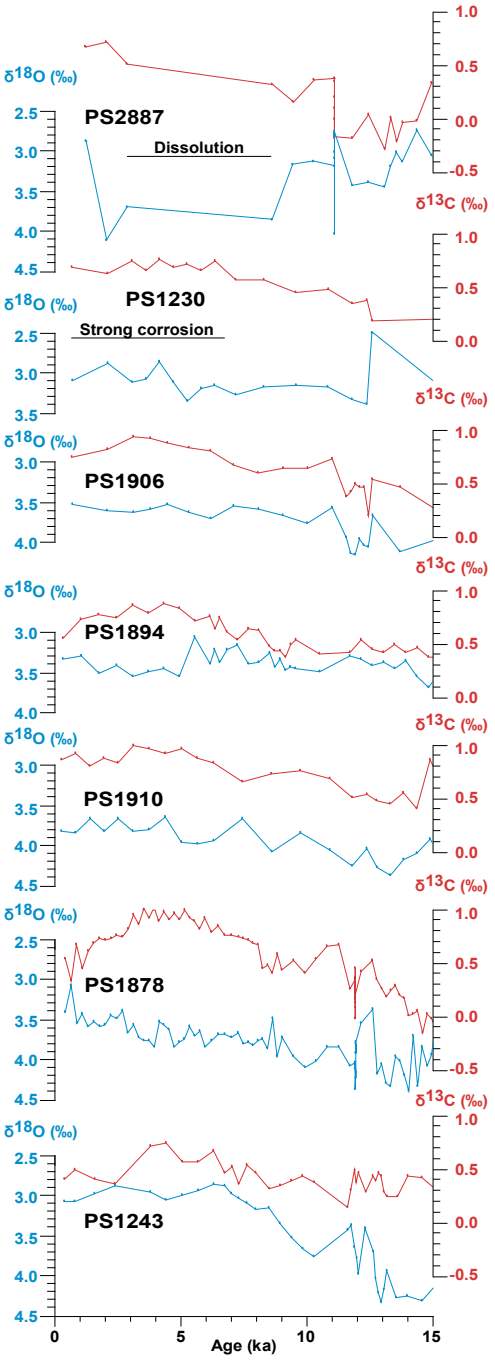


**Fig. 5.** Planktic oxygen and carbon stable isotope records of cores from the Nordic Seas plotted vs. age (since 15 ka).

seems obvious in a perennially ice-covered ocean. However, relatively high $\delta^{13}$C values (> 0.7 ‰) are found at present also in the perennially ice-covered areas of the central Arctic Ocean (Spielhagen and Erlenkeuser, 1994). Therefore, we hesitate to relate the low $\delta^{13}$C solely to the sea ice and/or strong stratification of the upper water layers. In addition, the carbon cycle in the glacial ocean may have been much

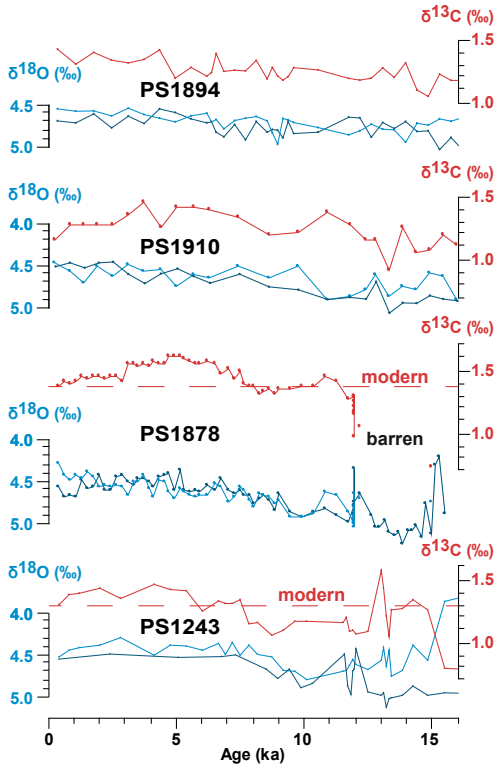


**Fig. 6.** Benthic oxygen (light and dark blue for *C. wuellerstorfi* and *O. umbonatus*, respectively) and carbon (red, *C. wuellerstorfi*) stable isotope records (in ‰ vs. PDB) of cores PS1894, PS1910, PS1878 and PS1243 vs. age (since 16 ka). Broken lines in PS1878 and PS1243 mark modern (core-top) $\delta^{13}$C values of *C. wuellerstorfi* from the central Greenland Sea and site PS1243, respectively (Bauch and Erlenkeuser, 2003).

different than at present, which makes it difficult to unambiguously interpret the carbon isotope record in this interval.

The LGM sediments, especially in cores PS1906 and PS1910, contain high amounts of coarse ice-rafted debris if compared to younger layers (Fig. 3). This indicates that numerous icebergs were passing the area and dropping parts of their freight. The IRD concentration is highly variable and marked by numerous prominent peaks. These peaks clearly coincide with foraminiferal abundance peaks in cores PS1894, PS1878 and partly in core PS1906. As already discussed previously at site PS1878, the IRD peaks may represent sporadic and relatively short intervals of somewhat ameliorated conditions during times of decreased seasonal sea ice and slightly warmer surface water that resulted in a higher biological productivity, an increased IRD delivery, and thus, a higher sedimentation rate (Telesiński et al., 2013). The duration of these intervals may be overrepresented in the sediment record, the most compelling example being the IRD and foraminiferal peaks in core PS1906 at ca. 25–30 cm (ca. 20–22 ka). Variable sedimentation rates and the uncertainties in our age models for the LGM make it difficult to say whether the ameliorated conditions occurred basin wide or had a diachronous nature.

### 6.2 Deglaciation

Prominent low $\delta^{18}$O peaks accompanied by low $\delta^{13}$C values are recorded in the deglacial parts of cores PS1878 (ca. 18 ka) and PS1906 (19.7 ka), as well as PS1230 (19.2 ka, Bauch et al., 2001) and PS2887 (19.6–18.7 ka, Nørgaard-Pedersen et al., 2003). Similar, though more obscure features can be traced in cores PS1894 and PS1910 (Fig. 2). We interpret them as a result of the occurrence of isotopically light freshwater that lowered the regional surface and near-surface water salinity (Sarnthein et al., 1995; Spielhagen et al., 2004; Telesiński et al., 2013). In cores PS1906 and PS1878 the high amplitude of the $\delta^{18}$O peaks is accompanied by low IRD abundance in the respective intervals, which may suggest that the freshwater originated from catastrophic discharges from remote and/or terrestrial sources (e.g., outbursts from ice-dammed or subglacial lakes) rather than from a delivery by melting icebergs or nearby glaciers.

On the other hand, in the well-dated record from core PS2887 (Nørgaard-Pedersen et al., 2003) $\delta^{18}$O values remained low for more than 2 kyr and the interpolated age of the spike in PS1878 (18–15 ka) fits well with the duration of the Heinrich stadial 1 (HS1). This may suggest that the freshwater persisted in the Greenland Sea for several thousand years and that the low foraminiferal abundance during this time might be a result of a salinity decrease below the level tolerated by planktic foraminifers. The lack of IRD might then be caused by a decrease in iceberg mobility and melt rate due to a rigid sea-ice cover that is expected to grow on top of a cold and freshened water surface.

We realize that the reservoir ages during the deglaciation, especially in the event when massive freshwater discharges rapidly affected the ocean's surface, remain highly uncertain and may have been considerably larger than at present (Waelbroeck et al., 2001; Hanslik et al., 2010; Stern and Lisiecki, 2013). Although the low sedimentation rates in some of our cores increase the uncertainty of the $^{14}$C-based age models, our regional comparison shows that the major deglacial freshwater discharges into the western Nordic Seas were roughly coeval. We consider that these events were likely triggered by the global sea level rise that started around 20 ka (Clark and Mix, 2002) and came from the Greenland Ice Sheet and, perhaps, other circum-Arctic ice sheets (e.g., Sarnthein et al., 1995).

The low carbon isotope ratios during these freshwater events (Fig. 2) might be an indication of a reduced ventilation of the upper water column that was forced by a stable, highly stratified surface water lid (cf. Sarnthein et al., 1995; Spielhagen et al., 2004). If the surface stratification of the Greenland Sea was indeed a basin-wide phenomenon, as shown by our records, it supports the interpretation of a slowdown of the Atlantic Meridional Overturning Circulation

(AMOC) during HS1 (McManus et al., 2004; Stanford et al., 2011; Telesiński et al., 2013). Furthermore, it also gives a rough chronological framework for the onset of the deglaciation (ca. 18 ka).

Although our benthic oxygen isotope records do not cover the initial part of HS1, the $\delta^{18}$O data of *O. umbonatus* indicate, like the planktic record, a distinct decrease around 15.5–15.0 ka in PS1878 (Fig. 6). Such simultaneously occurring surface and bottom water depletions in $\delta^{18}$O are often interpreted as a result of brines rejected during sea-ice formation (e.g., Dokken and Jansen, 1999; Hillaire-Marcel and de Vernal, 2008). The likelihood that such brines formed in this way and could sink into intermediate or even much greater depths without significant dilution remains unproven (for a discussion see also Bauch and Bauch, 2001; Rasmussen and Thomsen, 2009). More recently, another scenario was proposed to explain the occurrence of light $\delta^{18}$O excursions during HS1 (Stanford et al., 2011). It suggests that meltwater loaded with fine sediments entered the Nordic Seas below the sea surface as a hyperpycnal flow. In our record, the negative benthic $\delta^{18}$O excursion at 15.5–15.0 ka may result from such a mechanism. However, in the record studied by Stanford et al. (2011), the benthic oxygen isotope depletion has an amplitude larger than the planktic record, which is not observed in our record. Stanford et al. (2011) explain that, after losing the sediment load, the remaining relatively fresh, low density and low-$\delta^{18}$O water rose towards the surface (while strongly mixing with ambient water), resulting in the amplitude difference. Possibly the freshwater event in or close to the Greenland Sea released both a sediment-loaded and a largely sediment-free freshwater plume, which in combination may explain the strong near-surface and weaker bottom water $\delta^{18}$O decreases. The sediment-loaded plume mechanism may also explain the significant thickness of the layers in cores PS1878 and PS2887 with light $\delta^{18}$O values. While the plume was losing its load, sedimentation rates likely increased dramatically in the affected areas, resulting in relatively thick fine-grained deposits. The duration of the freshwater outbursts was probably significantly shorter than what appears from the linear age interpolation between the dating points. However, sea ice may have played a role as a further freshwater supplier by extending the range and duration of the freshwater event.

Following the freshwater event(s), planktic $\delta^{18}$O values increased to $\sim$ 4 ‰ or more (Figs. 2, 5), indicating that the freshwater influence had decreased by this time. Also, the increasing $\delta^{13}$C values may further suggest that either the ventilation and/or the subsurface water structure with respect to stratification and bioproductivity had changed again.

The gradual and low–amplitude changes in the oxygen isotope record of PS1910 make it likely that the site was not directly influenced by major freshwater discharges. Short-lived freshwater events like those recorded in PS1878 between 15 and 13 ka may have taken place at site PS1910 (as well as PS1906 after the major event) but may be obscured by the core's low resolution. The generally heavy $\delta^{18}$O values throughout the deglaciation, as well as later on, do indicate a notable inflow of Atlantic waters to this area.

Site PS1894 is located on the Greenland continental slope, in direct proximity to the EGC and under the sea-ice cover. Thus, the lowest $\delta^{18}$O values in this record might result from the weakest influence of AW and the lowest salinity, compared to other sites. Today, the salinity at site PS1894 is 1–2 psu (practical salinity units) lower than farther to the east, in the ice-free areas (Thiede and Hempel, 1991). In contrast to the other sites, the main onset of the deglaciation (after 17 ka) seems to be characterized by a warming of the (sub)surface water rather than by a freshwater inflow, as the oxygen isotope ratio decrease is accompanied by the appearance of subpolar foraminiferal species (Figs. 2, 4). It is possible that a minor enhancement of the Atlantic Water inflow into the northwestern Greenland Sea coincided with and probably also contributed to the termination of LGM-type conditions and to the onset of deglacial changes at this site. It might seem counterintuitive that at this site, which is the one most affected by PW today, the subpolar species appeared so early and in such high amounts (around 20 %), especially since even in late Holocene sediments this group constitute less than 20 % of the planktic fauna in this area (Husum and Hald, 2012). However, an occurrence of subpolar species, in particular those of smaller sizes, might indicate the advection of Atlantic waters subducted below stratified and sea-ice covered surface water layers (Bauch et al., 2001). Such a mechanism is confirmed by modern oceanographic measurements on a W–E profile across the Greenland Sea, showing higher subsurface temperatures at stations covered with sea ice than in ice-free areas (Thiede and Hempel, 1991).

Although the PS1894 oxygen isotope record does not indicate any major direct freshwater discharges in this area (Fig. 2), surface water salinity was apparently lower than at the other sites, as indicated by the low $\delta^{18}$O values, probably as a result of the proximity of the ice margin and the EGC.

### 6.3 Younger Dryas (YD)

Only core PS1878 contains a clear light $\delta^{18}$O excursion (12.8–11.9 ka) that, according to our age model, fits into the time span of the YD (12.9–11.7 ka, cf. Broecker et al., 2010). However, less prominent oxygen isotope peaks of the same age can be found in cores PS1906 and PS1910, as well as in PS1230 and PS1243 (Bauch et al., 2001). We associate these peaks also with the YD and used them for the correlation of the cores (Figs. 2, 5). The oxygen isotope record of core PS1894 contains no indications that could be linked to the YD cooling. However, as already mentioned above, this record exhibits generally low $\delta^{18}$O values ($< 3.5$ ‰ across the YD interval), often lower than those of the light $\delta^{18}$O excursions in the other records. It indicates that this site was under a constant influence of relatively fresh PW, which makes the identification of a YD freshwater signal difficult.

In general, the origin and cause of the YD has been a matter of debate for decades now (e.g., Broecker et al., 1989; Teller et al., 2005; Murton et al., 2010; Fahl and Stein, 2012; Fisher and Lowell, 2012; Not and Hillaire-Marcel, 2012). A discharge of large amounts of freshwater from the deglacial Lake Agassiz to the North Atlantic and, in particular, to the areas of deep water convection is still considered the most likely cause for the YD (Broecker et al., 2010). While a rerouting from the Gulf of Mexico to the St. Lawrence River was proposed earlier as one triggering mechanism (Broecker et al., 1989), recent modeling results of Condron and Winsor (2012) indicate that only a freshwater discharge to the Arctic (probably via the Mackenzie Valley; cf. Tarasov and Peltier, 2006) was able to reach the deep water formation regions in the North Atlantic (including our study area) and weaken the AMOC sufficiently to trigger the YD. Our finding of a coeval low $\delta^{18}$O signal at ~ 13 ka in Fram Strait and Greenland Sea records is in support of hypotheses that suggest the Arctic region (including the East Greenland margin) as the main source area for the freshwater pulse. It seems unlikely that a large-volume freshwater transport occurred from the south, i.e., opposite to the dominant flow direction in the Greenland Sea. Following the modeling results of Condron and Winsor (2012), our data make the hypothesis of an Arctic trigger for the YD cold event more convincing.

### 6.4 Holocene

Although the onset of the Holocene in our records is expressed by the typical proxy changes for a glacial–interglacial transition, it looks different at the individual sites. In the southern Fram Strait (site PS1906) both the foraminiferal abundance and the percentage of subpolar species increased relatively rapidly around 12 ka. This was possibly related to the onset of enhanced surface flow of the NAC branch along the eastern Nordic Seas following shortly upon the YD (e.g., Sarnthein et al., 2003; Hald et al., 2007; Risebrobakken et al., 2011). Farther south, at sites PS1910 and PS1878, that increase was much more gradual and highest values there were reached between 10 and 8 ka. Subsurface waters at site PS1878 also warmed more slowly reaching ~ 3 °C only around 8 ka (Fig. 7). This confirms that in the earliest Holocene the influence of the melting Greenland Ice Sheet was strong and acted as a negative feedback to the orbitally forced climatic optimum (cf. Blaschek and Renssen, 2013). The decrease of IRD deposition at three of our sites (PS1906, PS1910, PS1878) indicates that only few icebergs still reached the southeastern Greenland Sea due to a northwestward expansion of the warmer water masses. The decrease in IRD deposition was less prominent in the southern Fram Strait at this time, most probably due to the proximity of the Transpolar Drift which still brought numerous icebergs from the Arctic Ocean into this region. Site PS1894 showed the least significant changes at the onset of the Holocene (Figs. 8, 9). The proxy data indicate that the eastern part of

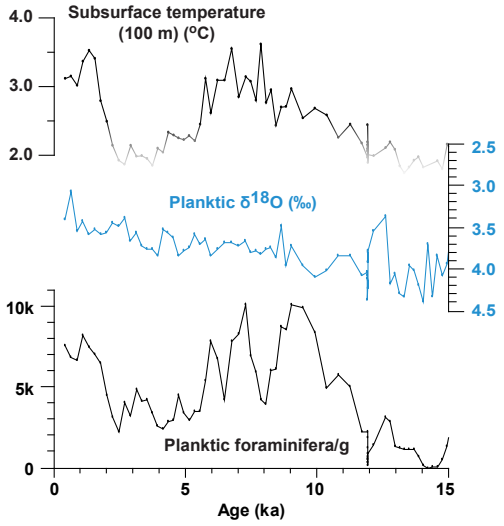


**Fig. 7.** Absolute subsurface temperatures calculated using the transfer function of Husum and Hald (2012) on planktic foraminifera from core PS1878 and planktic oxygen isotope and total planktic foraminiferal abundance records. Calculated temperatures below 2 °C should be considered uncertain.

the Greenland Sea remained under polar conditions with cold surface water, numerous icebergs and sea-ice cover for most of the time.

For the entire study area it is difficult to determine a coeval thermal maximum, which we define as the interval with the highest percentage of subpolar species (or highest absolute temperatures in core PS1878). Not only the course of the initial warming but also the duration and termination of the warmest interval differed between the individual sites. In the southern Fram Strait (site PS1906) the thermal maximum interval apparently started already around 11.5 ka and ended gradually between 7 and 3 ka. At sites PS1894, PS1910 and PS1878 it was significantly shorter and can be dated to ca. 11–9.5, 10.5–7 and 8–5.5 ka, respectively. This might at least in part be attributed to uncertainties in the correlation between the records, which was mainly based on the isotope records. Nevertheless, the onset of the warmest interval around 11–9 ka accords with many other Nordic Seas records (e.g., Bauch et al., 2001; Sarnthein et al., 2003; Giraudeau et al., 2010; Risebrobakken et al., 2011; Husum and Hald, 2012) where the beginning of the Holocene thermal maximum (HTM) was related to maximum insolation in the high latitudes (e.g., Andersen et al., 2004; Risebrobakken et al., 2011) and the maximum in northward oceanic heat transport by the NAC (Risebrobakken et al., 2011). The late onset of the thermal maximum at site PS1878 might have resulted from the large distance between the site and the core of the NAC (Fig. 1). Since this onset was time-transgressive along the main pathway of the NAC (Hald et al., 2007), a similar development may also be expected westward. In principle, the presence of freshwater in the earliest Holocene (Fig. 5)

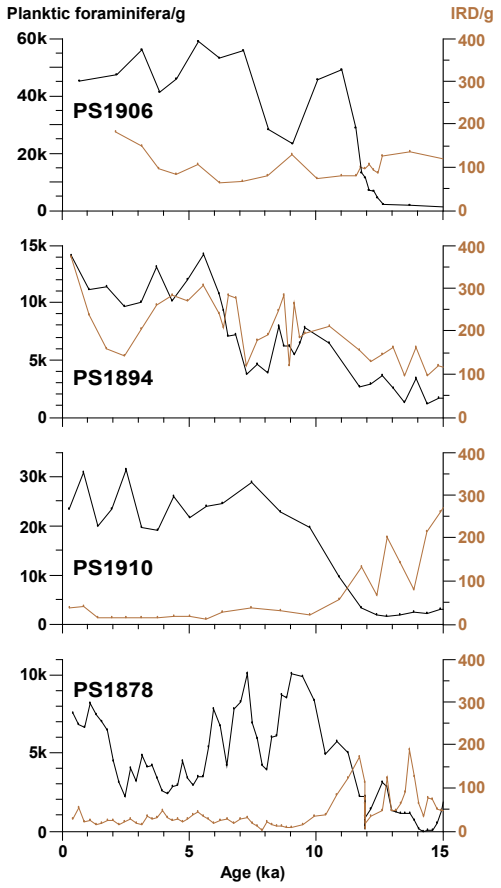


**Fig. 8.** Planktic foraminifera and IRD abundance (per 1 g dry sediment) of cores used in this study, plotted vs. age (since 15 ka).

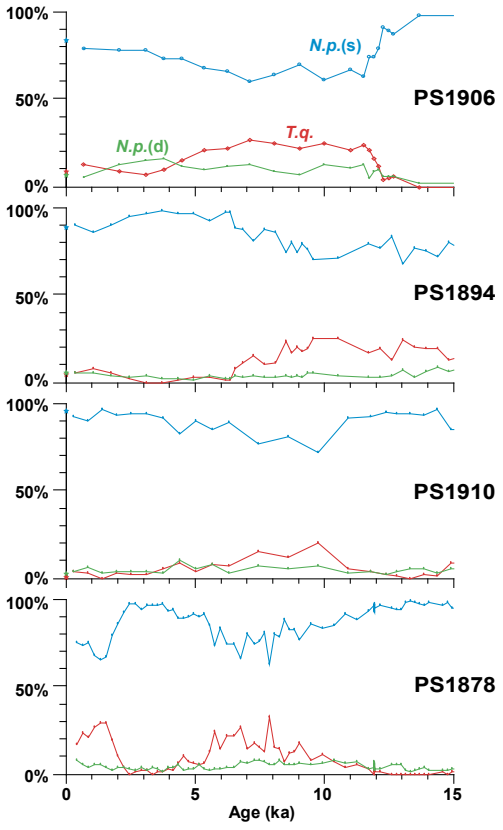


**Fig. 9.** Relative abundance of the three most common planktic foraminifera species in cores used in this study, plotted vs. age (since 15 ka). Abbreviations as in Fig. 4. Asterisks mark the modern (core-top) values (own data).

may have had a cooling effect, but this should have also been the case at the other three sites. Furthermore, the relative proximity of the remnant Greenland Ice Sheet, still delivering cold meltwater, could have acted as a negative feedback for the early Holocene warming (Blaschek and Renssen, 2013). The transfer function yielded temperatures of 3–3.5 °C at 100 m water depth between 8 and 5.5 ka. This is significantly warmer than modern temperatures at this depth in the Vesterisbanken area (max. 2 °C, Thiede and Hempel, 1991) and indicates that the advection of Atlantic waters to the area between 8 (or even 10.5) and 5.5 ka was stronger than at present.

The transition between the thermal maximum and the Neoglacial cooling as found in our records between ca. 6–5 and 3 ka was also not simultaneous and, with the exception of PS1878, was much more gradual than the early Holocene warming (Figs. 7, 9). Although in cores PS1906 and PS1878 relatively late, such a timing is in good general agreement with other studies (e.g., Bauch et al., 2001; Sarnthein et al., 2003; Hald et al., 2007; Giraudeau et al., 2010; Rasmussen and Thomsen, 2010; Husum and Hald, 2012; Werner et al., 2013; for some remarkable exceptions see Risebrobakken et al., 2011). The Neoglacial cooling was very likely forced primarily by decreasing insolation (Andersen et al., 2004), while the regional variations in its timing and scale are a manifestation of the reorganization of the specific water mass configuration in the Nordic Seas. This reorganization involved, e.g., changes in the strength and routing of the individual NAC and EGC branches, the amount of meltwater, and the relocation of the convection centers and eventually resulted in the establishment of a type of overall water mass distribution and circulation as we see it today (Bauch et al., 2001).

The $\delta^{13}$C "plateau" between ca. 7 and 3 ka (Fig. 5) is common in Nordic Seas records (e.g., Vogelsang, 1990; Fronval and Jansen, 1997; Bauch et al., 2001; Sarnthein et al., 2003; Risebrobakken et al., 2011; Werner et al., 2013) and reflects a period of maximum ventilation of subsurface waters, relatively stable and modern-like environmental conditions (Bauch et al., 2001; Sarnthein et al., 2003), and perhaps a significantly changed surface water structure (Bauch and Weinelt, 1997). Its onset also corresponds to the establishment of the modern Iceland–Scotland Overflow Water (Thornalley et al., 2010) and AMOC strengthening (Hall

et al., 2004). Our benthic $\delta^{13}$C records (Fig. 6) and other benthic records from the Nordic Seas (Bauch et al., 2001; Sarnthein et al., 2003) also exhibit relatively high values in this interval. This implies good ventilation of the bottom water and suggests that intensive deep water convection took place in the Nordic Seas between 7 and 3 ka. An AMOC intensification after 7 ka would also imply enhanced inflow of AW and PW into the Greenland Sea since the increased convection rate must be compensated by an increased inflow of both saline AW from the south and cold PW from the north. The increasing influence of cold PW amplified the Neoglacial cooling in the area, which might explain the relatively rapid warm–cold transition at site PS1878 at 5.5 ka, similar to what was found in the eastern Fram Strait (Werner et al., 2013). The cooling, in turn, likely enhanced sea-ice formation and strong winds, which opened up ice leads and provoked super-cooling processes further intensifying deep water formation. The bottom water at site PS1878 was particularly well ventilated compared to other Holocene records from the Nordic Seas (Fig. 6, cf. Bauch et al., 2001; Sarnthein et al., 2003). This indicates that deep convection was taking place in the central Greenland Sea, in the proximity of this site, with maximum vigor between 7 and 3 ka.

The planktic $\delta^{13}$C decrease after around 3 ka, observed in all our records (Fig. 5), appears to be a sound stratigraphic time marker in many Nordic Seas records (Bauch and Weinelt, 1997). Moreover, as it occurs all across the Nordic Seas including the Barents Sea (e.g., Vogelsang, 1990; Fronval and Jansen, 1997; Bauch et al., 2001; Sarnthein et al., 2003; Risebrobakken et al., 2011; Werner et al., 2013) this event clearly bears a supraregional implication. A reconstruction of sea-ice conditions in the Fram Strait (Müller et al., 2012) revealed increasing sea-ice coverage since 8 ka. At about 3 ka a further significant expansion of the sea-ice cover occurred and sea-ice conditions became more fluctuating. Although in the record from the East Greenland Shelf (Müller et al., 2012) no increase in sea-ice coverage is observed before 3 ka (perhaps because this area was strongly influenced by sea ice during the entire Holocene), the total sea-ice cover in the Nordic Seas was probably increasing. A similar timing in ice increase is also confirmed for the western Barents Sea slope (Sarnthein et al., 2003). Renssen et al. (2006) indicated that a negative solar irradiance anomaly and associated cooling may cause an expansion of sea ice and a temporary relocation of deep water formation sites in the Nordic Seas. One of the strongest anomalies in the Holocene occurred between 2.85 and 2.6 ka and could have triggered the sudden increase in sea-ice extent, increased the stratification of the upper water layers and decreased the ventilation of the subsurface water. This solar irradiance anomaly may also have triggered the increase in ice rafting in the North Atlantic around that time (Bond et al., 2001; Renssen et al., 2006).

In two of our benthic carbon isotope records (PS1910 and PS1878, Fig. 6) we observe a decrease of values around 3 ka, which paralleled that in the planktic record. This is, however, not generally the case elsewhere (e.g., at site PS1894 or in the central and eastern Nordic Seas; Bauch et al., 2001; Sarnthein et al., 2003; Werner et al., 2013). The decrease in benthic $\delta^{13}$C values suggests that, probably as a result of a more extensive sea-ice cover and a stronger stratification of the upper water layers, deep convection diminished or did not reach down to maximum depth of the basins any longer (Renssen et al., 2006). Sites PS1910 and PS1878 were most likely located closest to the convection center and the decrease in convection rate or depth was recorded here as a benthic $\delta^{13}$C decrease. At other sites that were located farther from the convection center, the bottom waters were not as well ventilated before 3 ka and therefore the relative decrease in ventilation was not large enough to be recorded in the sediment archive.

As described earlier (Telesiński et al., 2013), significant changes are observed in core PS1878 since 3 ka. The total foraminiferal abundance (Fig. 8) and percentage of subpolar species (Fig. 9) increase and planktic carbon and oxygen isotope ratios decrease. These changes were interpreted as evidence of a warming of subsurface waters caused by an NAO-induced increase in AW inflow, amplified by stronger upper water layers stratification (Telesiński et al., 2013). The benthic data from core PS1878 show that the planktic and the two benthic oxygen isotope records, which in the older part of the record ran roughly parallel to each other, diverge after 3 ka (Figs. 5, 6). The planktic values begin to decrease after the stable interval of the Middle Holocene and *O. umbonatus* values start to increase, while *C. wuellerstorfi* oxygen isotope ratios follow the earlier slightly decreasing trend. As a result of the decrease in convection rate and depth, probably not only the surface and bottom waters began to differentiate from each other, but also, at a smaller scale, the epibenthic and infaunal biotopes became more distinct than before due to more stagnant conditions.

In the other records from the Greenland Sea the changes after 3 ka are not as obvious. At site PS1894, strongly affected by PW, the conditions seem to be similar to those at other sites during the LGM, with at least seasonally open water conditions and somewhat warmer upper water layers (Figs. 5, 8, 9; see discussion above). Virtually no indications of warming or increased AW influence can be found at sites PS1906 and PS1910 at that time.

The high-resolution subsurface temperature reconstruction from site PS1878 indicates a warming from ca. 2 °C at 2.5 ka to 3.5 °C at 1.5 ka, confirming that conditions in the central Greenland Sea in the late Holocene were comparable to the early Holocene warm interval (cf. Telesiński et al., 2013). The scale of this warming (1.5 °C) is comparable to that of the modern warming in the Arctic (e.g., Spielhagen et al., 2011) though, of course, on a significantly longer timescale. A comparison with the faunal data from other Greenland Sea cores (Fig. 9) shows that this phenomenon was confined to the central part of the Greenland Sea and may have resulted from the co-occurrence of the stronger

water column stratification and the enhanced inflow of Atlantic waters to the site.

## 7 Summary and conclusions

With the records presented in this study we were able here to reconstruct for the first time a millennial- to multicentennial-scale image of the late glacial and Holocene paleoceanographic evolution in the northern and central Greenland Sea. Despite the low sedimentation rates in the northern part of the study area and the related chronological uncertainties, the correlation and comparison with a high resolution record PS1878 (Telesiński et al., 2013) allowed us to study the spatial and temporal variability of the most important oceanographic processes. The integration of surface, subsurface and bottom water proxies gave an almost complete image.

During the LGM environmental conditions were to a large extent similar across the Greenland Sea. Cold conditions with a dense sea-ice cover, numerous icebergs and low biological productivity prevailed in the area. During the deglaciation the Greenland Sea was affected by freshwater discharges. Although we argue that they were roughly simultaneous (between 18 and 15 ka) and may have had a common trigger mechanism, their sources and character were probably different. During the YD the Greenland Sea was affected by a major deglacial freshwater discharge most probably originating from the Arctic. Our data suggest a thicker but weaker halocline and a deepening of AW.

The onset, duration and decline of the early Holocene warm interval were apparently different in age and scale at each site, reflecting regional differences in the reorganization of the ocean circulation of the area. As peak warming occurred not simultaneously at all sites, the thermal maximum in the central Greenland Sea was not reached until ca. 8 ka, which is relatively late compared to other Nordic Seas records. Maximum subsurface temperatures ($> 3\,^{\circ}C$) were higher than at present, indicating a strong influence of Atlantic waters. Since 7 ka high $\delta^{13}C$ values, both planktic and benthic, indicate the establishment of the modern ocean circulation system in the Nordic Seas with maximum deep convection in the Greenland Sea. Despite a strong AMOC, decreasing insolation led to the Neoglacial cooling and an increase in sea-ice coverage. At 3–2.8 ka a solar irradiance minimum may have triggered a rapid expansion of the sea-ice cover that led to a stronger stratification of the upper water layers and, subsequently, to a weakening of deep convection in the Greenland Sea and of the AMOC. Eventually, an increase in AW inflow into the Nordic Seas led to subsurface warming in the central Greenland Sea (site PS1878). Probably due to a relatively stable water stratification, as well as increased presence of sea ice (and thus an isolation of the subsurface water from the atmosphere and other water masses), subsurface temperatures rose again to a level comparable with the early Holocene thermal maximum at this site.

Comparison of the Greenland Sea records suggests insolation to be the primary driver controlling the regional paleoceanographic evolution while the routing and intensity of AW inflow seems to control the spatial variability in the area. Other processes – such as sea-ice formation, deep convection, freshwater discharges, etc. – also played an important role in the observed local differences.

*Acknowledgements.* This work is a contribution to the CASE Initial Training Network funded by the European Community's 7th Framework Programme FP7 2007/2013, Marie Curie Actions, under Grant Agreement no. 238111. We thank reviewers Juliane Müller and Thomas Cronin, as well as Christelle Not and Kirstin Werner for their constructive criticism and suggestions which improved the manuscript. Our gratitude goes to Katrine Husum for her help with performing the transfer function calculations. We are grateful to Lulzim Haxhiaj as well as Helmut Erlenkeuser and his staff for performing the stable isotope measurements and to the Leibniz Laboratory, Kiel University, and the Poznan Radiocarbon Laboratory for the AMS $^{14}C$ datings.

The service charges for this open access publication have been covered by a Research Centre of the Helmholtz Association.

Edited by: H. Renssen

## References

Andersen, C., Koç, N., Jennings, A. E., and Andrews, J. T.: Nonuniform response of the major surface currents in the Nordic Seas to insolation forcing: Implications for the Holocene climate variability, Paleoceanography, 19, PA2003, doi:10.1029/2002PA000873, 2004.

Bauch, D. and Bauch, H. A.: Last glacial benthic foraminiferal $\delta^{18}O$ anomalies in the polar North Atlantic: A modern analogue evaluation, J. Geophys. Res., 106, 9135–9143, 2001.

Bauch, H. A. and Erlenkeuser, H.: Interpreting Glacial-Interglacial Changes in Ice Volume and Climate From Subarctic Deep Water Foraminiferal $\delta^{18}O$, in: Earth's Climate and Orbital Eccentricity: The Marine Isotope Stage 11 Question, Geoph. Monog. Series 137, edited by: Droxler, L. H., Poore, A. W., and Burckle, R. Z., American Geophysical Union, Washington, D.C., 87–102, 2003.

Bauch, H. A. and Weinelt, M. S.: Surface water changes in the Norwegian Sea during last deglacial and Holocene times, Quaternary Sci. Rev., 16, 1115–1124, 1997.

Bauch, H. A., Erlenkeuser, H., Spielhagen, R. F., Struck, U., Matthiessen, J., Thiede, J., and Heinemeier, J.: A multiproxy reconstruction of the evolution of deep and surface waters in the subarctic Nordic seas over the last 30,000 yr, Quaternary Sci. Rev., 20, 659–678, 2001.

Blaschek, M. and Renssen, H.: The Holocene thermal maximum in the Nordic Seas: the impact of Greenland Ice Sheet melt and other forcings in a coupled atmosphere–sea-ice–ocean model, Clim. Past, 9, 1629–1643, doi:10.5194/cp-9-1629-2013, 2013.

Bond, G. C., Kromer, B., Beer, J., Muscheler, R., Evans, M. N., Showers, W., Hoffmann, S., Lotti-Bond, R., Hajdas, I., and Bonani, G.: Persistent solar influence on North Atlantic climate during the Holocene, Science, 294, 2130–2136, doi:10.1126/science.1065680, 2001.

Broecker, W. S., Kennett, J. P., Flower, B. P., Teller, J. T., Trumbore, S., Bonani, G., and Wolfli, W.: Routing of meltwater from the Laurentide Ice Sheet during the Younger Dryas cold episode, Nature, 341, 318–321, 1989.

Broecker, W. S., Denton, G. H., Edwards, R. L., Cheng, H., Alley, R. B., and Putnam, A. E.: Putting the Younger Dryas cold event into context, Quaternary Sci. Rev., 29, 1078–1081, doi:10.1016/j.quascirev.2010.02.019, 2010.

Carstens, J., Hebbeln, D., and Wefer, G.: Distribution of planktic foraminifera at the ice margin in the Arctic (Fram Strait), Mar. Micropaleontol., 29, 257–269, 1997.

Clark, D. L. and Hanson, A.: Central Arctic Ocean sediment texture: A key to ice transport mechanism, in: Glacial-marine sedimentation, edited by: Molnia, B. F., Plenum Press, New York, 301–330, 1983.

Clark, P. U. and Mix, A. C.: Ice sheets and sea level of the Last Glacial Maximum, Quaternary Sci. Rev., 21, 1–7, doi:10.1016/S0277-3791(01)00118-4, 2002.

Condron, A. and Winsor, P.: Meltwater routing and the Younger Dryas, P. Natl. Acad. Sci. USA, 109, 19928–19933, doi:10.1073/pnas.1207381109, 2012.

Dokken, T. M. and Jansen, E.: Rapid changes in the mechanism of ocean convection during the last glacial period, Nature, 401, 458–461, 1999.

Duplessy, J. C., Labeyrie, L. D., and Blanc, P. L.: Norwegian Sea Deep Water Variations over the Last Climatic Cycle: Paleo-Oceanographical Implications, in: Long and Short Term Variability of Climate, edited by: Wanner, H. and Siegenthaler, U. Springer, New York, 83–116, 1988.

Fahl, K. and Stein, R.: Modern seasonal variability and deglacial/Holocene change of central Arctic Ocean sea-ice cover: New insights from biomarker proxy records, Earth Planet. Sc. Lett., 351-352, 123–133, doi:10.1016/j.epsl.2012.07.009, 2012.

Fisher, T. G. and Lowell, T. V.: Testing northwest drainage from Lake Agassiz using extant ice margin and strandline data, Quatern. Int., 260, 106–114, doi:10.1016/j.quaint.2011.09.018, 2012.

Fronval, T. and Jansen, E.: Eemian and early Weichselian (140–60 ka) paleoceanography and paleoclimate in the Nordic seas with comparisons to Holocene conditions, Paleoceanography, 12, 443–462, 1997.

Giraudeau, J., Grelaud, M., Solignac, S., Andrews, J. T., Moros, M., and Jansen, E.: Millennial-scale variability in Atlantic water advection to the Nordic Seas derived from Holocene coccolith concentration records, Quaternary Sci. Rev., 29, 1276–1287, doi:10.1016/j.quascirev.2010.02.014, 2010.

Hald, M., Andersson, C., Ebbesen, H., Jansen, E., Klitgaard-Kristensen, D., Risebrobakken, B., Salomonsen, G. R., Sarnthein, M., Sejrup, H. P., and Telford, R. J.: Variations in temperature and extent of Atlantic Water in the northern North Atlantic during the Holocene, Quaternary Sci. Rev., 26, 3423–3440, doi:10.1016/j.quascirev.2007.10.005, 2007.

Hall, I. R., Bianchi, G. G., and Evans, J. R.: Centennial to millennial scale Holocene climate-deep water linkage in the North Atlantic, Quaternary Sci. Rev., 23, 1529–1536, doi:10.1016/j.quascirev.2004.04.004, 2004.

Hansen, B. and Østerhus, S.: North Atlantic–Nordic Seas exchanges, Prog. Oceanogr., 45, 109–208, doi:10.1016/S0079-6611(99)00052-X, 2000.

Hanslik, D., Jakobsson, M., Backman, J., Björck, S., Sellén, E., O'Regan, M., Fornaciari, E., and Skog, G.: Quaternary Arctic Ocean sea ice variations and radiocarbon reservoir age corrections, Quaternary Sci. Rev., 29, 3430–3441, doi:10.1016/j.quascirev.2010.06.011, 2010.

Hillaire-Marcel, C. and de Vernal, A.: Stable isotope clue to episodic sea ice formation in the glacial North Atlantic, Earth Planet. Sc. Lett., 268, 143–150, doi:10.1016/j.epsl.2008.01.012, 2008.

Husum, K. and Hald, M.: Arctic planktic foraminiferal assemblages: Implications for subsurface temperature reconstructions, Mar. Micropaleontol., 96–97, 38–47, doi:10.1016/j.marmicro.2012.07.001, 2012.

Juggins, S.: C2, Version 1.7.2, Software for Ecological and Palaeoecological Data Analysis and Visualization, http://www.campus.ncl.ac.uk/staff/Stephen.Juggins/index.html, University of Newcastle, Newcastle upon Tyne, UK, 2011.

Marshall, J. and Schott, F.: Open-ocean convection: Observations, theory, and models, Rev. Geophys., 37, 1–64, 1999.

McManus, J. F., Francois, R., Gherardi, J.-M., Keigwin, L. D., and Brown-Leger, S.: Collapse and rapid resumption of Atlantic meridional circulation linked to deglacial climate changes, Nature, 428, 834–837, doi:10.1038/nature02494, 2004.

Müller, J., Werner, K., Stein, R., Fahl, K., Moros, M., and Jansen, E.: Holocene cooling culminates in sea ice oscillations in Fram Strait, Quaternary Sci. Rev., 47, 1–14, doi:10.1016/j.quascirev.2012.04.024, 2012.

Murton, J. B., Bateman, M. D., Dallimore, S. R., Teller, J. T., and Yang, Z.: Identification of Younger Dryas outburst flood path from Lake Agassiz to the Arctic Ocean, Nature, 464, 740–743, doi:10.1038/nature08954, 2010.

Nørgaard-Pedersen, N., Spielhagen, R. F., Erlenkeuser, H., Grootes, P. M., Heinemeier, J., and Knies, J.: Arctic Ocean during the Last Glacial Maximum: Atlantic and polar domains of surface water mass distribution and ice cover, Paleoceanography, 18, 1–19, doi:10.1029/2002PA000781, 2003.

Not, C. and Hillaire-Marcel, C.: Enhanced sea-ice export from the Arctic during the Younger Dryas, Nature Comm., 3, 647, doi:10.1038/ncomms1658, 2012.

Nürnberg, D., Wollenburg, I., Dethleff, D., Eicken, H., Kassens, H., Letzig, T., Reimnitz, E., and Thiede, J.: Sediments in Arctic sea ice: implications for entrainment, transport and release, Mar. Geol., 104, 185–214, 1994.

Rasmussen, T. L. and Thomsen, E.: Stable isotope signals from brines in the Barents Sea: Implications for brine formation during the last glaciation, Geology, 37, 903–906, doi:10.1130/G25543A.1, 2009.

Rasmussen, T. L. and Thomsen, E.: Holocene temperature and salinity variability of the Atlantic Water inflow to the Nordic seas, Holocene, 20, 1223–1234, doi:10.1177/0959683610371996, 2010.

Reimer, P., Baillie, M., Bard, E., Bayliss, A., Beck, J. W., Blackwell, P. G., Bronk Ramsey, C., Buck, C. E., Burr, G. S., Edwards, R. L., Friedrich, M., Grootes, P. M., Guilderson, T. P., Hajdas, I., Heaton, T. J., Hogg, A. G., Hughen, K. A., Kaiser, K. F., Kromer, B., McCormac, F. G., Manning, S. W., Reimer, R. W., Richards, D. A., Southon, J. R., Talamo, S., Turney, C. S. M., van der Plicht, J., and Weyhenmeyer, C. E.: IntCal09 and Marine09 radiocarbon age calibration curves, 0–50,000 years cal BP, Radiocarbon, 51, 1111–1150, 2009.

Renssen, H., Goosse, H., and Muscheler, R.: Coupled climate model simulation of Holocene cooling events: oceanic feedback amplifies solar forcing, Clim. Past, 2, 79–90, doi:10.5194/cp-2-79-2006, 2006.

Risebrobakken, B., Dokken, T., Smedsrud, L. H., Andersson, C., Jansen, E., Moros, M., and Ivanova, E. V.: Early Holocene temperature variability in the Nordic Seas: The role of oceanic heat advection versus changes in orbital forcing, Paleoceanography, 26, PA4206, doi:10.1029/2011PA002117, 2011.

Rudels, B. and Quadfasel, D.: Convection and deep water formation in the Arctic Ocean-Greenland Sea System, J. Mar. Syst., 2, 435–450, doi:10.1016/0924-7963(91)90045-V, 1991.

Rudels, B., Friedrich, H. J., and Quadfasel, D.: The Arctic Circumpolar Boundary Current, Deep Sea-Res. Pt. II, 46, 1023–1062, doi:10.1016/S0967-0645(99)00015-6, 1999.

Sarnthein, M., Jansen, E., Weinelt, M., Arnold, M., Duplessy, J. C., Erlenkeuser, H., Flatøy, A., Johannessen, G., Johannessen, T., Jung, S., Koc, N., Labeyrie, L., Maslin, M., Pflaumann, U., and Schulz, H.: Variations in Atlantic surface ocean paleoceanography, 50°–80° N: A time-slice record of the last 30,000 years, Paleoceanography, 10, 1063–1094, 1995.

Sarnthein, M., van Kreveld, S., Erlenkeuser, H., Grootes, P. M., Kucera, M., Pflaumann, U., and Schulz, M.: Centennial-to-millennial-scale periodicities of Holocene climate and sediment injections off the western Barents shelf, 75° N, Boreas, 32, 447–461, doi:10.1080/03009480310003351, 2003.

Spielhagen, R. F. and Erlenkeuser, H.: Stable oxygen and carbon isotopes in planktic foraminifers from Arctic Ocean surface sediments: Reflection of the low salinity surface water layer, Mar. Geol., 119, 227–250, doi:10.1016/0025-3227(94)90183-X, 1994.

Spielhagen, R. F., Baumann, K.-H., Erlenkeuser, H., Nowaczyk, N. R., Nørgaard-Pedersen, N., Vogt, C., and Weiel, D.: Arctic Ocean deep-sea record of northern Eurasian ice sheet history, Quaternary Sci. Rev., 23, 1455–1483, doi:10.1016/j.quascirev.2003.12.015, 2004.

Spielhagen, R. F., Werner, K., Aagaard-Sørensen, S., Zamelczyk, K., Kandiano, E., Budeus, G., Husum, K., Marchitto, T. M., and Hald, M.: Enhanced Modern Heat Transfer to the Arctic by Warm Atlantic Water, Science, 331, 450–453, doi:10.1126/science.1197397, 2011.

Stanford, J. D., Rohling, E. J., Bacon, S., Roberts, A. P., Grousset, F. E., and Bolshaw, M.: A new concept for the paleoceanographic evolution of Heinrich event 1 in the North Atlantic. Quaternary Sci. Rev., 30, 1047–1066, doi:10.1016/j.quascirev.2011.02.003, 2011.

Stern, J. V. and Lisiecki, L. E.: North Atlantic circulation and reservoir age changes over the past 41,000 years, Geophys. Res. Lett., 40, 3693–3697, doi:10.1002/grl.50679, 2013.

Stuiver, M. and Reimer, P. J.: Radiocarbon calibration program, Radiocarbon, 35, 215–230, 1993.

Swift, J.: The Arctic Waters, in: The Nordic Seas, edited by: Hurdle, B., Springer, New York, 129–151, 1986.

Tarasov, L. and Peltier, W. R.: A calibrated deglacial drainage chronology for the North American continent: evidence of an Arctic trigger for the Younger Dryas, Quaternary Sci. Rev., 25, 659–688, doi:10.1016/j.quascirev.2005.12.006, 2006.

Telesiński, M. M., Spielhagen, R. F., and Lind, E. M.: A high-resolution Late Glacial and Holocene paleoceanographic record from the Greenland Sea, Boreas, doi:10.1111/bor.12045, in press, 2013.

Teller, J. T., Boyd, M., Yang, Z., Kor, P. S. G., and Mokhtari Fard, A.: Alternative routing of Lake Agassiz overflow during the Younger Dryas: new dates, paleotopography, and a re-evaluation, Quaternary Sci. Rev., 24, 1890–1905, doi:10.1016/j.quascirev.2005.01.008, 2005.

Thiede, J. and Hempel, G.: The Expedition ARKTIS-VII/1 of RV "POLARSTERN" in 1990, Ber. Polarforsch., 80, 137 pp., 1991.

Thornalley, D. J. R., Elderfield, H., and McCave, I. N.: Intermediate and deep water paleoceanography of the northern North Atlantic over the past 21,000 years, Paleoceanography, 25, 1–17, doi:10.1029/2009PA001833, 2010.

Vogelsang, E.: Paläo-Ozeanographie des Europäischen Nordmeeres an Hand stabiler Kohlenstoff- und Sauerstoffisotope – Paleoceanography of the Nordic seas on the basis of stable carbon and oxygen isotopes, Berichte aus dem Sonderforschungsbereich 313, Nr. 23, Univ. Kiel, Kiel, 1990.

Waelbroeck, C., Duplessy, J. C., Michel, E., Labeyrie, L., Paillard, D., and Duprat, J.: The timing of the last deglaciation in North Atlantic climate records, Nature, 412, 724–727, doi:10.1038/35089060, 2001.

Werner, K., Spielhagen, R. F., Bauch, D., Christian Hass, H., and Kandiano, E.: Atlantic Water advection versus sea-ice advances in the eastern Fram Strait during the last 9 ka: Multiproxy evidence for a two-phase Holocene, Paleoceanography, 28, 283–295, doi:10.1002/palo.20028, 2013.

# 5. Evolution of the central Nordic Seas over the last 20 thousand years

# Evolution of the central Nordic Seas over the last 20 thousand years

M. M. Telesiński[1], H. A. Bauch[1, 2], R. F. Spielhagen[1, 2], and E. S. Kandiano[1, 3]

[1] GEOMAR Helmholtz Centre for Ocean Research Kiel, Wischhofstrasse 1-3, 24148 Kiel, Germany,

[2] Academy of Sciences, Humanities, and Literature, 53151 Mainz, Germany

[3] Currently: Royal Netherlands Institute for Sea Research, Texel, The Netherlands

## Abstract

The deep and surface water paleoceanographic evolution of the central Nordic Seas over the last 20 thousand years was reconstructed using various micropaleontological, isotopic and lithological proxy data. The comparison with other records from the region shows high spatial and temporal complexity of the oceanic circulation in the region. During the early deglaciation a roughly simultaneous collapse of the ice sheets surrounding the Nordic Seas released large amounts of freshwater that affected both the surface and bottom water circulation and significantly contributed to Heinrich stadial 1. During the Younger Dryas the central Nordic Seas were affected by the last major freshwater plume originating most probably from the Arctic Ocean. After ice rafting ceased around 11 ka subsurface temperatures started to rise. Enhanced Atlantic Water advection and subsurface temperatures reached their maximum later than in the eastern Nordic Seas due to the gradual re-routing of the Atlantic Water flow

and the establishment of the Greenland Sea gyre. A distinct temperature and bioproductivity anomaly related with the 8.2 ka event was observed, especially in the Lofoten Basin. The Holocene thermal maximum ended in the Greenland Basin ca. 5.5 ka, triggered by an increase in sea-ice export from the Arctic. In the Lofoten Basin the cooling occurred later, after 4 ka, and was associated with a weakening of the overturning circulation. The Neoglacial cooling was reached ca. 3 ka, together with low solar irradiance, expanding sea-ice and a weakened deep convection. At ca. 2 ka subsurface temperatures began to rise again due to increasing influence of Atlantic Waters.

## 5.1. Introduction

The transition from the Last Glacial Maximum (LGM) into the Holocene and the paleoceanographic evolution of the present interglacial in the Nordic Seas have been a focus of numerous studies (e.g., Hald et al., 2007; Lekens et al., 2005; Müller et al., 2009; Nørgaard-Pedersen et al., 2003; Rasmussen et al., 2013; Risebrobakken et al., 2011; Weinelt et al., 2003; Werner et al., 2013). However, apart from a small number of exceptions (Bauch and Weinelt, 1997; Bauch et al., 2001a; Fronval and Jansen, 1997; Müller et al., 2012), most of the studies concentrate on records from along the Norwegian-Svalbard continental margin. The central part of the basin, despite its importance for the overturning circulation (Marshall and Schott, 1999; Rudels and Quadfasel, 1991), remains largely unexplored in terms of the oceanographic development. The two main reasons for this situation are the difficult accessibility of the appropriate study areas and problems to find high resolution, undisturbed sedimentary sequences in this remote, cold and largely sea ice-covered region.

A study of high resolution sedimentary records from the central Nordic Seas helps to gain a better understanding of processes and forcings that govern the oceanographic evolution not only of the basin itself, but of the overall North Atlantic region in general. Freshwater outbursts from glaciated areas and melting icebergs affected the proximal ocean environment increasingly since the onset of the last deglaciation (Álvarez-Solas et al., 2011; Condron and Winsor, 2012; Seidenkrantz et al., 2012). That situation enhanced surface stratification, weakened the overturning circulation, and the resulting surface freshening enabled more seasonal sea-ice production. However, the intensity of these meltwater events, their sources and their influence on the climate evolution remains largely unknown (e.g., Sarnthein et al., 1995; Tarasov and Peltier, 2006). While the onset of the Holocene warmth was to a large extent induced by high summer insolation in the northern polar latitudes, a detailed image of the deglacial-interglacial transition appears much more complex (Andersen et al., 2004a; Risebrobakken et al., 2011). The exact timing of the warming, the duration and amplitude of the thermal maximum and the character of its termination depended largely on the intensity and routing of the Atlantic Water advected into the Nordic Seas (e.g., Giraudeau et al., 2010) and feedbacks from the remnant ice sheets (Blaschek and Renssen, 2013) or sea ice (Müller et al., 2009). The Holocene, earlier considered a relatively stable interval (Grootes et al., 1993), was punctuated by numerous cooling events (Andersen et al., 2004b; Renssen et al., 2006; Rohling and Pälike, 2005; Wanner et al., 2011; Werner et al., 2013). Even the late Holocene, the most recent part of the present interglacial, still seems to bear some mysteries (Aagaard-Sørensen et al., 2014a; Spielhagen et al., 2011) and also requires further studies to be better understood.

In previous studies Telesiński et al. (2014a, 2014b) investigated a multicentennial record from the central Greenland Sea, which shed some more light on the

paleoceanographic evolution of this area. However, due to the high oceanographic complexity of the Nordic Seas a major gap remained between this cold Greenland Basin and the area farther east, the Lofoten Basin where the warm Norwegian Atlantic Current passes through on its way into the Arctic Ocean. Here we present the relatively high resolution core M17730-4 from the Lofoten Basin, in the northern Norwegian Sea. We compare it with core PS1878 from the Greenland Basin (Telesiński et al., 2014b) as well as other high-resolution records from the region to relate the evolution of the Greenland Sea and the eastern Nordic Seas and to obtain a more complete view on the evolution of the Nordic Seas since the LGM.

## 5.2. Study area

At present, the Nordic Seas are bathed by two main surface-water currents (Fig. 5.1.). The main flow of the North Atlantic Current (NAC) propagates northward from the Faroe-Shetland Channel, along the Norwegian and Barents Sea continental margins and through the eastern Fram Strait where it enters the Arctic Ocean, transporting relatively warm and saline Atlantic Water (AW). The East Greenland Current (EGC) enters the Nordic Seas from the north through the western Fram Strait, flows southward along the Greenland continental margin, and leaves through the Denmark Strait. It transports cold and low-saline Polar Water (PW) carrying sea-ice and icebergs from the Arctic Ocean. Due to this oceanographic pattern a strong east-west gradient across the Nordic Seas exists both in surface water temperature and salinity. Two north-south trending oceanographic fronts run roughly parallel to the main current flow directions. The Polar Front separates PW from Arctic Water (ArW), a product of PW and AW mixing, while the Arctic Front constitutes a boundary between ArW and AW (Swift,

1986). The strong zonation of the Nordic Seas makes them highly susceptible to any changes in the oceanographic pattern.

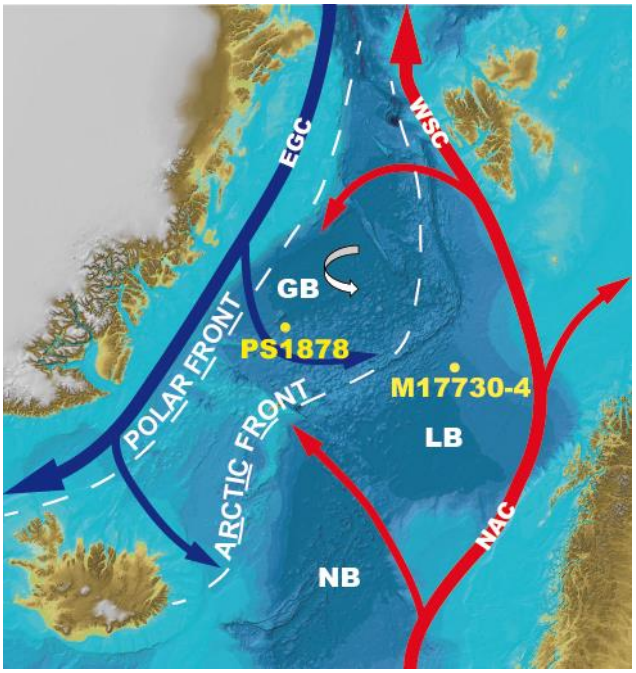


Fig. 5.1. Present day surface water circulation in the Nordic Seas. Cores used in this study are marked by yellow dots. Red arrows indicate Atlantic Water, blue arrows – Polar Water, white broken lines – oceanographic fronts. White arrow – present-day deep convection (Marshall and Schott, 1999). EGC – East Greenland Current, GB – Greenland Basin, LB – Lofoten Basin, NAC – North Atlantic Current, NB – Norwegian Basin, WSC – West Spitsbergen Current. Bathymetry from The International Bathymetric Chart of the Arctic Ocean (http://www.ibcao.org, 2012).

The ArW domain between the Polar and Arctic fronts is the area where branches of NAC and EGC create a cyclonic gyre and where deep water convection and formation of North Atlantic Deep Water (NADW) takes place, with sea-ice playing a decisive preconditioning role (Marshall and Schott, 1999). In early winter the formation of sea-ice leads to brine rejection, an increase in surface layer density, and cooling of the mixed layer. Later in winter, the ice forms a wedge (the Is Odden) enclosing an ice-free bay (the Nord Bukta) – a result of the southward ice transport by winds. Subsequently, the mixed layer deepens to 300-400 m, also as a result of strong winds. Finally, typically around

March, preconditioning is advanced enough for the deep (>2000 m) convection to develop in the ice-free areas (Marshall and Schott, 1999; Rudels and Quadfasel, 1991).

At present, site M17730-4 is located under the direct influence of the NAC and its westerly branches but relatively close to the Arctic Front. Site PS1878 belongs to the ArW domain and is located near the convection center (Telesiński et al., 2014b). Thus, paleoceanographic records from these sites will allow a comparative study of the temporal evolution of the Greenland Sea gyre and westward advection of AW into the central Nordic Seas.

## 5.3. Material and methods

Core M17730-4 (72°06.7'N, 07°23.3'E, 2749 m water depth) is a kasten core retrieved from the Lofoten Basin in the northern Norwegian Sea (Fig. 5.1.). It has previously been studied by Weinelt (1993) and Bauch and Weinelt (1997) but with a lower sampling resolution. Similar to core PS1878 (Telesiński et al., 2014a, 2014b), it was sampled continuously every 1 cm. Samples were freeze-dried, wet-sieved with deionized water through a 63 μm mesh, and dry-sieved into size fractions using 125 μm, 150 μm, 250 μm, 500 μm and 1000 μm mesh sizes. Each size fraction was weighed.

As the original, onboard-made depth scale of the core (Weinelt, 1993) did not quite match with our new measurements (likely due to some drying up and shrinking of the material during storage) we had to correlate the two depth scales using characteristic lithological horizons in the actual core material and in the original core photographs to be able to apply the $^{14}C$ dates of Weinelt (1993) to our record. Thus, a new depth scaling was

established (Table 5.1.) and all the depths given here refer to it unless otherwise indicated (Fig. 5.2.).

Table 5.1. Tie points between the original depth scale of core M17730-4 (Weinelt, 1993) and the depth scale used in this study.

| Depth (Weinelt, 1993) (cm) | Depth (this study) (cm) |
|---|---|
| 21,0 | 21,5 |
| 32,0 | 32,5 |
| 64,6 | 63,5 |
| 88,5 | 85,5 |
| 110,0 | 104,5 |
| 131,0 | 123,5 |

Planktic foraminifera census counts were conducted on representative splits (>300 specimens) of the >150 μm size fraction and were used to calculate the absolute faunal abundances (specimens per 1 g dry sediment) and relative abundances of individual species.

Rock grains >150 μm were counted every 1-2 cm and provided information on ice-rafting. As ice-rafted debris (IRD) we interpret here all lithic grains >150 μm. Such coarse particles can be transported into a deep ocean basin preferentially by icebergs while sea ice often transports finer material (Nürnberg et al., 1994). To provide clues on the origin of IRD, several types were identified, the most common of them being crystalline and clastic rock fragments. Organic-rich, clastic IRD is common in glacial sediments from the eastern Nordic Seas (e.g., Bischof, 1994; Bischof et al., 1997) and is interpreted as originating from the wide and shallow western Eurasian shelves (Bauch et al., 2001a; Wagner and Henrich, 1994). For comparison we present similar data from core PS1878 but for the >250 μm size fraction.

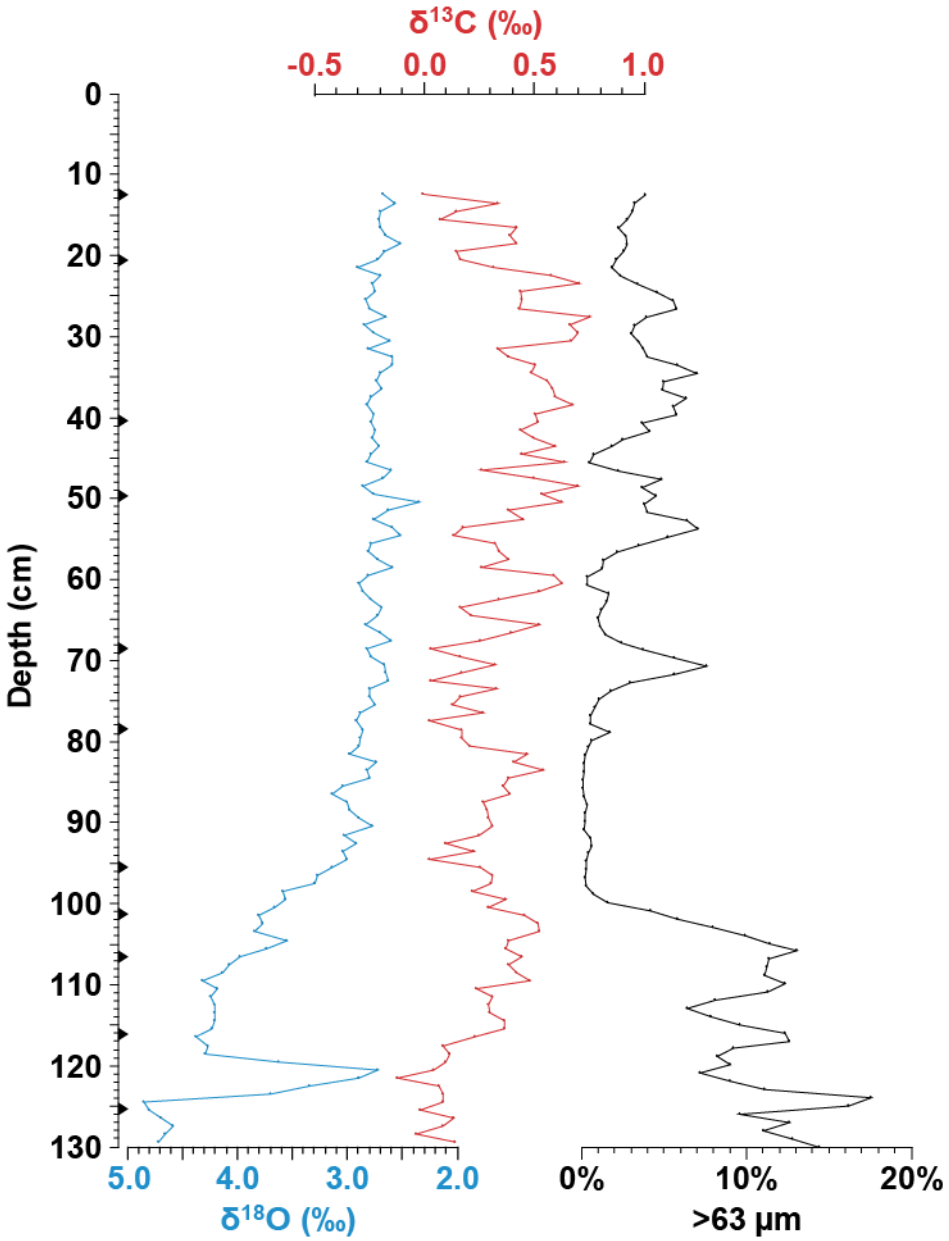


Fig. 5.2. M17730-4 proxy records versus depth: oxygen (blue) and carbon (red) isotope ratios of planktic foraminifera *N. pachyderma* (sin), >63 µm fraction content (black). Black triangles mark the AMS $^{14}$C dates.

Stable oxygen and carbon isotope analyses were performed on planktic species Neogloboquadrina *pachyderma* (sin.) and two benthic species - the epibenthic *Cibicidoides wuellerstorfi* and the shallow infaunal *Oridorsalis umbonatus*. Twenty-five specimens were picked from the 125–250 µm (*N. pachyderma* (sin) and *O. umbonatus*) or 250-500 µm (*C. wuellerstorfi*) size fraction and crushed to minimize the risk of

performing the measurements on reworked/anomalous material. All stable isotope analyses were carried out in the stable isotope laboratory of GEOMAR using a Finnigan MAT 253 mass spectrometer system and a Kiel IV Carbonate Preparation Device. Results are expressed in the δ notation referring to the PDB standard and are given as $\delta^{18}O$ and $\delta^{13}C$. Because of departures from isotopic calcite equilibrium, the measured $\delta^{18}O$ values of *C. wuellerstorfi* and *O. umbonatus* were corrected by +0.64 and +0.36‰, respectively (Duplessy et al., 1988).

To retrieve subsurface temperatures (SSTs) from foraminiferal census data the SIMMAX technique, a variation of the modern analogue technique (MAT) approach, was applied. The relation between foraminiferal diversities and SSTs was established by using the North Atlantic part of the surface sediment samples foraminiferal database (Pflaumann et al., 2003) linked to oceanographic atlas SST data of 100 m water depth layer (Levitus and Boyer, 1994). The used winter and summer temperatures represent average values for February to April and August to October, respectively. It should be noted that below 3°C SIMMAX tends to overestimate temperatures (Pflaumann et al., 2003).

## 5.4. Chronology

Details on the age control of core PS1878 were given by Telesiński et al. (2014b). For the present study we obtained an additional date at 73.5 cm (corrected core depth) to improve the older part of the age model. The chronology of core 17730-4 is based on eleven AMS $^{14}C$ dates measured on *N. pachyderma* (sin.) (Table 5.2.). Seven of them were taken from Bauch and Weinelt (1997) while the other four are from this study and were obtained to improve and verify the previous age model. All radiocarbon ages were

corrected for a reservoir age of 400 years, calibrated using Calib Rev 6.1.0 software (Stuiver and Reimer, 1993) and the Marine09 calibration curve (Reimer et al., 2009), and are given in thousand calendar years before AD 1950 (ka).

Table 5.2. AMS $^{14}$C measurements and their calibrated ages for the cores used in the study.

| Lab. no. | Original depth (cm) | Corrected depth (cm) | $^{14}$C age ± error | Calibrated age (a BP) |
|---|---|---|---|---|
| Core PS1878-2 | | | | |
| Poz-45376 | 0,5 | 0,5 | 775 ± 35 | 426 |
| Poz-45377 | 12,5 | 12,5 | 3300 ± 40 | 3143 |
| Core PS1878-3 | | | | |
| Poz-45378 | 11,5 | 12,5 | 3295 ± 35 | 3139 |
| Poz-45380 | 19,5 | 20,5 | 4525 ± 35 | 4746 |
| Poz-54381 | 25,5 | 26,5 | 5580 ± 50 | 5961 |
| Poz-54382 | 30,5 | 31,5 | 6760 ± 50 | 7295 |
| Poz-45384 | 39,5 | 40,5 | 8410 ± 60 | 9028 |
| Poz-45385 | 58,5 | 59,5 | 11100 ± 60 | 12613 |
| Beta-367894 | 72,5 | 73,5 | 14050 ± 60 | 16800 |
| KIA 47284 | 95,5 | 96,5 | 16620 ± 110 | 19266 |
| Core M17730-4 | | | | |
| Beta-367895 | 12,0 | 12,5 | 2240 ± 30 | 1850 |
| (Weinelt, 1993) | 20,0 | 20,5 | 3330 ± 100 | 3200 |
| (Weinelt, 1993) | 40,0 | 40,1 | 5610 ± 70 | 5990 |
| (Weinelt, 1993) | 50,0 | 49,7 | 6800 ± 110 | 7320 |
| (Weinelt, 1993) | 70,0 | 68,5 | 8470 ± 90 | 9080 |
| Beta-367896 | 81,0 | 78,5 | 8980 ± 40 | 9620 |
| (Weinelt, 1993) | 100,0 | 95,6 | 9520 ± 590 | 10400 |
| Beta-367897 | 106,6 | 101,5 | 10490 ± 50 | 11690 |
| (Weinelt, 1993) | 112,0 | 106,3 | 11590 ± 100 | 13110 |
| (Weinelt, 1993) | 123,0 | 116,3 | 13030 ± 120 | 15000 |
| Beta-367898 | 133,2 | 125,5 | 15590 ± 60 | 18540 |

The age–depth relations and sedimentation rates of both cores are shown in Fig. 5.3. The interval between 73.5 and 96.5 cm in core PS1878 shows a sedimentation rate that is anomalously high for this record, as discussed below. Therefore, to extrapolate the age of the lowermost section of the core we used the sedimentation rate of the 59.5 to 73.5 cm interval. As a result, the yielded age of the bottom of the core (24.4 ka) is ca. 2 kyr older than the one reported by Telesiński et al. (2014b). The average sedimentation

rate of core 17730-4 amounts to ~6.6 cm $kyr^{-1}$ and the record represents the time period between 19.6 and 1.8 ka. The dating at 95.6 cm (Weinelt, 1993; original depth 100 cm) gave an unusually large error (±590 $^{14}C$ years BP). Because the obtained calibrated age (10.4 ka) fits relatively well into our new age model, we did not leave this date out. However, it should still be kept in mind that the possible age range at this level may vary from 9.6 to 11.1 ka (1σ range).

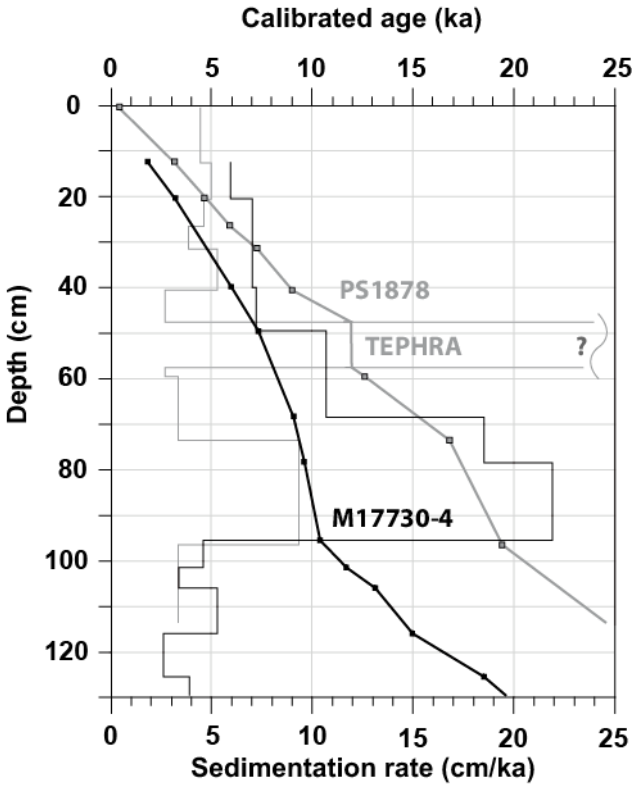


Fig. 5.3. Age-depth plot (thick lines with squares) and sedimentation rates (thin lines) of cores M17730-4 (black lines) and PS1878 (gray lines).

## 5.5. Results

As the results from core PS1878 were already described in detail by Telesiński et al. (2014a, 2014b) here we briefly present only some additional, new data from that core (crystalline and clastic IRD counts) and focus on core M17730-4.

### 5.5.1. Planktic foraminifera and reconstructed subsurface temperatures

The lowermost part of core M17730-4 contains a fauna which is dominated by the polar species *N. pachyderma* (sin) (Fig. 5.4.). The foraminiferal abundances remained low between 20 and 16.5 ka. They then increased slightly until 11 ka showing four broad peaks. Between 11 and 9.5 ka the abundances decreased again and reached an absolute minimum around 10 ka. In this period, subpolar species (mainly *N. pachyderma* (dex) but also *Turborotalita quinqueloba, Globigerina bulloides* and others) increased in relative abundance. Most significantly, the percentage of *N. pachyderma* (dex) rose to almost 30% around 9.8 ka. This is followed by a massive peak in foraminiferal abundance and percentage of *T. quinqueloba* at 9.1 ka. Both proxies reached their absolute maximum values. The following interval (9.1-1.9 ka) was characterized by high variability in both proxies. Intervals with high foraminiferal abundances (9.3-8.4, 8-7, 6.4-3.5 and after 2 ka) are also characterized by high percentages of subpolar species (mainly *T. quinqueloba*, up to 50-60%). They are separated by intervals with lower abundances and higher *N. pachyderma* (sin) percentages.

The reconstructed summer SSTs are generally ca. 0.6°C higher than the winter temperatures. Before 17 ka the summer SSTs increased slightly slightly above 1°C. Subsequently they decreased to ca. 0.5-1°C and remained at this level until ca. 10.5 ka. A warm episode centered around 10.2 ka with summer SSTs of up to 3.7°C was followed by a cooling around 10 ka. Subsequently, the SSTs reached their maximum of up to 6.3°C

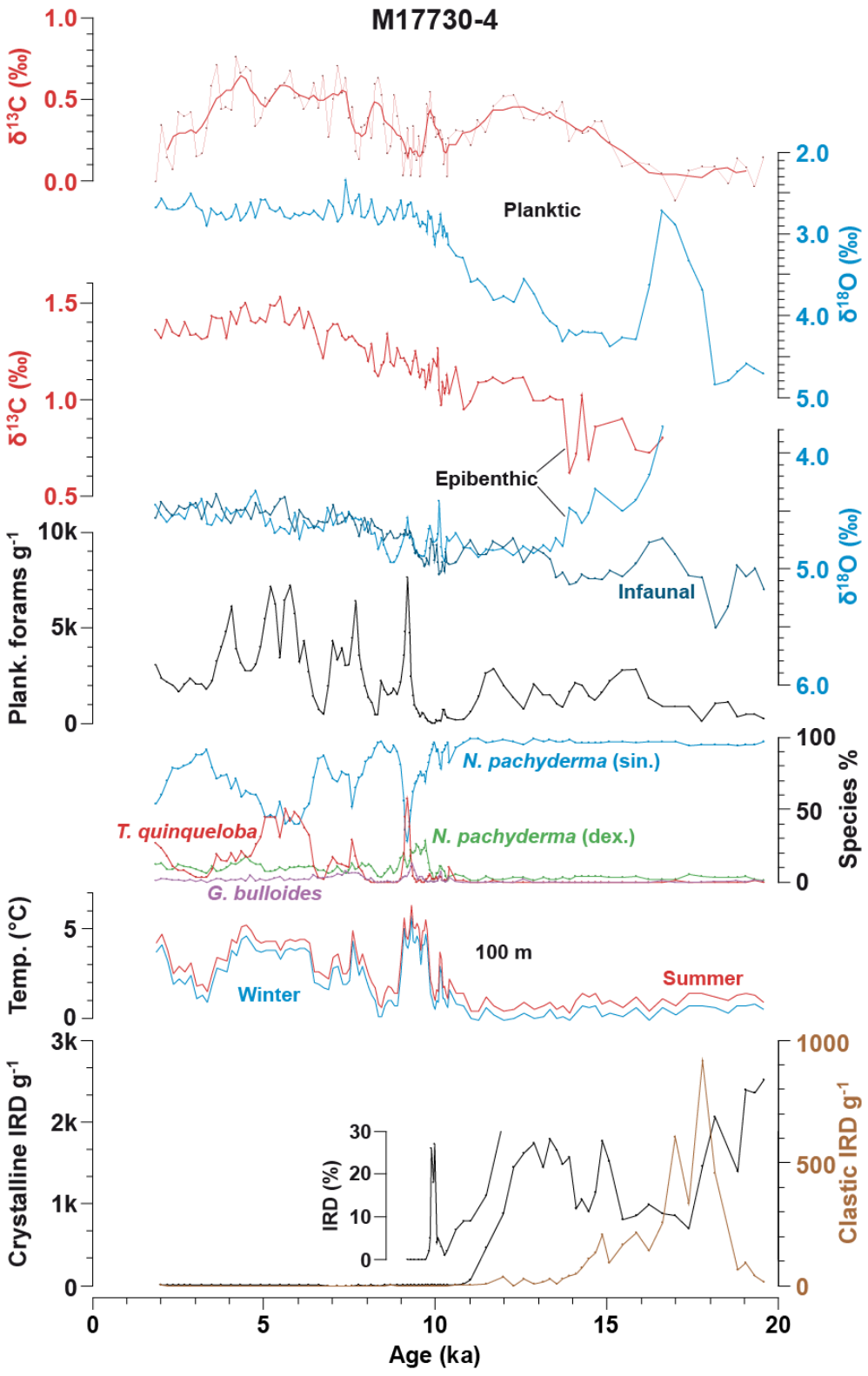


Fig. 5.4. M17730-4 paleoceanographic record: stable carbon (red, thin line – raw data, thick lines – five-point running means) and oxygen (blue) isotope ratios of planktic foraminifera *N. pachyderma* (sin), epibenthic *C. wuellerstorfi* and infaunal *O. umbonatus*, total abundance of planktic foraminifera, relative abundance of four dominant planktic foraminiferal species, reconstructed subsurface (100 m) summer (red) and winter (blue) temperatures, total abundance of crystalline (black) and clastic (brown) IRD, and relative abundance of IRD (vs. all grains >150 µm, 12-9 ka).

(summer) between 9.8 and 9 ka. A major cooling between 8.9 and 7.9 ka (summer SSTs down to 0.6°C) was followed by a relatively stable warm interval (summer SSTs 4-4.5°C) interrupted only by a cooling between 7.5 and 6.5 ka. After 4 ka the SSTs began to decrease to reach a minimum between 3.4 and 3 ka and they increased towards the end of the record.

### 5.5.2. Stable isotopes

The planktic oxygen isotope record shows relatively heavy values typical for the LGM (>4.5‰) in its oldest part (Fig. 5.4.). A small but remarkable excursion with light values was noted around 19 ka. The second, much stronger excursion peaked around 17 ka. Thereafter the values decreased with another distinct excursion around 12.6 ka and remained relatively stable after ca. 9 ka. The planktic carbon isotope record shows significant variability. Values were low until 16 ka. They were then increasing until 12 ka and subsequently decreasing. Since ca. 10 ka the carbon isotope ratio continued to rise to reach highest values after 7 ka and began to decrease after 3 ka.

Heavy $\delta^{18}O$ values (>5‰) were recorded for the benthic infaunal species (*O. umbonatus*). Contemporaneous with the planktic record, also a light benthic isotope excursion is found around 17 ka. The values then returned to the previous high level and remained relatively stable until 13.5 ka. The epibenthic $\delta^{18}O$ record (*C. wuellerstorfi*) starts only around 17 ka due to the absence of this species in the older interval. It also reveals the relatively light value peak noted in the other two species records, but rapidly increased values until ca. 13.5 ka. After that both benthic records run roughly parallel to each other. A trend towards lower values dominates the remaining part of the record with only minor variability. Epibenthic carbon isotope data (*C. wuellerstorfi*) show a steadily

increasing trend between 17 and 6.5 ka. The values remained relatively high until ca. 3.5 ka from when on they decreased in a stepwise manner.

### 5.5.3. IRD

Between 20 and 11 ka IRD content in core M17730-4 was high, the majority being crystalline fragments of various rock types (Fig. 5.4.). There are, however, a number of prominent peaks in the clastic IRD record (18, 17, 16 and 15 ka). Although after 11 ka the IRD concentration became extremely low, around 10 ka there is a prominent peak in the percentage record of IRD (predominantly crystalline) relative to all grains >150 μm (mineral grains and foraminifera).

The IRD record of core PS1878 is generally dominated by crystalline rock fragments (Fig. 5.5.). Only around 14.5 ka the amount of clastic IRD exceeded that of the crystalline grains. The total IRD content was high between 25 and 11 ka, with numerous prominent peaks. The younger part of the sedimentary record contains little IRD.

## 5.6. Discussion

### 5.6.1. Deglaciation

The first major deglacial freshwater event was centered at 17 ka (e.g., Bond et al., 1997; Hemming, 2004; Stanford et al., 2011; Telesiński et al., 2014b). However, a small, but conspicuous “precursor” $\delta^{18}O$ event occurred just prior to it. It is well recorded in cores PS1878 and M17730-4 around 19 ka (Figs. 5.4. and 5.5.) and can also be identified in other records from the Norwegian Sea (Lekens et al., 2005; Weinelt et al., 2003), Denmark Strait (Voelker et al., 2000) and Fram Strait (Nørgaard-Pedersen et al., 2003).

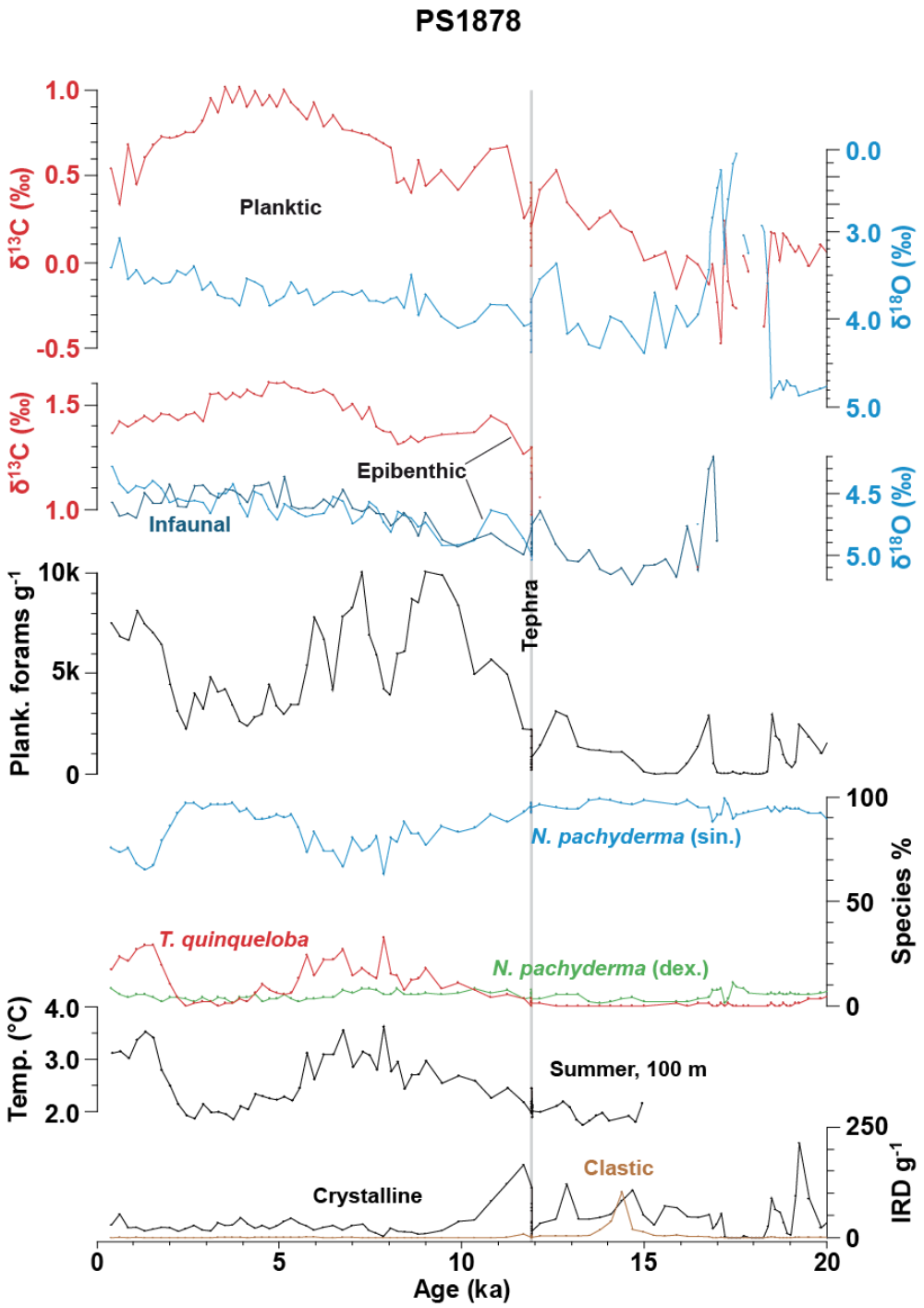


Fig. 5.5. PS1878 paleoceanographic record: stable carbon (red) and oxygen (blue) isotope ratios of planktic foraminifera *N. pachyderma* (sin), epibenthic *C. wuellerstorfi* and infaunal *O. umbonatus*, total abundance of planktic foraminifera, relative abundance of three dominant planktic foraminiferal species, reconstructed subsurface (100 m) summer temperatures, and total abundance of crystalline (black) and clastic (brown) IRD.

Although at the latter location the age of the event seems to be significantly older (ca. 21 ka), the difference might be attributable to variations in reservoir ages during the deglaciation (Stern and Lisiecki, 2013; Waelbroeck et al., 2001). The prevalence of this event across the entire Nordic Seas region, despite its low amplitude, suggests that it may have had multiple sources but a common trigger mechanism. As suggested by proxy (Hall et al., 2006) and modeling results (Álvarez-Solas et al., 2011), the Atlantic Meridional Overturning Circulation (AMOC) is sensitive to small-scale freshwater perturbations. Thus the "precursor" light $\delta^{18}O$ excursions at 19 ka could have been induced by a first, slight sea-level rise (cf. Clark et al., 2004) which resulted in transient and localized freshwater fluxes to the North Atlantic. This in turn may have led to a first weakening of the AMOC and NADW formation and subsurface warming (Fig. 5.4.) that ca. 1.2-1.3 kyr later caused ice shelves collapse and iceberg purges – events known as Heinrich stadial 1 (HS1) (Álvarez-Solas et al., 2011; Hall et al., 2006; Marcott et al., 2011).

The new dating result of core PS1878 just above the main deglacial light $\delta^{18}O$ excursion (Table 5.1.) limits the duration of the freshwater event attributed to HS1 to ca. 1.8 kyr (18.5-16.7 ka, Fig. 5.5.). This is comparable to the length of the event in core M17730-4 (ca. 2.0 kyr, 18-16 ka, Fig. 5.4.). The apparent difference in timing is likely a result of variable reservoir ages (Telesiński et al., 2014a). However, the HS1 freshwater event seems to have had a different character at each of the two sites. In the Greenland Basin (Fig. 5.5.) the event probably resulted from a discharge of fine sediment-loaded freshwater from the Greenland Ice Sheet (GIS), which caused a massive increase in sedimentation rates (cf. Hjelstuen et al., 2004; Lekens et al., 2005), thereby diluting the concentrations of IRD and planktic foraminifera (Evans et al., 2002; Lekens et al., 2005; Telesiński et al., 2014b). In the record from the Lofoten Basin (Fig. 5.4.) we observe only a slight decrease in IRD delivery during the event, but also a distinct peak of clastic

grains. This increase in the clastic IRD input suggests the western Eurasian shelves as the source of the ice-rafted material and connects the freshwater event with a partial collapse of the Barents Sea Ice Sheet (BSIS) (Bischof, 1994; Elverhøi et al., 1995). These differences clearly show that although the events were simultaneous and had a common trigger mechanism (see above), the sources of freshwater must have been different. Sarnthein et al. (1995) identified two deglacial freshwater tongues – one in the Denmark Strait and another southwest of the Barents Sea margin. The latter one probably also reached site M17730-4. The freshwater outburst recorded in PS1878 originated more likely from the GIS to the west (Telesiński et al., 2014b) whereas other records from farther north and south would indicate a freshwater outflow from the Arctic Ocean and/or the Fram Strait region (Nørgaard-Pedersen et al., 2003) and the Norwegian Channel (Lekens et al., 2005), respectively. Thus, there were at least five different freshwater sources around the Nordic Seas during the early deglaciation. Such a synchronized collapse, including the Laurentide (Hemming, 2004) and circum-Nordic Seas ice sheets, points to an external trigger mechanism (Bond et al., 1997) rather than internal instabilities of the individual ice sheets (Broecker, 1994) as a cause of HS1. Our observations confirm a significant contribution of the circum-Nordic Seas ice sheets to HS1 (Bond et al., 1997; Hemming, 2004), in contrast to earlier studies which indicated the Laurentide Ice Sheet as the only contributor (e.g., Broecker, 1994).

Contrary to core PS1878, the isotope record of the infaunal species *O. umbonatus* in M17730-4 is complete and covers the entire studied period (Figs. 5.4. and 5.5.). It reveals that the $\delta^{18}O$ decrease between 18 and 16 ka, although of lower amplitude, was simultaneous with the planktic shift. The epibenthic record also shows a decrease but it does not cover the entire $\delta^{18}O$ event. For the Greenland Sea, Telesiński et al. (2014b) suggested that the light oxygen isotope signal in PS1878 was injected into the bottom

water layers with a hyperpycnal (sediment-loaded) plume (cf. Stanford et al., 2011). A similar explanation seems less supportive for the Lofoten Basin record, as we do not observe any decrease neither in the concentration of planktic foraminifera or IRD nor in the >63 μm size fraction (Fig. 5.2.), as it is the case in core PS1878. The plume in the Lofoten Basin was likely associated with the partial collapse of the BSIS (see above), which partly explains why ice rafting did not decrease. Another mechanism that could result in the light benthic $\delta^{18}O$ values is the formation of supercooled water under the ice shelf, a process observed nowadays in the Weddell Sea (Bauch and Bauch, 2001). A relatively warm and saline water mass, in our case the AW, could subduct under the ice shelf, increasing its melting (Straneo and Heimbach, 2013; Straneo et al., 2010). The admixture of relatively small amounts of fresh, cold, and isotopically extremely light meltwater into the AW, combined with brine release, would altogether produce a low $\delta^{18}O$, but sufficiently dense (cold and saline) water mass capable of sinking to the bottom of an ocean basin (Bauch and Bauch, 2001). In the Lofoten Basin, the cascading of such water masses down the Barents Sea continental slope could also explain the peak in >63 μm size fraction content just prior to the light isotope excursion in core M17730-4 (Fig. 5.2.), as the finer material could be winnowed by the cascades. These two mechanisms (the hyperpycnal plume and the formation of supercooled water) do not exclude each other and might have both taken place at both sites, although with different relative importance.

During the time interval after the main freshwater event (between ca. 16 and 13 ka) core M17730-4 (Fig. 5.4.) reveals planktic $\delta^{18}O$ values similar to those in the Greenland Basin records (Telesiński et al., 2014a). However, the PS1878 record is much more variable, indicating that minor freshwater events were much more common in the western Nordic Seas, in the proximity of the GIS (Fig. 5.5.). Most of the BSIS (except for

the Svalbard Ice Sheet) had already disappeared by then (Bischof, 1994). Thus, the GIS remained the main source of freshwater thereafter, releasing it during smaller-scale discharges. A small but significant increase in the clastic IRD delivery to sites PS1878, M17730-4, as well as PS1243 (Bauch et al., 2001a) between 14.5 and 15 ka was most probably related to the advance of the Svalbard Ice Sheet at that time (Elverhøi et al., 1995). The arrival of Svalbard icebergs to the Greenland and Lofoten basins might therefore indicate the AMOC recovery at the onset of the Bølling-Allerød interval (Stanford et al., 2011).

The SST reconstructions in the deglacial part of both records indicate cold and relatively stable thermal conditions (Figs. 4 and 5). Both applied transfer functions do not perform well in low temperatures (Husum and Hald, 2012; Pflaumann et al., 2003; below ca. 2°C and 3°C, respectively), which may in part explain such results. However, the foraminiferal fauna composition also remained stable in the pre-Holocene part of the records and was strongly dominated by polar species. This might indicate that the water temperature at the planktic foraminiferal habitat depth was indeed low and relatively stable during the deglaciation. In our records, no indications of warming during Bølling-Allerød (B-A) can be found. B-A was an interval of relatively high air temperatures recorded at 14.7-12.9 ka over Greenland (Johnsen et al., 2001; Rasmussen et al., 2006) and Europe (e.g., Ammann et al., 2013; Friedrich et al., 2001). The lack of a distinct B-A warming in paleoceanographic records from the Nordic Seas is a common feature (e.g., Rasmussen et al., 2007), although the warming is found in the North Atlantic records (Waelbroeck et al., 2001). The onset of the B-A interstadial was concurrent with meltwater pulse 1A (mwp-1A, Weaver et al., 2003). The source area of mwp-1A remains unknown, ranging from Antarctica to the Laurentide or Fennoscandian ice sheets (Weaver et al., 2003). Our records do not contain indications of any prominent freshwater

discharges during the B-A interstadial, which seems to exclude the circum-Nordic Seas ice sheets as potential mwp-1A sources. It is possible, however, that significant amounts of freshwater were still present in the basin since HS1 due to the continuous replenishment from the surrounding melting ice sheets or advected into the area as a result of mwp-1A. The freshwater could have maintained a strong halocline and isolated the subsurface waters from the atmospheric warming during B-A.

Between 14 and 13 ka the offset between both benthic $\delta^{18}O$ records in core M17730-4 decreased and in the younger part of the records both species exhibit similar values (after correction for vital effects, Fig. 5.4.). This cannot be observed in core PS1878, due to the incompleteness of the records, but is a common feature in other Nordic Seas records during Marine Isotope Stage (MIS) 2 and Termination I (Bauch et al., 2001a; Telesiński et al., 2014a), as well as during MIS 6 and Termination II (Bauch et al., 2000). Although the reason for this shift still remains elusive, it might be an effect of a change in overall circulation in the Nordic Seas or a different ecology, and thus a specific change of the vital effect of these benthic foraminifera during times of enhanced IRD deposition (Bauch and Erlenkeuser, 2003).

During the Younger Dryas (YD) interval the central Nordic Seas were once again affected by some freshwater (Figs. 5.4. and 5.5.). Both cores show time-coeval planktic $\delta^{18}O$ peaks with a maximum around 12.6 ka, suggesting a rapid propagation of freshwater from the north (e.g., Fram Strait; Fahl and Stein, 2012) towards the south (cf. Condron and Winsor, 2012). The presence of a YD low $\delta^{18}O$ signal in the Lofoten Basin, together with the $\delta^{18}O$ data compilation of Sarnthein et al. (1995), might also indicate a southern origin. However, Sarnthein et al. (1995) showed a time slice from the late YD (ca. 12.3-11.3 ka), while the freshwater plume reached the Nordic Seas earlier (peak ca. 12.6 ka).

Besides, their map compilation contains very few data points from the northern and western Nordic Seas, the area most affected by the plume if the meltwater had come from the North. Absence of freshwater indications in high resolution records farther to the south (Risebrobakken et al., 2003) and their unambiguous occurrences in the northern part of the Nordic Seas (Bauch et al., 2001a; Fahl and Stein, 2012; Telesiński et al., 2014a) suggest the Arctic as an important or even the main source area. Our Lofoten Basin site seems to be the southeasternmost locality in the Nordic Seas which recorded a clear YD freshwater signal (Fig. 5.1.). This record therefore sets a geographical limit of the southward freshwater propagation into the Nordic Seas, but extending it beyond the area suggested by Condron and Winsor (2012). Such a broad spatial expansion of the freshwater lid might be in agreement with the paradigm of AMOC decline (McManus et al., 2004) and it certainly conforms to the regional reconstructions of increased sea-ice abundance in the Norwegian Sea and in the Fram Strait (Cabedo-Sanz et al., 2013; Müller et al., 2009) during the early YD.

### 5.6.2. Holocene

Iceberg rafting ceased almost completely in the central Nordic Seas shortly after the YD, as indicated by low IRD content in the sediments (Figs. 5.4. and 5.5.). This time was associated with an improvement of surface water conditions and the disappearance of the perennial sea-ice cover, as shown by increasing faunal abundances. While in the Greenland Basin the bioproductivity continued to increase almost continuously until ca. 9 ka, in the Lofoten Basin the foraminiferal concentration decreased again between 11 and 9.5 ka. This decline can at least partly be attributed to an increase in sedimentation rate around that time (Fig. 5.3.) - especially if the dated sample from 95.6 cm is in fact older than 10.4 ka. Large amounts of fine-grained material may have been delivered to the site during the final stage of the decay of the nearby Scandinavian Ice Sheet (SIS). Although

the ice rafting generally ceased at that time, as the ice front retreated from the coastline, continental runoff could have still provided significant amounts of suspended material (Mangerud, 2004).

A distinct, light-brown layer was observed at 86.5-84.5 cm depth (age around 9.95 ka) in core M17730-4. It is characterized by light $\delta^{18}O$ and heavy $\delta^{13}C$ peaks, both planktic and benthic, a slightly elevated IRD content and is almost barren of foraminifera (Fig. 5.4.). As the BSIS had already retreated at that time (Elverhøi et al., 1995, 1993; Svendsen et al., 2004) the emerged shallow shelf sea was an environment where sea-ice and brine formation must have occurred, at least seasonally. The final retreat of the SIS (Mangerud, 2004) mobilized sediment material, of which the finer size fractions possibly remained suspended in the water further increasing its density and allowing the water to cascade down the continental slope and into the deeper parts of the Lofoten Basin where the fine sediments were deposited. Thus we interpret this layer as a result of dense water cascading from the Barents Sea shelf. The brine formation and cascading around 10 ka could also have increased the ventilation of the subsurface and bottom water, as indicated by elevated planktic and benthic $\delta^{13}C$ values, respectively. Although the temperature reconstruction indicates a cooling around that time, it might be a result of selective winnowing and/or abrasion of the small, thin-walled subpolar foraminiferal tests.

The early Holocene SST increase in the Lofoten Basin started ca. 10.5 ka. The strengthening of the AW advection is reflected in consecutive peaks in the relative abundance record of *N. pachyderma* (dex), *G. bulloides* and *T. quinqueloba* (Fig. 5.4.). While the former species is the main warm counterpart of *N. pachyderma* (sin) in the Nordic Seas – with a present-day dominance in the SE Norwegian Sea region (Bauch and Kandiano, 2007) – the latter two species are directly related to the inflow of AW. Their

specific sequence of occurrence indicates either a gradual strengthening of the AW inflow or a westward lateral migration of the AW core towards our study site.

Although SSTs had already increased and reached a maximum by 9.8 ka in the Lofoten Basin, enhanced advection of AW occurred later, ca. 9.2 ka. This is similar in time to the northern Greenland Basin but earlier than in its central part (Telesiński et al., 2014a). Still, it appears relatively late compared to the records from other sites located near the main flow path of the NAC where it is found around 10 ka (Fig. 5.6., e.g., Hald et al., 2007; Risebrobakken et al., 2011). Most likely this illustrates the gradual decoupling of an AW branch from the main NAC and a re-routing of AW flow from a northward to a northwestward direction. The delay of AW advection in the central and western part of the Nordic Seas may also be a result of the activation ('an overshoot of the AMOC' suggested by Risebrobakken et al., 2011) and subsequent stabilization of the Greenland Sea gyre at this time. In addition, a deglacial freshwater input from the GIS may have also delayed the warming in the central Nordic Seas, thereby influencing the AMOC development in general (Blaschek and Renssen, 2013; Seidenkrantz et al., 2012). Only after 8-7 ka, when the freshwater input had ceased completely and the modern surface ocean circulation pattern and the flow strength of the AMOC were reached (Thornalley et al., 2010), did the heat advected into the Nordic Seas by the AW reach also significantly farther to the west, as seen in our Greenland Basin record (Fig. 5.5.). The absence or weakness of a westward heat transport during the early Holocene might have been also responsible for the high amplitude of the Holocene Thermal Maximum in paleotemperature records from the eastern and northeastern Nordic Seas (Fig. 5.6., e.g., Hald et al., 2007; Risebrobakken et al., 2011).

Similar to the situation in the eastern Nordic Seas (Risebrobakken et al., 2011), in the Lofoten Basin the thermal maximum seems to be at least partly decoupled from the

maximum AW advection indicated by the maximum abundances of subpolar species (Fig. 5.4.). However, while at the Norwegian and Barents Sea margins the SST maximum is delayed compared to the AW advection, in the Lofoten Basin it begins ca. 600 years earlier. The surface waters close to the Norwegian coast were affected by freshwater from the retreating SIS, which could have delayed the surface warming. Site M17730-4, located farther to the northwest, was probably less influenced by freshwater at that time and the high summer insolation caused the warming before the maximum AW advection was reached.

Between ca. 9 and 6 ka the foraminiferal concentration records in the Lofoten and Greenland basins seem to be in phase (Figs. 5.4. and 5.5.). However, while at site M17730-4 high faunal abundances corresponded with intervals rich in subpolar fauna, in core PS1878 these two proxies seem to be unrelated. While the relative proportions of subpolar species might be more directly related to temperature and salinity in the upper water layers (e.g., Hald et al., 2007), the changes in total foraminiferal productivity more likely depend on factors such as food availability, water ventilation, variations in sea-ice cover etc. The Lofoten Basin (Figs. 5.1. and 5.4.) was directly influenced by the NAC, and its changing intensity was the dominant factor for the environmental conditions (e.g., Giraudeau et al., 2010; Risebrobakken et al., 2011; Werner et al., 2013). By comparison, in the Greenland Basin (Figs. 5.1. and 5.5.) the oceanographic situation was more complex due to the interplay of NAC and EGC branches, the Greenland Sea gyre, the intensity of deep convection as well as the sea ice exported from the Arctic through the Fram Strait (Telesiński et al., 2014a, 2014b). Therefore the bioproductivity in this area, which resulted from these complex relationships, might have not been directly linked to the water temperature, but rather to the intensity of the AW inflow.

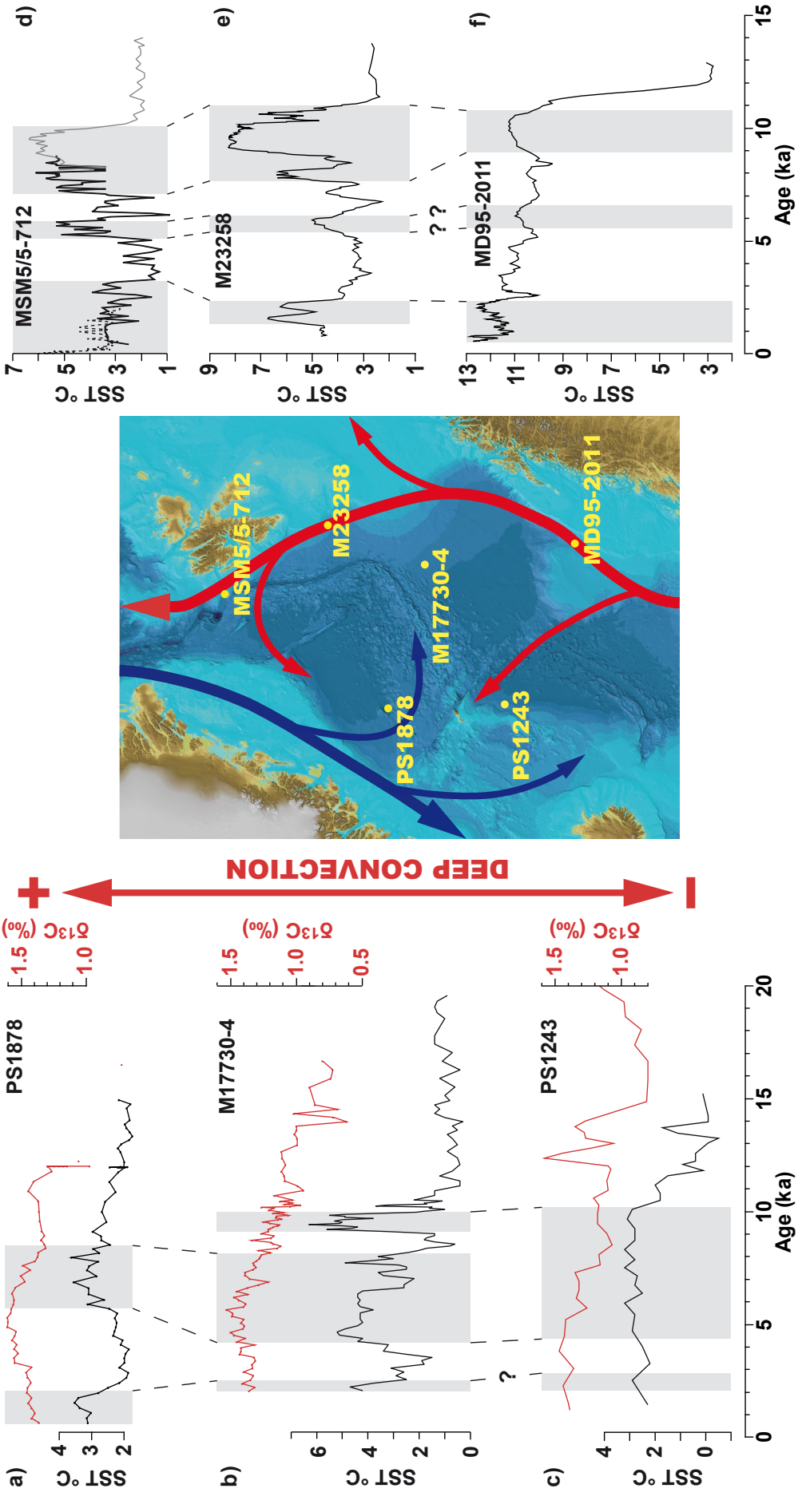
d)
e)
f)
MSM5/5-712
M23258
MD95-2011
? ?
SST °C
Age (ka)
MSM5/5-712
M23258
M17730-4
MD95-2011
PS1878
PS1243
DEEP CONVECTION
+
−
δ13C (‰)
a)
b)
c)
PS1878
M17730-4
PS1243
?
SST °C
Age (ka)

Fig. 6. (previous page) Comparison of high-resolution Nordic Seas records. a)-c) Central Nordic Seas SST and epibenthic $\delta^{13}C$ records. a) PS1878 (Telesiński et al., 2014), summer SST at 100 m water depth. b) M17730-4 (this study), summer SST at 100 m. c) PS1243 (Bauch et al., 2001a; Kandiano et al., 2012), winter SST at 100 m. d)-f) Eastern Nordic Seas SST records. d) MSM5/5-712 (gray line - Aagaard-Sørensen et al., 2014b; black line - Werner et al., 2013, dotted line - Werner et al., 2011), summer SST at 50 m. e) M23258 (Sarnthein et al., 2003), summer SST at 10 m, smoothed. f) MD95-2011 (Andersson et al., 2010), summer SST at 10 m, smoothed. Light gray shadings indicate early, middle and/or late Holocene warm intervals.

The sediments deposited between 9 and 6 ka, generally rich in planktic foraminifera, reveal two prominent intervals of impoverished fauna centered around 8.2 and 6.6 ka (Figs. 5.4. and 5.5.). The earlier one spans the interval of the 8.2 ka event, a widespread cooling event often related to a catastrophic freshwater release into the Labrador Sea and disruption of NADW formation (e.g., Rohling and Pälike, 2005). As shown by model simulations, the freshwater outburst strengthened the Atlantic subpolar gyre but apparently weakened the transport of AW into the Nordic Seas (Born and Levermann, 2010). This caused a cold and dry climate with overregional implications (Kobashi et al., 2007; Rohling and Pälike, 2005). At both of our sites, a SST decrease occurred around 8.2 ka (Fig. 5.6.). The cooling was much more pronounced in the Lofoten Basin, perhaps because the preceding early Holocene warming was much stronger here and because this area was more directly influenced by the intensity of the AW inflow than the Greenland Basin. A time-coeval increase in planktic $\delta^{13}C$ at site M17730-4 might either reflect the decreased inflow of poorly ventilated AW (cf. Sarnthein et al., 2003) or be related to enhanced sea-ice formation from the cool and fresh surface water (Müller et al., 2012, 2009) indicating that during the 8.2 ka event conditions in the Lofoten Basin resembled those in the present-day Arctic Ocean (cf. Spielhagen and Erlenkeuser, 1994). Low benthic $\delta^{13}C$ values indicate limited deep water renewal in accordance with a brief decrease in ISOW flow and AMOC collapse at that time (Hall et

al., 2004). The anomalies related to the 8.2 ka event in our records extend over several hundred years, which is in accordance with data from many other records. It corroborates that the sudden climate changes related with the freshwater outburst were probably superimposed on a longer-term climatic trend (Rohling and Pälike, 2005).

During the younger foraminifer-poor interval (6.8-6.4 ka) the decrease in foraminiferal abundance was of similar amplitude as during the 8.2 ka event (Figs. 5.4. and 5.5.). In the Greenland Basin it fell within the maximum of the early Holocene warm interval (Telesiński et al., 2014a) and no indications of cooling can be seen in the planktic assemblages. In the Lofoten Basin the cooling was significantly weaker than during the 8.2 ka event (Fig. 5.6.), but it was still one of the most pronounced cold Holocene anomalies, similar in scale to a brief cooling around 7.3 ka, accompanied by only a minor bioproductivity decrease. An event simultaneous to the 6.8-6.4 ka cooling is recorded in the northern Nordic Seas (Müller et al., 2012; Sarnthein et al., 2003; Werner et al., 2013), where it was associated with (sub)surface water cooling, expanded sea-ice occurrence and decreased bioproductivity. The event also coincides with an interval of lower current speed in the northern Fram Strait, possibly related to a slowdown of the overturning circulation (Hass, 2002). A decrease in our Lofoten Basin benthic $\delta^{13}C$ record confirms a possible brief AMOC weakening. It is difficult to determine unambiguously the cause and nature of this event, as indications of any kind of local (e.g., freshwater) or global (e.g., solar irradiance) forcing cannot be found around that time. Apparently the event was more of a local perturbation, restricted mainly to the northeastern Nordic Seas, perhaps related to internal oceanic variability (cf. Wanner et al., 2011).

Except for the two abovementioned events, the benthic carbon isotope values kept increasing at both sites, at least since the onset of the Holocene, and reached maximum

values between 7 and 6 ka (Fig. 5.6.). The same is true for the planktic $\delta^{13}C$ record. As already discussed by Telesiński et al. (2014a), this is a basin-wide feature that illustrates the development of deep convection in the Greenland Sea. The following interval (7-6 until 3 ka) was characterized by high convection rates as shown by high carbon isotope ratios, both planktic and benthic, in most areas of the Nordic Seas (e.g., Bauch et al., 2001a; Sarnthein et al., 2003). Sediment grain size data and modelling results also seem to support this interpretation (Thornalley et al., 2013). The fact that the convected water influenced the bottom environment not only of the Greenland Basin (Telesiński et al., 2014a) but also of the Lofoten Basin indicates a broad spreading of the well ventilated deepwater on both sides of the oceanic ridge separating the Greenland and Lofoten basins before flowing southward across the Greenland-Scotland Ridge and into the North Atlantic (cf. Mauritzen, 1996).

The middle Holocene warm interval lasted in the Greenland Basin until ca. 5.5 ka In the Lofoten Basin the cooling started ca. 4 ka, but its main phase occurred only ca. 3.5 ka (Fig. 5.6.). Such a long and late warm phase is in good agreement with numerous other Nordic Seas records (Andersen et al., 2004b; Bauch et al., 2001a; Giraudeau et al., 2010; Telesiński et al., 2014a; Werner et al., 2013). It differs from several eastern Nordic Seas records (Hald et al., 2007; Rasmussen et al., 2007; Risebrobakken et al., 2011) which show a relatively short thermal maximum in subsurface waters during the early Holocene. However, even at these sites the sea surface temperatures indicate a later and longer warm phase. Most probably, only in the areas directly influenced by the AW inflow there was a warm interval restricted to the period of maximum advection, which terminated shortly after. In other areas and/or water layers this warm phase was extended by the still relatively high summer insolation and, perhaps, other feedback mechanisms (Risebrobakken et al., 2011).

Interestingly, the termination of the middle Holocene warm interval in core PS1878 around 5.5 ka coincides with the time when the flooding of the vast Siberian shelves was concluded (Bauch et al., 2001b). The reach of the Holocene sea level highstand in the Arctic immensely increased sea-ice production on these Arctic shelves and its export through Fram Strait (Werner et al., 2013). This probably acted as a positive feedback for the Neoglaciation after the mid-Holocene, especially in the northwestern Nordic Seas. In the Lofoten Basin there was no cooling at that time as the Arctic sea ice probably did not expand that far south. Strong convection (maximum between ca. 7-6 and 3 ka, Telesiński et al., 2014a) might have also played a role in delaying the cooling in the Lofoten Basin as it required an enhanced inflow of Atlantic waters into the convection center (Marshall and Schott, 1999) that had to pass over site M17730-4. However, the decrease in foraminiferal abundance, especially of the subpolar species *T. quinqueloba*, between 5 and 4 ka might indicate some deterioration of the planktic foraminiferal environment in the Lofoten Basin. The subsequent cooling ca. 3.5 ka and the Neoglacial thermal minimum in the central Nordic Seas around 3 ka, which was very likely enforced or amplified by decreased solar irradiance (Renssen et al., 2006), also coincided with an increase in sea-ice occurrence in the northern Nordic Seas (Müller et al., 2012) and a weakening of deep convection in the Greenland Sea (Telesiński et al., 2014a).

Sediment grain size records and modelling results (Thornalley et al., 2013) suggest a rather gradual shoaling of deep convection in the Nordic Seas through the middle-late Holocene. Our results, however, show that there was a stepwise decrease in the convection strength around 3 ka (Telesiński et al., 2014a), perhaps superimposed on a longer-term trend starting in the middle Holocene (Fig. 5.6.). Even at sites farther from the convection center, where this stepwise decrease was not recorded, a brief reduction in the AMOC strength can be observed around 3 ka, indicating some kind of disruption to

the convection mechanism (Bauch et al., 2001a; Hall et al., 2004; Sarnthein et al., 2003; Werner et al., 2013). The highest benthic $\delta^{13}C$ values and their stepwise decrease ca. 3 ka, recorded only in cores PS1878, PS1910 (Telesiński et al., 2014a) and M17730-4, suggest that the convection center was located close to these sites. This means that the convection center was situated more or less in the same area as at present (Fig. 5.1., cf. Marshall and Schott, 1999). The location of the convection center strongly depends on the position of the ice edge and the Polar Front, as the interplay between ice-covered and ice-free areas is crucial for the deep convection preconditioning (Marshall and Schott, 1999). Therefore we suggest that, if during the Neoglacial cooling climax around 3 ka the ice edge was located farther to the southeast, the convection center was probably also shifted into this direction, as suggested earlier by modelling results of Renssen et al. (2006).

Although our Lofoten Basin record does not cover the last ca. 1.8 kyr, a warming trend is noticeable after 3 ka (Fig. 5.6.). After ca. 2 ka the SSTs reached a level comparable with the early and mid-Holocene thermal maxima. This implies that the warming of the subsurface waters reflected in data from core PS1878 (Telesiński et al., 2014a) was not a local phenomenon but affected a broader area. It may have been related to an increase in AW advection into the Nordic Seas due to a shift in the variability analogous to the modern North Atlantic Oscillation (Giraudeau et al., 2010; Olsen et al., 2012). In the southeastern Norwegian Sea (Giraudeau et al., 2010) and at our two sites the observed changes had an amplitude comparable to that of the Holocene thermal maximum (Telesiński et al., 2014a). In other areas of the Nordic Seas where a warming or an increase of AW inflow can also be observed in the late Holocene (e.g., Andersen et al., 2004a, 2004b; Hald et al., 2007; Werner et al., 2013), it was clearly much weaker than during the early/middle Holocene. However, a Mg/Ca subsurface temperature reconstruction from the eastern Fram Strait (Aagaard-Sørensen et al., 2014a) indicates

that also in the northeastern Nordic Seas the early and late Holocene warming may have been equally strong. In contrast to the early Holocene, during the last 2-3 kyr the summer insolation in the high northern latitudes was low and therefore the warming must have been entirely forced by the AW advection aided by stronger water column stratification. These reconstructions differ from the common view of the Holocene climatic and oceanographic evolution with an orbitally-induced early Holocene thermal maximum and a gradual cooling thereafter (e.g., Andersen et al., 2004a). It shows that short-scale dynamical processes can play a very important role on a regional scale which decouples them from larger-scale, long-term trends (Wanner et al., 2011).

## 5.1. Summary and conclusions

The study of the central Nordic Seas records shows that the paleoceanographic evolution of this area was significantly different from that in the well-explored eastern part of the basin. It illustrates the complexity of the oceanographic variability in the region, both on the spatial and temporal scale (Fig. 5.6.).

The deglaciation in the Nordic Seas started ca. 19 ka with non-catastrophic freshwater discharges. These were likely caused by an early sea-level rise and led to a first weakening of the AMOC, enhanced subsurface warming, and eventually, to a dramatic collapse of circum-Nordic Seas marine-based ice sheets and the major deglacial freshwater discharge (ca. 18-16 ka). This strong freshwater outburst in the region, which was crucial to the deepwater formation processes, indicate that the Nordic Seas significantly contributed to the onset of HS1. When the BSIS had disintegrated, the GIS remained the main source of freshwater releasing it in minor quantities into the Greenland Sea. The last major freshwater plume which affected the northern and central Nordic Seas

occurred during the early YD (ca. 12.6 ka). Most probably it came from the Arctic Ocean and reached as far as the Lofoten Basin, thereby affecting the AMOC.

Ice rafting and sea-ice cover in the central Nordic Seas diminished after the YD, but the subsurface warming started only ca. 10.5 ka. The thermal maximum and the maximum in AW advection were reached later in the Lofoten Basin (ca. 9.8 and 9.2 ka, respectively) than in the eastern Nordic Seas. This was caused by the gradual re-routing of an AW branch towards the northwest. In the Greenland Basin it was even later (after 8 ka) due to the activation of the Greenland Sea gyre and the negative influence of the GIS, still delivering freshwater. A distinct temperature and bioproductivity anomaly, related to the 8.2 ka event and spanning a few centuries, stood out in the central Nordic Seas, predominantly in the Lofoten Basin. It was most probably related to a weakening of AW transport into the Nordic Seas. A similar, though less distinct and probably more local cold event occurred in the area ca. 6.6 ka. The thermal maximum ended in the Greenland Basin quite abruptly ca. 5.5 ka in connection with the increasing sea-ice export from the Arctic. In the Lofoten Basin the cooling started only after 4 ka as the Arctic sea ice did not reach that far.

Deep convection developed in the central Nordic Seas since the early Holocene and reached its maximum strength 7-6 ka. The convection center was located approximately in the same area as at present, migrating slightly together with the sea-ice edge. At 3 ka, a solar irradiance minimum fostered an expansion of seasonal sea ice, which in turn significantly limited the convection rate. These events correspond to the thermal minimum in the central Nordic Seas. Since ca. 2 ka a shift in the variability analogous to the North Atlantic Oscillation enhanced the AW inflow into the well-stratified Nordic Seas. Most of the warmth was then routed into the central Nordic Seas

resulting in subsurface temperatures comparable with the early-middle Holocene thermal maximum.

## Acknowledgements

This work is a contribution to the CASE Initial Training Network funded by the European Community's 7th Framework Programme FP7 2007/2013, Marie Curie Actions, under Grant Agreement no. 238111. We are grateful to Lulzim Haxhiaj and Christelle Not for performing the stable isotope measurements and to the Poznan Radiocarbon Laboratory, Beta Analytic, and the Leibniz Laboratory, Kiel University, for the AMS $^{14}C$ datings.

## References

Aagaard-Sørensen, S., Husum, K., Hald, M., Marchitto, T.M., Godtliebsen, F., 2014a. Sub sea surface temperatures in the Polar North Atlantic during the Holocene: Planktic foraminiferal Mg/Ca temperature reconstructions. The Holocene 24, 93–103.

Aagaard-Sørensen, S., Husum, K., Werner, K., Spielhagen, R.F., Hald, M., Marchitto, T.M., 2014b. A Late Glacial-early Holocene multiproxy record from the eastern Fram Strait, Polar North Atlantic. Mar. Geol. in press.

Álvarez-Solas, J., Montoya, M., Ritz, C., Ramstein, G., Charbit, S., Dumas, C., Nisancioglu, K., Dokken, T.M., Ganopolski, A., 2011. Heinrich event 1: an example of dynamical ice-sheet reaction to oceanic changes. Clim. Past 7, 1297–1306.

Ammann, B., van Raden, U.J., Schwander, J., Eicher, U., Gilli, A., Bernasconi, S.M., van Leeuwen, J.F.N., Lischke, H., Brooks, S.J., Heiri, O., Nováková, K., van Hardenbroek, M., von Grafenstein, U., Belmecheri, S., van der Knaap, W.O., Magny, M., Eugster, W., Colombaroli, D., Nielsen, E., Tinner, W., Wright, H.E., 2013. Responses to rapid warming at Termination 1a at Gerzensee (Central Europe):

Primary succession, albedo, soils, lake development, and ecological interactions. Palaeogeogr. Palaeoclimatol. Palaeoecol. 391, 111–131.

Andersen, C., Koç, N., Jennings, A.E., Andrews, J.T., 2004a. Nonuniform response of the major surface currents in the Nordic Seas to insolation forcing: Implications for the Holocene climate variability. Paleoceanography 19, PA2003.

Andersen, C., Koç, N., Moros, M., 2004b. A highly unstable Holocene climate in the subpolar North Atlantic : evidence from diatoms. Quat. Sci. Rev. 23, 2155–2166.

Andersson, C., Pausata, F.S.R., Jansen, E., Risebrobakken, B., Telford, R.J., 2010. Holocene trends in the foraminifer record from the Norwegian Sea and the North Atlantic Ocean. Clim. Past 6, 179–193.

Bauch, D., Bauch, H.A., 2001. Last glacial benthic foraminiferal $\delta^{18}O$ anomalies in the polar North Atlantic: A modern analogue evaluation. J. Geophys. Res. 106, 9135–9143.

Bauch, H.A., Erlenkeuser, H., 2003. Interpreting Glacial-Interglacial Changes in Ice Volume and Climate From Subarctic Deep Water Foraminiferal $\delta^{18}O$, in: Droxler, A.W., Poore, R.Z., Burckle, L.H. (Ed.), Earth's Climate and Orbital Eccentricity: The Marine Isotope Stage 11 Question. American Geophysical Union, Washington, D. C., pp. 87–102.

Bauch, H.A., Erlenkeuser, H., Jung, S.J.A., Thiede, J., 2000. Surface and deep water changes in the subpolar North Atlantic during Termination II and the last interglaciation. Paleoceanography 15, 76–84.

Bauch, H.A., Erlenkeuser, H., Spielhagen, R.F., Struck, U., Matthiessen, J., Thiede, J., Heinemeier, J., 2001a. A multiproxy reconstruction of the evolution of deep and surface waters in the subarctic Nordic seas over the last 30,000 yr. Quat. Sci. Rev. 20, 659–678.

Bauch, H.A., Kandiano, E.S., 2007. Evidence for early warming and cooling in North Atlantic surface waters during the last interglacial. Paleoceanography 22, PA1201.

Bauch, H.A., Mueller-Lupp, T., Taldenkova, E., Spielhagen, R.F., Kassens, H., Grootes, P.M., Thiede, J., Heinemeier, J., Petryashov, V. V., 2001b. Chronology of the Holocene transgression at the North Siberian margin. Glob. Planet. Change 31, 125–139.

Bauch, H.A., Weinelt, M.S., 1997. Surface water changes in the Norwegian Sea during last deglacial and Holocene times. Quat. Sci. Rev. 16, 1115–1124.

Bischof, J.F., 1994. The decay of the Barents ice sheet as documented in nordic seas ice-rafted debris. Mar. Geol. 117, 35–55.

Bischof, J.F., Lund, J.J., Ecke, H.-H., 1997. Palynomorphs of ice rafted clastic sedimentary rocks in Late Quaternary glacial marine sediments of the Norwegian

Sea as provenance indicators. Palaeogeogr. Palaeoclimatol. Palaeoecol. 129, 329–360.

Blaschek, M., Renssen, H., 2013. The Holocene thermal maximum in the Nordic Seas: the impact of Greenland Ice Sheet melt and other forcings in a coupled atmosphere–sea-ice–ocean model. Clim. Past 9, 1629–1643.

Bond, G.C., Showers, W., Cheseby, M., Lotti, R., Almasi, P., DeMenocal, P., Priore, P., Cullen, H., Hajdas, I., Bonani, G., 1997. A Pervasive Millennial-Scale Cycle in North Atlantic Holocene and Glacial Climates. Science 278, 1257–1266.

Born, A., Levermann, A., 2010. The 8.2 ka event: Abrupt transition of the subpolar gyre toward a modern North Atlantic circulation. Geochemistry, Geophys. Geosystems 11, Q06011.

Broecker, W.S., 1994. Massive iceberg discharges as triggers for global climate change. Nature 372, 421–424.

Cabedo-Sanz, P., Belt, S.T., Knies, J., Husum, K., 2013. Identification of contrasting seasonal sea ice conditions during the Younger Dryas. Quat. Sci. Rev. 79, 74–86.

Clark, P.U., McCabe, A.M., Mix, A.C., Weaver, A.J., 2004. Rapid rise of sea level 19,000 years ago and its global implications. Science 304, 1141–1144.

Condron, A., Winsor, P., 2012. Meltwater routing and the Younger Dryas. Proc. Natl. Acad. Sci. U. S. A. 109, 19928–19933.

Duplessy, J.C., Labeyrie, L.D., Blanc, P.L., 1988. Norwegian Sea Deep Water Variations over the Last Climatic Cycle: Paleo-Oceanographical Implications, in: Wanner, H., Siegenthaler, U. (Eds.), Long and Short Term Variability of Climate. Springer, New York, pp. 83–116.

Elverhøi, A., Andersen, E.S., Dokken, T.M., Hebbeln, D., Spielhagen, R.F., Svendsen, J.I., Sorflaten, M., Rornes, A., Hald, M., Forsberg, C.F., 1995. The growth and decay of the Late Weichselian ice sheet in western Svalbard and adjacent areas based on provenance studies of marine sediments. Quat. Res. 44, 303–316.

Elverhøi, A., Fjeldskaar, W., Solheim, A., Nyland-Berg, M., Russwurm, L., 1993. The Barents Sea Ice Sheet—a model of its growth and decay during the last ice maximum. Quat. Sci. Rev. 12, 863–873.

Evans, J., Dowdeswell, J.A., Grobe, H., Niessen, F., Stein, R., Hubberten, H.W., Whittington, R.J., 2002. Late Quaternary sedimentation in Kejser Franz Joseph Fjord and the continental margin of east Greenland, in: Dowdeswell, J.A., Ó Cofaigh, C. (Eds.), Glacier-Influenced Sedimentation on High-Latitude Continental Margins. The Geological Society of London, London, pp. 149–179.

Fahl, K., Stein, R., 2012. Modern seasonal variability and deglacial/Holocene change of central Arctic Ocean sea-ice cover: New insights from biomarker proxy records. Earth Planet. Sci. Lett. 351-352, 123–133.

Friedrich, M., Kromer, B., Kaiser, K.F., Spurk, M., Hughen, K.A., Johnsen, S.J., 2001. High-resolution climate signals in the Bølling–Allerød Interstadial (Greenland Interstadial 1) as reflected in European tree-ring chronologies compared to marine varves. Quat. Sci. Rev. 20, 1223–1232.

Fronval, T., Jansen, E., 1997. Eemian and early Weichselian (140-60 ka) paleoceanography and paleoclimate in the Nordic seas with comparisons to Holocene conditions. Paleoceanography 12, 443–462.

Giraudeau, J., Grelaud, M., Solignac, S., Andrews, J.T., Moros, M., Jansen, E., 2010. Millennial-scale variability in Atlantic water advection to the Nordic Seas derived from Holocene coccolith concentration records. Quat. Sci. Rev. 29, 1276–1287.

Grootes, P.M., Stuiver, M., White, J.W.C., Johnsen, S.J., Jouzel, J., 1993. Comparison of oxygen isotope records from the GISP2 and GRIP Greenland ice cores. Nature 366, 552–554.

Hald, M., Andersson, C., Ebbesen, H., Jansen, E., Klitgaard-kristensen, D., Risebrobakken, B., Salomonsen, G.R., Sarnthein, M., Petter, H., Telford, R.J., 2007. Variations in temperature and extent of Atlantic Water in the northern North Atlantic during the Holocene. Quat. Sci. Rev. 26, 3423–3440.

Hall, I.R., Bianchi, G.G., Evans, J.R., 2004. Centennial to millennial scale Holocene climate-deep water linkage in the North Atlantic. Quat. Sci. Rev. 23, 1529–1536.

Hall, I.R., Moran, S.B., Zahn, R., Knutz, P.C., Shen, C.-C., Edwards, R.L., 2006. Accelerated drawdown of meridional overturning in the late-glacial Atlantic triggered by transient pre-H event freshwater perturbation. Geophys. Res. Lett. 33, L16616.

Hass, H.C., 2002. A method to reduce the influence of ice-rafted debris on a grain size record from northern Fram Strait, Arctic Ocean. Polar Res. 21, 299–306.

Hemming, S.R., 2004. Heinrich events: Massive late Pleistocene detritus layers of the North Atlantic and their global climate imprint. Rev. Geophys. 42, 1–43.

Hjelstuen, B.O., Sejrup, H.P., Haflidason, H., Nygård, A., Berstad, I.M., Knorr, G., 2004. Late Quaternary seismic stratigraphy and geological development of the south Vøring margin, Norwegian Sea. Quat. Sci. Rev. 23, 1847–1865.

Husum, K., Hald, M., 2012. Arctic planktic foraminiferal assemblages: Implications for subsurface temperature reconstructions. Mar. Micropaleontol. 96-97, 38–47.

Kandiano, E.S., Bauch, H. a., Fahl, K., Helmke, J.P., Röhl, U., Pérez-Folgado, M., Cacho, I., 2012. The meridional temperature gradient in the eastern North Atlantic during MIS 11 and its link to the ocean–atmosphere system. Palaeogeogr. Palaeoclimatol. Palaeoecol. 333-334, 24–39.

Kobashi, T., Severinghaus, J.P., Brook, E.J., Barnola, J.-M., Grachev, A.M., 2007. Precise timing and characterization of abrupt climate change 8200 years ago from air trapped in polar ice. Quat. Sci. Rev. 26, 1212–1222.

Lekens, W.A.H., Sejrup, H.P., Haflidason, H., Petersen, G., Hjelstuen, B., Knorr, G., 2005. Laminated sediments preceding Heinrich event 1 in the Northern North Sea and Southern Norwegian Sea: Origin, processes and regional linkage. Mar. Geol. 216, 27–50.

Levitus, S., Boyer, T.P., 1994. World Ocean Atlas 1994, vol. 4, Temperature, NOAA Atlas. ed. U.S. Department of Commerce, Washington, D.C.

Mangerud, J., 2004. Ice sheet limits on Norway and the Norwegian continental shelf, in: Ehlers, J., Gibbard, P.L. (Eds.), Quaternary Glaciations: Extent and Chronology, Vol. 1, Europe. Elsevier, Oxford, pp. 271–294.

Marcott, S.A., Clark, P.U., Padman, L., Klinkhammer, G.P., Springer, S.R., Liu, Z., Otto-Bliesner, B.L., Carlson, A.E., Ungerer, A., Padman, J., He, F., Cheng, J., Schmittner, A., 2011. Ice-shelf collapse from subsurface warming as a trigger for Heinrich events. Proc. Natl. Acad. Sci. U. S. A. 108, 13415–13419.

Marshall, J., Schott, F., 1999. Open-ocean convection: Observations, theory, and models. Rev. Geophys. 37, 1–64.

Mauritzen, C., 1996. Production of dense overflow waters feeding the North Atlantic across the Greenland-Scotland Ridge. Part 1: Evidence for a revised circulation scheme. Deep Sea Res. 43, 769–806.

McManus, J.F., Francois, R., Gherardi, J.-M., Keigwin, L.D., Brown-Leger, S., 2004. Collapse and rapid resumption of Atlantic meridional circulation linked to deglacial climate changes. Nature 428, 834–837.

Müller, J., Massé, G., Stein, R., Belt, S.T., 2009. Variability of sea-ice conditions in the Fram Strait over the past 30,000 years. Nat. Geosci. 2, 772–776.

Müller, J., Werner, K., Stein, R., Fahl, K., Moros, M., Jansen, E., 2012. Holocene cooling culminates in sea ice oscillations in Fram Strait. Quat. Sci. Rev. 47, 1–14.

Nørgaard-Pedersen, N., Spielhagen, R.F., Erlenkeuser, H., Grootes, P.M., Heinemeier, J., Knies, J., 2003. Arctic Ocean during the Last Glacial Maximum: Atlantic and polar domains of surface water mass distribution and ice cover. Paleoceanography 18, 1–19.

Nürnberg, D., Wollenburg, I., Dethleff, D., Eicken, H., Kassens, H., Letzig, T., Reimnitz, E., Thiede, J., 1994. Sediments in Arctic sea ice: Implications for entrainment, transport and release. Mar. Geol. 119, 185–214.

Olsen, J., Anderson, N.J., Knudsen, M.F., 2012. Variability of the North Atlantic Oscillation over the past 5,200 years. Nat. Geosci. 5, 808–812.

Pflaumann, U., Sarnthein, M., Chapman, M.R., D'Abreu, L., Funnel, B., Huels, M., Kiefer, T., Maslin, M.A., Schulz, H., Swallow, J., van Kreveld, S., Vautravers, M., Vogelsang, E., Weinelt, M.S., 2003. Glacial North Atlantic: Sea-surface conditions reconstructed by GLAMAP 2000. Paleoceanography 18, 1065.

Rasmussen, T.L., Thomsen, E., Skirbekk, K., Ślubowska-Woldengen, M., Klitgaard Kristensen, D., Koç, N., 2013. Spatial and temporal distribution of Holocene temperature maxima in the northern Nordic seas: interplay of Atlantic-, Arctic- and polar water masses. Quat. Sci. Rev.

Rasmussen, T.L., Thomsen, E., Ślubowska, M.A., Jessen, S., Solheim, A., Koç, N., 2007. Paleoceanographic evolution of the SW Svalbard margin (76°N) since 20,000 $^{14}$C yr BP. Quat. Res. 67, 100–114.

Reimer, P.J., Baillie, M.G.L., Bard, E., Bayliss, A., 2009. IntCal09 and Marine09 radiocarbon age calibration curves, 0–50,000 years cal BP. Radiocarbon 51, 1111–1150.

Renssen, H., Goosse, H., Muscheler, R., 2006. Coupled climate model simulation of Holocene cooling events: oceanic feedback amplifies solar forcing. Clim. Past 2, 79–90.

Risebrobakken, B., Dokken, T.M., Smedsrud, L.H., Andersson, C., Jansen, E., Moros, M., Ivanova, E. V., 2011. Early Holocene temperature variability in the Nordic Seas: The role of oceanic heat advection versus changes in orbital forcing. Paleoceanography 26, PA4206.

Risebrobakken, B., Jansen, E., Andersson, C., Mjelde, E., Hevrøy, K., 2003. A high-resolution study of Holocene paleoclimatic and paleoceanographic changes in the Nordic Seas. Paleoceanography 18, 1017.

Rohling, E.J., Pälike, H., 2005. Centennial-scale climate cooling with a sudden cold event around 8,200 years ago. Nature 434, 975–979.

Rudels, B., Quadfasel, D., 1991. Convection and deep water formation in the Arctic Ocean-Greenland Sea System. J. Mar. Syst. 2, 435–450.

Sarnthein, M., Jansen, E., Weinelt, M.S., Arnold, M., Duplessy, J.C., Erlenkeuser, H., Flatøy, A., Johannessen, G., Johannessen, T., Jung, S.J.A., Koç, N., Labeyrie, L.D., Maslin, M., Pflaumann, U., Schulz, H., 1995. Variations in Atlantic surface ocean paleoceanography, 50°-80°N: A time-slice record of the last 30,000 years. Paleoceanography 10, 1063–1094.

Sarnthein, M., van Kreveld, S., Erlenkeuser, H., Grootes, P.M., Kucera, M., Pflaumann, U., Schulz, M., 2003. Centennial-to-millennial-scale periodicities of Holocene climate and sediment injections off the western Barents shelf, 75°N. Boreas 32, 447–461.

Seidenkrantz, M.-S., Ebbesen, H., Aagaard-Sørensen, S., Moros, M., Lloyd, J.M., Olsen, J., Knudsen, M.F., Kuijpers, A., 2012. Early Holocene large-scale meltwater

discharge from Greenland documented by foraminifera and sediment parameters. Palaeogeogr. Palaeoclimatol. Palaeoecol. 391, 71–81.

Spielhagen, R.F., Erlenkeuser, H., 1994. Stable oxygen and carbon isotopes in planktic foraminifers from Arctic Ocean surface sediments: Reflection of the low salinity surface water layer. Mar. Geol. 119, 227–250.

Spielhagen, R.F., Werner, K., Aagaard-Sørensen, S., Zamelczyk, K., Kandiano, E.S., Budeus, G., Husum, K., Marchitto, T.M., Hald, M., 2011. Enhanced Modern Heat Transfer to the Arctic by Warm Atlantic Water. Science 331, 450–453.

Stanford, J.D., Rohling, E.J., Bacon, S., Roberts, A.P., Grousset, F.E., Bolshaw, M., 2011. A new concept for the paleoceanographic evolution of Heinrich event 1 in the North Atlantic. Quat. Sci. Rev. 30, 1047–1066.

Stern, J. V., Lisiecki, L.E., 2013. North Atlantic circulation and reservoir age changes over the past 41,000 years. Geophys. Res. Lett. 40, 3693–3697.

Straneo, F., Hamilton, G.S., Sutherland, D.A., Stearns, L.A., Davidson, F., Hammill, M.O., Stenson, G.B., Rosing-Asvid, A., 2010. Rapid circulation of warm subtropical waters in a major glacial fjord in East Greenland. Nat. Geosci. 3, 182–186.

Straneo, F., Heimbach, P., 2013. North Atlantic warming and the retreat of Greenland's outlet glaciers. Nature 504, 36–43.

Stuiver, M., Reimer, P.J., 1993. Radiocarbon calibration program. Radiocarbon 35, 215–230.

Svendsen, J.I., Alexanderson, H., Astakhov, V.I., Demidov, I., Dowdeswell, J.A., Funder, S., Gataullin, V., Henriksen, M., Hjort, C., Houmark-Nielsen, M., Hubberten, H.W., Ingólfsson, Ó., Jakobsson, M., Kjær, K.H., Larsen, E., Lokrantz, H., Lunkka, J.P., Lyså, A., Mangerud, J., Matiouchkov, A., Murray, A., Möller, P., Niessen, F., Nikolskaya, O., Polyak, L., Saarnisto, M., Siegert, C., Siegert, M.J., Spielhagen, R.F., Stein, R., 2004. Late Quaternary ice sheet history of northern Eurasia. Quat. Sci. Rev. 23, 1229–1271.

Swift, J., 1986. The Arctic waters, in: Hurdle, B. (Ed.), The Nordic Seas. New York, pp. 129–151.

Tarasov, L., Peltier, W.R., 2006. A calibrated deglacial drainage chronology for the North American continent: evidence of an Arctic trigger for the Younger Dryas. Quat. Sci. Rev. 25, 659–688.

Telesiński, M.M., Spielhagen, R.F., Bauch, H.A., 2014a. Water mass evolution of the Greenland Sea since late glacial times. Clim. Past 10, 123–136.

Telesiński, M.M., Spielhagen, R.F., Lind, E.M., 2014b. A high-resolution Lateglacial and Holocene palaeoceanographic record from the Greenland Sea. Boreas 43, 273–285.

Thornalley, D.J.R., Blaschek, M., Davies, F.J., Praetorius, S., Oppo, D.W., McManus, J.F., Hall, I.R., Kleiven, H., Renssen, H., McCave, I.N., 2013. Long-term variations in Iceland–Scotland overflow strength during the Holocene. Clim. Past 9, 2073–2084.

Thornalley, D.J.R., Elderfield, H., McCave, I.N., 2010. Intermediate and deep water paleoceanography of the northern North Atlantic over the past 21,000 years. Paleoceanography 25, 1–17.

Voelker, A.H.L., Grootes, P.M., Nadeau, M.-J., Sarnthein, M., 2000. Radiocarbon Levels in the Iceland Sea From 25-53 kyr and their Link to the Earth's Magnetic Field Intensity. Radiocarbon 42, 437–452.

Waelbroeck, C., Duplessy, J.C., Michel, E., Labeyrie, L., Paillard, D., Duprat, J., 2001. The timing of the last deglaciation in North Atlantic climate records. Nature 412, 724–727.

Wagner, T., Henrich, R., 1994. Organo-and lithofacies of glacial-interglacial deposits in the Norwegian-Greenland Sea: Responses to paleoceanographic and paleoclimatic changes. Mar. Geol. 120, 335–364.

Wanner, H., Solomina, O., Grosjean, M., Ritz, S.P., Jetel, M., 2011. Structure and origin of Holocene cold events. Quat. Sci. Rev. 30, 3109–3123.

Weaver, A.J., Saenko, O.A., Clark, P.U., Mitrovica, J.X., 2003. Meltwater pulse 1A from Antarctica as a trigger of the Bølling-Allerød warm interval. Science 299, 1709–1713.

Weinelt, M.S., 1993. Veränderungen der Oberflächenzirkulation im Europäischen Nordmeer während der letzten 60.000 Jahre. Berichte aus dem Sonderforschungsbereich 313 41, 105.

Weinelt, M.S., Vogelsang, M., Kucera, M., Pflaumann, U., Sarnthein, M., Voelker, A.H.L., Erlenkeuser, H., Malmgren, B.A., 2003. Variability of North Atlantic heat transfer during MIS 2. Paleoceanography 18, 1071.

Werner, K., Spielhagen, R.F., Bauch, D., Hass, H.C., Kandiano, E.S., 2013. Atlantic Water advection versus sea-ice advances in the eastern Fram Strait during the last 9 ka: Multiproxy evidence for a two-phase Holocene. Paleoceanography 28, 283–295.

Werner, K., Spielhagen, R.F., Bauch, D., Hass, H.C., Kandiano, E.S., Zamelczyk, K., 2011. Atlantic Water advection to the eastern Fram Strait — Multiproxy evidence for late Holocene variability. Palaeogeogr. Palaeoclimatol. Palaeoecol. 308, 264–276.